

THESIS ON NATURAL AND EXACT SCIENCES

Heterogeneity of diffusion restrictions in cardiomyocytes

NATALJA JEPIHHINA

TUT
PRESS

TALLINN UNIVERSITY OF TECHNOLOGY

School of Science

Department of Cybernetics

Laboratory of Systems Biology

This dissertation was accepted for the defense of the degree of Doctor of Philosophy (Gene Technology) on 11 May, 2017.

Supervisor: Marko Vendelin, PhD
Laboratory of Systems Biology, Department of Cybernetics, School of Science,
Tallinn University of Technology, Tallinn, Estonia

Opponents: Prof. Anders Arner, MD, PhD
Department of Physiology and Pharmacology,
Karolinska Institutet, Stockholm, Sweden

Prof. Allen Kaasik, PhD
Department of Pharmacology,
University of Tartu, Tartu, Estonia

Defense of the thesis: 15 September, 2017

Declaration:

I hereby declare that this doctoral thesis, submitted for the doctoral degree at Tallinn University of Technology, is my original investigation and achievement and has not been submitted for the defense of any academic degree elsewhere.

Natalja Jepihhina

Copyright: Natalja Jepihhina, 2017, Creative Commons Attribution-NonCommercial-NoDerivs 3.0 Unported License

Colophon: This thesis was typeset with \LaTeX 2 ϵ using André Miede's *classicthesis* style with modifications by David Schryer and Ardo Illaste to conform with Tallinn University of Technology style guidelines. The main font is Times. Biolinum is used for sans-serif text.

ISSN 1406-4723

ISBN 978-9949-83-128-9 (publication)

ISBN 978-9949-83-129-6 (PDF)

LOODUS- JA TÄPPISTEADUSED

**Difusioonitakistuste
heterogeensus
südamelihasrakkudes**

NATALJA JEPHINA

TTÜ
KIRJASTUS

CONTENTS

SUMMARY	vi
KOKKUVÕTE	vii
LIST OF PUBLICATIONS	viii
LIST OF CONFERENCE PRESENTATIONS	ix
ACKNOWLEDGMENTS	x
ACRONYMS	xi
THESIS	13
1 INTRODUCTION	15
2 MITOCHONDRIAL AUTOFLUORESCENCE	19
3 RESULTS	23
3.1 Autofluorescence measurements in permeabilized cardiomyocytes	23
3.2 Diffusion restrictions in cardiomyocytes	25
4 DISCUSSION	29
4.1 Diffusion restrictions at the level of the mitochondrial outer membrane	30
4.2 Energetic compartments in cardiomyocytes	32
5 CONCLUSIONS	35
REFERENCES	37
CURRICULUM VITAE	49
APPENDIX	55
PUBLICATION I	57
PUBLICATION II	75
PUBLICATION III	93

SUMMARY

IN A HEALTHY HEART, the energy supply and demand should be in balance. This is achieved by an efficient transport of high energy phosphates. The researchers of heart muscle cells, cardiomyocytes, however, discovered that the diffusion of adenine nucleotide molecules is restricted in the heart muscle cells. Interestingly enough, the diffusion restriction diminishes in the ischemic heart cells, implying that the mechanisms of the diffusion restrictions are important to maintain the normal functioning of the heart and heart muscle cells. Thus, it is crucial to understand the origin of diffusion obstacles in cardiomyocytes.

This thesis is a part of the project studying diffusion restrictions in adult rat cardiomyocytes. The main goal of this thesis was to understand whether the diffusion of adenine nucleotides is restricted in a single heart muscle cell and, if so, to evaluate the distribution of diffusion restrictions. The novelty of the used approach is making experiments at the single cell level, whereas previous reports were based on cell population studies. The advantage of such approach is the ability to distinguish intracellular diffusion obstacles from overall diffusion restrictions in the system. This was achieved by measurements of the kinetics of cell respiration using autofluorescence-based methods.

The work conducted in this thesis showed that diffusion restrictions in cardiomyocytes exist at the single cell level. This was shown on adult rat cardiomyocytes and confirmed on cardiomyocytes of wild type and creatine deficient mice. Combination of experimental data and mathematical modeling made it possible to conclude that restricting obstacles found in cardiomyocytes are caused by two distinct features: closing of voltage-dependent anion channels (VDACs) on the mitochondrial outer membrane (MOM) and barriers in cell cytoplasm, which both contribute equally to diffusion restrictions. Specifically, it was found that 98% of the VDACs on the MOM were not available for adenosine phosphate transport and thus restricted its diffusion.

The findings presented in the current thesis enhance our insight into the distribution of diffusion restrictions in cardiomyocytes. Since the diffusion restrictions influence the transport of molecules from the cytosol to mitochondria and, hence, are one of the factors that determine the cell fate, better understanding of their regulatory mechanisms may help to develop new treatments for diseased hearts.

KOKKUVÕTE

TERVES SÜDAMES peavad energia nõudlus ja varustamine olema tasakaalus. Seda saavutatakse energiakandja molekulide efektiivse transportimisega. Varasemalt on leitud, et südamelihaskuded ehk kardiomüotsüütides on energiakandja molekulide (adeniinnukleotiidide) difusioon oluliselt takistatud. Lisaks sellele on näidatud, et need takistused adeniinnukleotiidide difusioonile vähenevad patoloogilistes seisundites nagu isheemia. See viitab asjaolule, et difusioonibarjäärid omavad olulist rolli südame ja kardiomüotsüütide korrektse talitluse säilitamiseks. Seetõttu, on oluline mõista difusioonitakistuste täpset päritolu ja funktsiooni südamelihaskudedes.

Antud doktoritöö on osa projektist, mis käsitleb difusioonitakistusi roti kardiomüotsüütides. Töö põhieesmärgiks oli uurida kas ja kui palju on takistatud adeniinnukleotiidide difusioon ühe südamelihasku tasemel. Kuna leidis kinnitust, et tõepoolest ühe raku tasemel on difusioon märkimisväärselt takistatud, siis järgmise sammuna keskenduti difusioonibarjääride jaotuse ja võimalike põhjustajate välja selgitamisele. Selleks töötati välja uudne meetod, mis põhineb raku hingamise kineetika mõõtmisel autofluorestsentsi abil. Kui varasemalt tehtud katsed raku populatsioonidel annavad vastuse ainult üldise difusioonitakistuse suuruselt raku, siis välja töötatud meetodi suurimaks eeliseks on võime määrata üldise difusioonitakistuse jaotust raku.

Tehtud töö tulemusena leidis kinnitust difusioonitakistuste olemasolu ühe südamelihasku tasemel. Seda näidati roti kardiomüotsüütides ning kinnitati kreatiini puudulikkusega ja vastava liini metsiktüüpi hiire südamelihaskudedes. Interdistsiplinaarne lähenemine, mis kombineeris eksperimentaalsete andmete kogumist ja nende analüüsi matemaatiliste mudelite abil, aitas tuvastada difusioonitakistuste jaotumist kaheks osaks. Leiti, et VDAC kanalite sulgumine mitokondri välismembraanis ja barjäärid raku tsütoplasmas pannustavad difusioonitakistustele võrdsel määral. Lisaks näitavad töö tulemused, et puhkeolekus kardiomüotsüütides ei ole 98% VDAC kanalitest läbitavad adenosinofosfaatidele.

Kõkkuvõtteks annavad antud töö tulemused suure panuse difusioonitakistuste uuringute valdkonda. Kuna difusioonibarjäärid mõjutavad molekulide transporti tsütosoolist mitokondrisse, siis seega on need raku saatuse üheks määravaks asjaoluks. Selliste adeniinnukleotiidide difusiooni reguleerivate mehhanismide uurimine võib saada oluliseks uute südameravis kasutatavate ravimite väljatöötamises.

LIST OF PUBLICATIONS

- I **Jepihhina N**, Beraud N, Sepp M, Birkedal R, Vendelin M; **Permeabilized rat cardiomyocyte response demonstrates intracellular origin of diffusion obstacles**, *Biophysical Journal*, 101, 2112–2121, 2011
- II Branovets J, Sepp M, Kotlyarova S, **Jepihhina N**, Sokolova N, Aksentijevic D, Lygate CA, Neubauer S, Vendelin M, Birkedal R; **Unchanged mitochondrial organization and compartmentation of high-energy phosphates in creatine-deficient $GAMT^{-/-}$ mouse hearts**, *AJP-Heart and Circulatory Physiology*, 305(4), 506–520, 2013
- III Simson* P, **Jepihhina* N**, Laasmaa M, Peterson P, Birkedal R, and Vendelin M; **Restricted ADP movement in cardiomyocytes: Cytosolic diffusion obstacles are complemented with a small number of open mitochondrial voltage-dependent anion channels**, *Journal of Molecular and Cellular Cardiology*, 97, 197–203, 2016

* authors contributed equally

Summary of the author's contributions

- I In Publication I, the author isolated cardiomyocytes and performed all the experiments in the fluorescence microscope and spectrofluorometer. The author made figures with experimental results and analyzed the experimental data. The author also participated in writing the manuscript.
- II For Publication II, the author participated in some isolations of cardiomyocytes and made all the experiments in the fluorescence microscope. The author also analyzed the data from her experiments and prepared the figures.
- III In Publication III, the author isolated cardiomyocytes, performed all the experiments and participated in manuscript revision.

LIST OF CONFERENCE PRESENTATIONS

- I **Jepihhina*** N, Beraud, N, Sepp, M, Birkedal, R, Vendelin, M; **Permeabilized rat cardiomyocyte response demonstrates intracellular origin of diffusion obstacles**; *Biophysical Society 56th Annual Meeting*, San Diego, California, USA, February 25 – 29, 2012
- II **Jepihhina*** N, Simson P, Laasmaa M, Peterson P, Birkedal R, Vendelin M; **The characterization of diffusion obstacles in rat cardiomyocytes**; *Biophysical Society 59th Annual Meeting*, Baltimore, Maryland USA, February 7 – 11, 2015
- III **Jepihhina*** N, Simson P, Laasmaa M, Birkedal R, Vendelin M; **The characterization of diffusion obstacles in rat cardiomyocytes**; *The Joint Meeting of the Federation of European Physiological Societies and the Baltic Physiological Societies (FEPS2015)*, Kaunas, Lithuania, August 26 – 29, 2015
- IV Simson P, **Jepihhina** N, Laasmaa M, Birkedal R, Vendelin* M; **The characterization of diffusion obstacles in rat cardiomyocytes**; *44th European Muscle Conference 2015*, Warsaw, Poland, September 21 – 26, 2015
- V Simson P, **Jepihhina** N, Laasmaa M, Branovets J, Peterson P, Birkedal R, Vendelin* M; **Number of open mitochondrial VDACs and intracellular diffusion coefficient in heart muscle**; *Biophysical Society 60th Annual Meeting*, Los Angeles, California, USA, February 27 – March 2, 2016

* *presented at the conference*

ACKNOWLEDGMENTS

I would like to thank my supervisor Dr. Marko Vendelin for his positive thinking, motivation and guidance in work. I am grateful to Dr. Rikke Birkedal for helping me with experimental difficulties. Special thanks to Dr. Martin Laasmaa, who was always willing to improve the technical part of the experiments and organize crosstalk between physicists and biologists in our lab. I thank all my colleagues for making working days more exciting.

I also thank Dr. Nathalie Beraud and all the members of Bioenergetics lab in the NICPB for guiding me through the first steps I took in this field.

I would like to thank my friends for sharing our high and low moments. Special thanks go to Dr. Olesja Bondarenko for both fruitful discussions and being a good friend.

My very special thanks for the support, friendship and valuable experience provided by the great team within the Veterinaardiagnostikakeskus. It has always been a great pleasure for me to take part in our mutual activities.

I am very grateful for my parents for their love, continuous support and patience. Without their believing in me, it would be much harder to achieve my goals.

Financial support from the Wellcome Trust (081755), the Estonian Science Foundation (ETF8041), the European Union through the European Regional Development Fund (CENS Estonian Center of Excellence in Research), Estonian Research Council (IUT33-7) as well as Archimedes Foundation is appreciated.

ACRONYMS

ADP	adenosine diphosphate
ANT	adenine nucleotide translocator
ATP	adenosine triphosphate
ATPase	adenosine triphosphatase
cAMP	cyclic adenosine monophosphate
CK ^{-/-}	creatine kinase knock-out
CK	creatine kinase
Cr	creatine
DC	diffusion coefficient
ETC	electron transport chain
FADH ₂	reduced form of flavin adenine dinucleotide
FCCP	carbonyl cyanide-4-(trifluoromethoxy)phenylhydrazone
Fp	flavoprotein
GAMT	guanidinoacetate N-methyltransferase
GAMT ^{-/-}	GAMT knock-out
ICEUs	intracellular energetic units
K _M (ADP)	apparent Michaelis-Menten constant of mitochondrial respiration to ADP
LipDH	lipoamide dehydrogenase
MOM	mitochondrial outer membrane
NAD ⁺	oxidized nicotinamide adenine dinucleotide
NADH	reduced nicotinamide adenine dinucleotide
PCr	phosphocreatine
PDH	pyruvate dehydrogenase complex
Pi	phosphate ion
SR	sarcoplasmic reticulum
TCA	citric acid cycle
VDAC	voltage-dependent anion channel
WT	wild type

THESIS

INTRODUCTION

ADEQUATE GENERATION of energy is crucial for heart functioning. Therefore, energy production and energy utilization should be in balance to maintain proper and efficient work of the heart. In failing hearts, this mechanism is disrupted and this powerful organ cannot function properly [1, 2], which causes high mortality rates worldwide [3–5]. Better understanding of factors that regulate heart metabolism and application of gained knowledge in the development of new drugs may help to overcome heart failure problems. Numerous studies have been performed to understand the mechanisms of heart failure. Studies with the tissues of diseased patients and transgenic animal models have been introduced in recent publications [6–9]. Animal models with induced heart failure improve our understanding of the energetic machinery in the heart [10–13].

Every day our heart produces and uses energy in the form of adenosine triphosphate (ATP) in the amount that is 15 times greater than the organ weighs [14]. It is therefore important to have sufficient amounts of energetic molecules for constant cell needs. Neubauer and coworkers examined the energetic pool of the hearts of diseased patients with cardiomyopathy through phosphocreatine (PCr)-to-ATP ratio, and suggested applying this factor to estimate future mortality [15]. It was shown that failing human hearts have 25–30% lower ATP content than healthy hearts [16], which is also confirmed by phosphorus-31 magnetic resonance spectroscopy (^{31}P -MRS) studies in diseased patients [17]. Thus, energetics of PCr and ATP inside the affected heart muscle cells is disturbed. However, it is not clear what causes the disturbance in high energy phosphate levels. It is therefore important to study the effects of energy transfer alterations on cell functioning and mechanisms underlying their action.

In this doctoral thesis, the research is focused on energy transfer in single heart muscle cells, cardiomyocytes. It was hypothesized that the ATP transport inside the heart muscle cells is guided by diffusion restrictions. This phenomenon was previously studied on permeabilized fibers and populations of cardiomyocytes, where mitochondrial affinity to extracellular adenosine phosphates was lower than in isolated mitochondria [18]. The intracellular environment of cardiac muscle cells is

highly organized and heterogeneous, as indicated by the “crystal-like” pattern of the mitochondria distribution [19, 20]. It was shown that diffusion restrictions tend to depend on cellular structure, being less evident in cells with more random organization of mitochondrial patterns such as cultured cardiomyocytes HL-1 and non-beating HL-1 [21], neonatal cardiomyocytes [22, 23] and cells having simpler morphology, such as fish cardiomyocytes [24], compared to adult mammalian cardiomyocytes. Moreover, diffusion in the cell cytoplasm can be obstructed because of macromolecular crowding, interactions and phase separation [25].

Interestingly, ischemia/reperfusion damage causes partial loss of diffusion restrictions implying an important role in maintaining the heart function [26]. At the moment, ischemic preconditioning, first introduced by Murry and coworkers in 1986, is shown to be an effective method to keep tissues from damage caused by ischemia/reperfusion injury [27]. Understanding the factors that contribute to fatal repercussions may widen survival opportunities of cardiac patients.

There is a controversy in the determination of the obstacles limiting diffusion. Some researchers suggest the obstruction of diffusion of adenine nucleotides by closure of voltage-dependent anion channels (VDACs) on the mitochondrial outer membrane (MOM) [28, 29]. The mathematical model in the publication by Saks and coworkers demonstrates how MOM permeability affects adenosine diphosphate (ADP) transport [30]. Alternatively, diffusion restrictions may come from the intracellular environment that group ATP producing and consuming units [31].

Notably, all the above-described knowledge on diffusion restriction in heart muscle cells was gained by studying populations of cardiomyocytes. However, such experiments must be interpreted with caution, because in this case cells may stick together, thereby limiting diffusion of metabolites to the inner cells [32]. Besides, laminar flow and unstirred solution layers may also create the possibility of misinterpreting the measurements [32].

The main aim of this thesis was to test whether diffusion restrictions exist at the single cell level and subsequently determine the cellular components involved in this process. To unravel the factors that might affect experimental results, single cells were used instead of cell populations. Studies on cell populations were also performed to compare our data with previous results. Cardiomyocytes were permeabilized and titrations of ADP and ATP were performed. The autofluorescence changes of reduced nicotinamide adenine dinucleotide (NADH) and flavoprotein (Fp) compounds were recorded on the fluorescence microscope for single cell experiments and in the spectrofluorometer chamber for populations of cardiomyocytes. This enabled us to make measurements on live cells and follow changes in their redox state in real time.

This work had a logical concept starting with checking the hypothesis of diffusion restrictions at the single cell level and subsequently finding the distribution

of diffusion restrictions inside the cell. Cardiomyocytes from three different animal models were used in a series of experiments: rat, wild type (WT) mice and transgenic creatine (Cr)-deficient mice.

In Publication I, we determined the presence of diffusion obstacles in a single cell, demonstrating that low apparent Michaelis-Menten constant of mitochondrial respiration to ADP ($K_M(\text{ADP})$) for exogenous ADP and ATP is of cellular origin. Measurements were performed on single cell and on a population of cells, enabling connecting data from respiration measurements to autofluorescence. The current finding was confirmed with a mathematical model, proving that the low affinity was not caused by an incomplete separation or clumping of cells.

In Publication II, we examined the effect of Cr deficiency on the energy metabolism of cardiomyocytes from WT and GAMT knock-out ($\text{GAMT}^{-/-}$) mice that lacked guanidinoacetate N-methyltransferase (GAMT) enzyme to synthesize Cr, causing the deficiency of the latter. The lack of Cr inhibits the creatine kinase (CK) system, which is proposed to be a spatial and a temporal energy buffer in cardiomyocytes [33, 34]. This system facilitates transport of ADP and ATP between the sites of their production and utilization, compensating for the diffusion obstacles. We showed that CK inactivation in these mice does not affect either respiration kinetics or mitochondrial organization at basal workloads.

Publication III gives insight into possible causes of heterogeneity of diffusion inside a single cell. The work reported in Publication III was a logical extension of my previous studies that enabled a deeper look into the problem of diffusion restrictions, concentrating on the location of diffusion barriers. These series of experiments shed light on the distribution of diffusion restrictions in cardiomyocytes and quantified the role of the MOM and cytoplasmic obstacles in the origin of diffusion restrictions.

A great advantage of the current work is that experimental procedures were complemented with mathematical modeling. This fusion helped to quantify the distribution of diffusion restrictions in the cell on the basis of the measured autofluorescence signal. Such way of analyzing results gives the possibility of using and understanding the obtained data more precisely and gain maximal knowledge. The research of such complicated processes like cellular metabolism has to rely on exact calculations on how small processes influence the whole picture.

MITOCHONDRIAL AUTOFLUORESCENCE

STUDYING THE PROCESSES occurring in live cells has always been a challenge for researchers all over the world. One of the complexities is caused by the fact that usually it is needed to somehow influence the cellular environment, thereby manipulating processes inside. Researchers either stain cells with special dyes or have to fix the experimental material. Fortunately, some processes can be monitored by using naturally fluorescent biomarkers from the cell. In the middle of 1950s Chance and colleagues developed a technique to monitor intracellular processes through intracellular coenzymes, NADH and Fp [35–38]. The advantage of this method is that the monitoring of cellular activities is non-invasive and the cellular response can be studied in the live environment.

NADH is involved in many activities of mitochondria metabolism, such as respiration and electron transport, oxidative stress, aging and apoptosis [39–41]. NADH monitoring has a promising potential in clinical applications, enabling to evaluate malignancy probability and proliferation of the affected tissue. It could be used to detect early stages of cancer in vivo in gastrointestinal, cervix [42], ovarian [43] and bladder [44] malignant processes. Moreover, the efficiency of new drugs can also be tested using intrinsic autofluorescence [43]. Using autofluorescence properties of these two intracellular biomarkers was previously described to help to estimate cancer development [45] and therapeutic efficiency [46]. Analyzing autofluorescence properties and redox ratio of NADH and Fps at the cellular level can be a tool to monitor tumor heterogeneity and response to anti-cancerous treatment. This can improve the therapy and survival of patients, minimizing tumor regeneration due to resistant populations of cells [47]. Cellular autofluorescence rise in response to ionic radiation could serve as a marker of exposure in cases of incidental radiation or following radiation therapy [48].

Mitochondrial autofluorescence has been used earlier by several researchers to study aspects of the heart function. Studies of mitochondrial NADH and Fp signal changes during ischemia/reperfusion injury were performed on the whole rat heart, enabling to detect myocardial damage at the beginning [49]. Mitochondrial dysfunction in heart failure and cardiac hypertrophy was recognized based on NADH

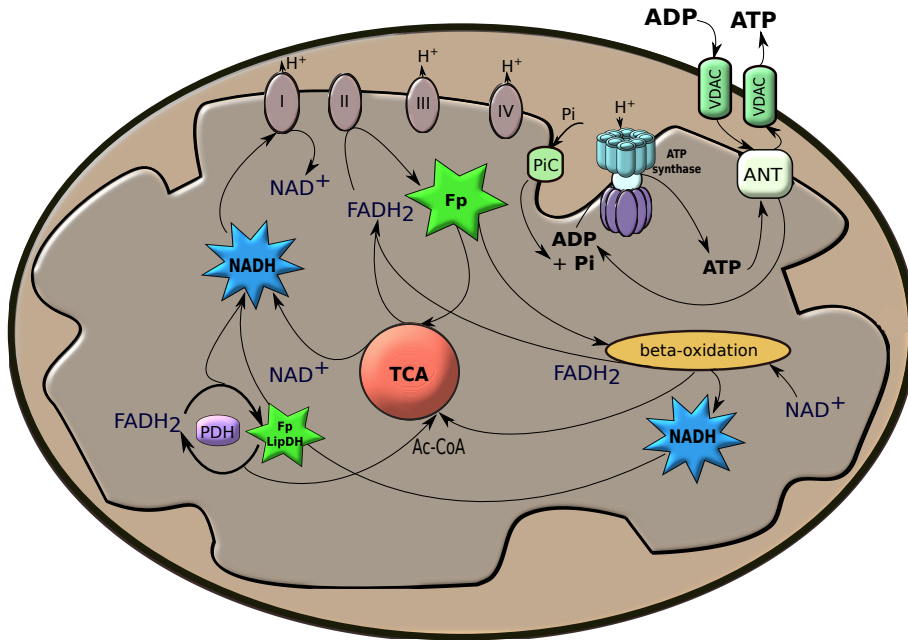


Figure 1 – Schematic representation of energetic pathways in mitochondria. VDACs provide a pathway for many molecules to enter the mitochondrial intermembrane space. ADP and ATP then enter the mitochondrial matrix via adenine nucleotide translocator (ANT). Substrates for cytric acid cycle (TCA), pyruvate dehydrogenase complex (PDH) and beta-oxidation enter the mitochondria matrix through specific channels. Pi is transferred into mitochondrial matrix via the Pi carrier (PiC). Electrons from TCA are transferred by electron carrier NADH to complex I of electron transport chain (ETC). FADH₂ transports electrons from TCA to complex II of ETC. PDH and beta-oxidation provide electrons to ETC via NADH and FADH₂. Reduced NADH is fluorescent. When NADH gives electrons to ETC and becomes NAD⁺, it is not fluorescent. At the same time reduced FADH₂ molecule is not fluorescent, while oxidized Fp emits light in the blue spectrum. When electrons go through ETC, protons are being pumped out of the mitochondrial matrix, creating a gradient needed to activate ATP synthesis to produce ATP from ADP and Pi. Newly synthesized ATP is transported out of mitochondria to be used for cellular needs.

and Fp signal changes [50]. NADH response to different pacing rates was observed by Asfour et al. [51] in the rabbit heart. Such monitoring would benefit patients undergoing surgery on the open heart, allowing surgens to estimate the metabolic function of the organ and also helping to improve protocols for transplantology [49]. NADH and Fp redox couple monitoring was applied to evaluate the interaction of drugs on the mitochondria electron transport chain (ETC) of cardiomyocytes [52].

In the current thesis the focus is on the NADH and Fp ability to reflect the redox state of cardiomyocytes. Similar studies were performed in different labs [45, 53, 54], indicating the power of the method to follow metabolic activities of the cell.

A simplified scheme of NADH/Fp cycling inside mitochondria is introduced in Fig. 1. NADH and Fps carry electrons from the citric acid cycle (TCA) to the (ETC) in the inner membrane of mitochondria. To obtain a NADH fluorescence signal, cells are excited in the UV spectrum with 330–350 nm light and the emission peak is 460 nm. When NADH donates electrons to complex I in the ETC, NAD^+ loses fluorescence properties [55]. The reduced form of flavin adenine dinucleotide (FADH_2) provides electrons for complex II in the ETC. Contrary to NADH, Fp becomes fluorescent in the oxidized state with excitation light 450 nm and emission 550 nm.

The major part of the signal of Fps comes from mitochondrial lipoamide dehydrogenase (LipDH) and the electron transfer Fp. Their emission and excitation spectra, 480 nm and 545 nm for LipDH and 435 nm and 485 nm for Fp, respectively, were distinguished by Kunz, who measured the rat liver mitochondria response to redox changes [56, 57]. The signals are close, and without a special experimental setup researchers see both at the same time [58]. However, both represent mitochondrial metabolism and are not involved in other cellular activities [59]. Redox states of LipDH flavoprotein and NAD^+/NADH pool are in equilibrium, because NADH is serving in the dehydrogenase reactions. Thus, an increase in mitochondrial NADH autofluorescence is accompanied by a decrease of the LipDH autofluorescence signal [60]. Some intracellular flavins are redox-independent, giving background fluorescence, which is quenched in case of their binding to protein cofactors [56]. In that case their contribution to intracellular autofluorescence is negligible [60]. By monitoring NADH and Fp autofluorescence in the current work, we analyzed the bioenergetic response of permeabilized cardiomyocytes to adenine nucleotide titrations.

RESULTS

THE PROBLEM OF DIFFUSION RESTRICTIONS has been widely studied for decades [61, 62]. It is not clear what causes diffusion restrictions in the cell and which structures are responsible for that. In the current thesis we built up a study to characterize the mitochondrial response to ADP titration in a single cell. The main results are briefly summarized in this section, giving a short overview of the obtained data with minimal repetition of the attached Publications I–III.

3.1 AUTOFLUORESCENCE MEASUREMENTS IN PERMEABILIZED CARDIOMYOCYTES

As the main method used in this work, cells were permeabilized and continuously superfused with a solution containing ADP and ATP in different concentrations. ADP and Pi in the solutions stimulate oxidative phosphorylation and ATP synthesis [35, 63]. The addition of ATP activates intracellular adenosine triphosphatases (ATPases) first, and the obtained ADP stimulates respiration. Glutamate and malate, substrates metabolized in the TCA cycle, increase the NADH/NAD⁺ ratio, which in turn provides more electrons for the functioning of the ETC. A widefield fluorescence microscope and a sensitive camera were used to image the cardiomyocytes. The fluorescence signals were normalized by adding oligomycin (inhibitor of ATP synthase) and cyanide (inhibitor of cytochrome c oxidase) followed by carbonyl cyanide-4-(trifluoromethoxy)phenylhydrazone (FCCP) (uncoupler) to the cell. This enabled to record minimal and maximal signals, respectively, and subtract the fluorescence background from the signal change caused by respiration.

Representative experimental data are shown in the Fig. 2. It was shown that the fluorescence signal of NADH and Fp changed in a stepwise manner in correlation with the applied extracellular ADP. The opposite behavior of these two signals was also advantageous, justifying the experimental protocol. Thus, we can conclude that signal changes were due to respiration, as both signals responded simultaneously to the addition of ADP. We focused on the change of the NADH signal, as

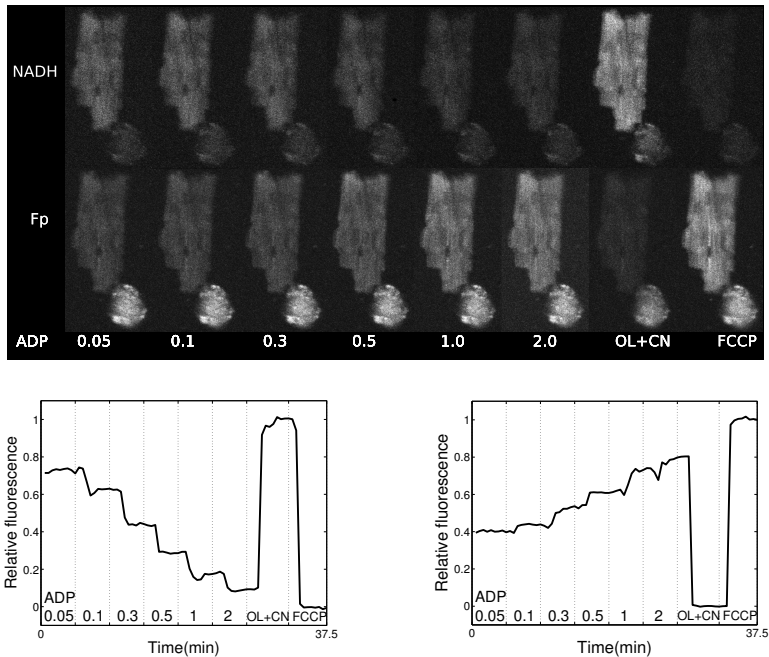


Figure 2 – Example of NADH and Fp autofluorescence changes in response to ADP titrations in a single permeabilized cardiomyocyte (top). Autofluorescence signal was induced by excitation light of 340 nm for NADH and 465 nm for Fp. Viable rod-shaped cell and hypercontracted cell are shown. Towards the end of the experiment, inhibitors of mitochondrial respiration (oligomycin (OL) and cyanide (CN)) followed by the uncoupler FCCP were used to record the maximal and minimal levels of the autofluorescence signal. Below, representative traces of NADH (left) and Fp (right) autofluorescence changes during ADP titrations are shown. Note that the autofluorescence of NADH and Fp changes in a stepwise manner and in the opposite way in response to the increasing ADP concentration.

in general it was brighter and the signal-to-noise ratio was larger than for the Fp signal in our experimental conditions.

As our previous study on respiration was performed on populations of cells [64], we needed to relate the autofluorescence changes in single cells to the respiration rate. For that, ADP titration was performed in a spectrofluorometer, where autofluorescence signals of NADH and Fp were recorded on cell populations. Both the experiments carried out under the microscope (experiments with single cells) and in the spectrofluorometer (experiments with cell populations) showed that the cells responded similarly to the titrations of adenine nucleotides. Autofluorescence changes in the spectrofluorometer cuvette were then related to oxygen consumption measurements [64]. After that, we compared autofluorescence changes in the single cell and the population of cells. This gave us a possibility of making a connection between population studies and single cell observations. The most im-

portant result of the work reported in Publication I was the demonstration of the intracellular nature of diffusion restrictions. In other words, we showed that intracellular diffusion barriers exist.

3.2 DIFFUSION RESTRICTIONS IN CARDIOMYOCYTES

As our first study (Publication I) confirmed the existence of diffusion restrictions inside the cell, our next goal was to assess the contribution of different cellular structures to the diffusion restrictions. In the study described in Publication III, we followed changes in the autofluorescence of NADH from a single permeabilized cardiomyocyte in response to ADP titration. The experimental protocol was built up to characterize mitochondrial respiration in different parts of the cell, comparing the NADH autofluorescence signals in the middle of the cell and at the edges.

The experimental design and modeling taken together gave us a possibility of distinguishing contributions of the MOM from the barriers situated in the cell cytoplasm (Fig. 3). In this case, signal normalization with oligomycin, cyanide and FCCP was performed at each location of the cell to see how the relative fluorescence distribution changes within a single cell. After determining the geometry of each particular cell we were able to construct a mathematical model of diffusion. The heterogeneity of the NADH signal distribution, as we see it, is caused by the thickness of the current cell as well as mitochondrial distribution and response. As we were able to exclude differences in the fluorescence signal caused by differences in cell thickness by normalizing the signal to references taken in the presence of respiration chain blockers and uncoupler, we were able to see how mitochondria reacted to ADP. We examined two models of the distribution of diffusion restrictions. One was composed to reflect the state when all the diffusion restrictions between the surrounding solution and inner mitochondria were due to the MOM. The other model took into account both, the MOM contribution to diffusion restrictions and the cytosolic barriers. If we compare modeling data with the results from our experiments, it is obvious that the MOM is not the only diffusion obstacle in the permeabilized cardiomyocytes (Fig. 3).

The numerical analysis of the recorded data indicated that nearly half of the $K_M(\text{ADP})$ of the permeabilized cardiomyocyte respiration was caused by the closure of VDACs in the MOM and the other half was due to diffusion obstacles in cytoplasm. The striking new result was that only 2% of the VDACs are open for ADP in the MOM. This discovery raises many questions about their role in cellular metabolism.

The closing of VDACs on the MOM contributes to intracellular diffusion restrictions. It is therefore important to study other cellular mechanisms that contribute to the energy transfer between ATPases and mitochondria. Higher affinity of mito-

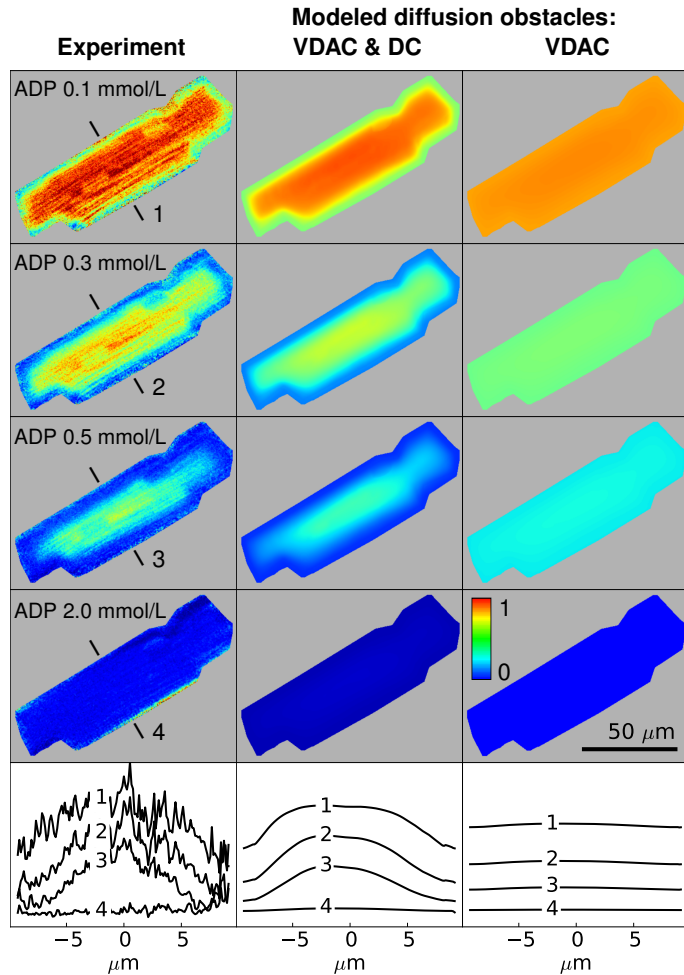


Figure 3 – Comparison of experimental data with images calculated by the model. The variation of NADH fluorescence in response to ADP titrations in a single permeabilized cardiomyocyte. The autofluorescence signal with every ADP concentration was additionally normalized by the maximal and minimal signals obtained in the presence of inhibitors of mitochondrial respiration, oligomycin and cyanide, in each location. The middle and the right columns represent the images calculated by the model. The model either takes into account both cytosolic diffusion barriers and the barriers at the MOM level (middle column), or the diffusion obstacles at the MOM level only. Comparison of experimental results with the modeled data show that the model in the middle column fits experimental results.

chondria to extracellular ADP and significant cytoarchitectural changes were previously observed in heart muscle fibers of CK-deficient mice ($CK^{-/-}$), who differently from WT mice lack cytosolic and mitochondrial CKs [65]. As CK facilitates energy transfer, in the absence of a functional CK system diffusion could be restricted less to compensate for the lack of CK [65].

3.2 DIFFUSION RESTRICTIONS IN CARDIOMYOCYTES

The research reported in Publication II emerged from the idea to observe whether cardiomyocytes isolated from WT and Cr-deficient $GAMT^{-/-}$ mice hearts have similar properties of diffusion restrictions, or whether absence of Cr influences this parameter, showing differences between WT mice and their transgenic littermates. The same protocol as used in Publication I was used to test this hypothesis. Our study revealed that there was no statistically significant difference in the NADH and Fp response to ADP titrations between WT and $GAMT^{-/-}$ cardiomyocytes. Other examinations, including kinetic measurements of oxygen consumption and evaluation of mitochondrial positioning, performed in the study, also confirmed that no differences occurred between knock-out and WT mice heart cardiomyocytes in resting conditions.

DISCUSSION

THIS DOCTORAL THESIS is focused on understanding the mitochondrial energy transfer in a single permeabilized cardiac muscle cell. The experimental results of the current work demonstrate the existence of diffusion obstacles for adenine nucleotides inside a single cardiomyocyte. Moreover, it was shown that the obstacles are partly caused by cytosolic structures, while the other part is due to MOM (VDAC) permeability. In addition, as this study combines both the single cell and cellular population measurement approaches, it enables to compare existing data on diffusion restrictions with the results obtained by applying new experimental strategies. In this part of the thesis the role of compartments causing diffusion restrictions will be discussed and the contribution of the work to the field will be pointed out.

As described above in detail, methods based on autofluorescence properties that naturally occur in the cells were used, which allowed us to perform experiments in less manipulated conditions. The use of single cells as a model was a novel approach in the studies of diffusion restrictions that enabled to get new insights into this phenomenon. Experiments carried out at the single cell level are perspective in modern science, helping to examine intracellular processes in healthy and affected cells. At the same time such approach enables to choose the cell of proper shape and size, its reaction to certain stimuli or any other parameter that may characterize its condition. For example, we chose viable rod-shaped cells for our experiments, while hypercontracted non-rod-shaped cells, damaged during the isolation procedure, might show a different kinetic response because of malfunctional mitochondria (Fig. 2). By studying diffusion restrictions at the single cell level we managed to resolve the controversy existing previously in the field. As mentioned above, Kongas et al. raised a concern that diffusion restrictions may be caused by clumping of cells or unseparated tissue fragments [32]. In this case, diffusion distances to the inner cells are larger and this would cause a higher apparent $K_M(\text{ADP})$ for respiration. In addition, unstirred solution layers around the cells might also limit the diffusion of molecules to the cells. The flow profile of the measuring chamber, estimated in Publication I, also indicated the contribution of intracellular diffusion obstacles, separating them from diffusion caused by solution flow properties. In

the first part of the thesis it was demonstrated that diffusion restrictions exist in a single permeabilized cardiomyocyte and can not be attributed to misinterpretation of experimental results.

The main result of this thesis is the finding that both the MOM and cytosolic structures are responsible for diffusion restrictions in cardiomyocytes. The importance and possible mechanisms of the regulation of both are discussed below.

4.1 DIFFUSION RESTRICTIONS AT THE LEVEL OF THE MITOCHONDRIAL OUTER MEMBRANE

Surprisingly, the MOM of cardiomyocytes was shown to have low permeability to ADP and this is caused by the closure of 98% of the VDACs (Fig. 4). The action of VDACs is very important in maintaining appropriate work of mitochondria, helping to keep energetic balance in cells. VDACs are found in the MOM of all eukaryotic species [66], providing transport of molecules, needed for the metabolic function of the cell, between mitochondria and cytoplasm [67]. They play an important role in energy circulation, cell growth [68], proliferation [69] and death [67].

Our data show that only 2% of the VDACs are accessible to ADP in the MOM. The fact that only a minor fraction of VDACs are opened for ADP is of high interest and may be important for future studies, given the crucial role of VDACs in multiple cellular processes. For example, such studies could provide new insights into the regulation of these porines. However, as the percentage of ADP-accessible VDACs was calculated partly on the basis of literature data and for our experimental conditions, it is currently not clear how this number is relevant for different experimental setups. In addition, the exact regulatory mechanism for VDAC action is still under investigation and the conditions at which VDACs are opened or closed are not fully understood.

VDACs are known to be regulated by the binding of tubulin, which regulates their closure [70] or interaction of other intracellular structures, such as sarcoplasmic reticulum (SR) [71, 72]. The role of tubulin in VDACs permeability is supported by the observation that mitochondria in the presence of tubulin have a higher apparent $K_M(\text{ADP})$ [70]. The conductivity of the VDACs depends also on the membrane potential, being higher at potential values below 30 mV and lower at potential values above 30 mV [73]. There are reasons to believe that VDACs permeability can be adjusted by pH changes, when mild alkalization promotes hexokinase binding to VDACs [74].

The conductance of porine channels was shown to depend on temperature, being higher at higher temperatures [75]. These data were taken into account in our model to convert experimental results obtained at room temperature to the phys-

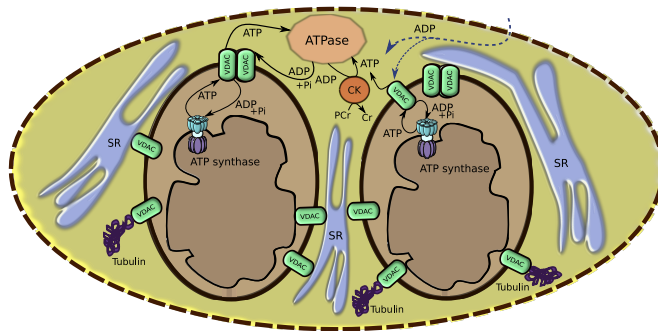


Figure 4 – The accessibility of VDACs on the MOM for ADP in a permeabilized cardiomyocyte. A VDAC may be closed due to the binding of tubulin, interaction with a sarcoplasmic reticulum (SR) or other factors (see 4.1). ADP from the solution enters through the permeabilized sarcolemma. It is either transferred into mitochondria via VDACs on the MOM, where it together with Pi stimulates ATP synthesis by ATP synthase or diffuses to creatine kinase (CK), which converts it to ATP with the involvement of PCr. ATPases hydrolyze ATP to ADP and Pi. It was shown that 98% of the VDACs are not accessible for adenosine phosphate transport in resting rat cardiomyocytes.

iological temperature of 37 °C. It is known that Ca^{2+} levels influence metabolite and ATP transport through the MOM [76]. The maintaining of Ca^{2+} homeostasis is crucial for heart contractions, and VDACs were found to work as Ca^{2+} transporters through the MOM [77]. As we performed our experiments on passive cells and Ca^{2+} levels were kept low, this could explain the small number of active VDACs. It is possible that a higher energy demand of contracting cells would cause more VDACs to open. Besides, VDAC permeability is limited for adenine nucleotides, while Cr and PCr diffusion is not restricted [78]. This may help to organize better crosstalk between ATP producers and consumers through the Cr-PCr shuttle. In Publication II we did not observe any adaptational differences in cardiomyocytes from $\text{GAMT}^{-/-}$ mice compared to WT. Diffusion restrictions were similar in both preparations showing that at moderate workloads cells can preserve their function without active CK.

Transport regulation through the MOM is of particular importance in many physiological processes where mitochondria play a pivotal role. In this sense, it is important to understand the mechanisms regulating the permeability of VDACs. The involvement of VDACs in lots of processes that are crucially important for life makes these mechanisms a very interesting subject for research. The fact that this protein can serve as a target for therapy of numerous diseases has lots of implications. Diffusion restrictions, which are the main study object in the thesis, are lower in ischemic hearts, this is probably due to some damage made to the intracellular structure. Imahashi et al. suggest that during ischemia pro-apoptotic protein Bcl-2

associates with VDACs, and this may be involved in cardioprotection [79]. Preconditioning is known to help to preserve the structures and diffusion barriers that are needed for the healthy functioning of the heart. This cardioprotective function may be connected to VDACs and adenine nucleotide transport regulation. Their possible role is to limit the transport of nucleotides and guard cardiac cells from acidification and reactive oxygen species generation. Therapeutic approaches that help to preserve or restore diffusion restrictions in affected hearts can decrease alterations. In clinical practice it should help to keep the function of the operated organ, minimizing complications and damage to cells.

4.2 ENERGETIC COMPARTMENTS IN CARDIOMYOCYTES

By comparing models in which diffusion restrictions were associated either with only the MOM or with the MOM with cytosolic barriers with the results of the experiments, it was shown that half of the diffusion restrictions were caused by cytosolic barriers. Experimental conditions did not allow us to see the certain areas of the cell where diffusion barriers are situated. According to previous studies, potential cytosolic diffusion barriers can be either functional or structural, and the candidates are discussed below. In 2001, Saks and colleagues described the intracellular energetic units (ICEUs), i.e. compartments that may limit diffusion in the cytoplasm of red muscle cells [80]. These complexes are conceivably organized by mitochondria and ATPases of myofibrils and SR, enabling faster and more efficient exchange of adenine nucleotides between the sites of their production and consumption. It is still under investigation of what structures ICEUs are built. Possible candidates may be t-tubules, intracellular organelles and proteins associated with them. The hypothesis of ICEUs was set as a result of a number of experiments showing that some structural barriers in the cytosol are limiting the diffusion of adenine nucleotides [65, 80] and most of endogenously generated ADP is transferred to nearby mitochondria rather than into the solution [81]. Diffusion restrictions in the cytosol were analyzed by mathematical modeling that predicted their heterogeneous localization in the cell [82]. Mathematical modeling, tested by Ramay and Vendelin, predicted the role of SR and intracellular proteins [31]. Another study in our laboratory revealed that barriers inside cardiomyocyte are distributed $\sim 1 \mu\text{m}$ apart in “lattice-like” structure and, surprisingly, in that environment the diffusion of larger molecules is relatively less restricted than the motility of smaller ones [83]. Theoretically, each of these factors could cause diffusion restrictions in our experimental setup.

However, from the results of Publication II, showing no differences between $\text{GAMT}^{-/-}$ mice and their healthy littermates, we can conclude that the formation

of ICEUs, which channel ADP/ATP between ATPases and mitochondria, provides sufficient energy transfer in the absence of a functional CK system. Thus, a disruption of the CK energy system at low workload does not cause perceptible differences in the heart muscle cells of $GAMT^{-/-}$ deficient mice. This observation may be explained by the close interaction of mitochondria with SR ATPases within ICEUs, forming a diffusion obstacle at this level. The functional and structural evidences of such energetic compartment were provided in recent publications [65, 71].

The possible involvement of SR-mitochondria interaction in the process of diffusion restrictions comes from the fact that cells with a less developed SR-mitochondria network, such as neonatal mammal cardiomyocytes [84] or cardiomyocytes from fish [85], show higher affinity for exogenous adenine nucleotides [22–24]. The finding of the current thesis that cytosolic composition plays an important role in the intracellular molecule transport was further confirmed by recent publications. Namely, it was reported that calcein and fluorescently labeled cyclic adenosine monophosphate (cAMP) molecules showed faster diffusion in neonatal cardiac muscle cells compared to diffusion rates in adult cardiomyocytes [86], which was explained by greater tortuosity and higher order of mitochondria arrangement of the latter. This is in the agreement with the finding that diffusion is restricted more in cells with strictly organized mitochondrial network, like adult mammal cardiomyocytes, while cells with simpler morphology, like neonatal cardiomyocytes and fish cardiac muscle cells, seem to have less restrictions for adenine nucleotides [22–24].

Overall, the work conducted in this thesis showed that a large fraction of diffusion restrictions are located in cytosolic barrier structures. However, it raises questions regarding their composition, location and role, which would have to be addressed in future studies.

CONCLUSIONS

THIS THESIS PROVIDES new insights into the topic of diffusion restrictions in cardiomyocytes, giving perspectives for future research. The main findings and conclusions of the work are summarized below.

- 1) Experimental data together with mathematical modeling show that diffusion of adenosine phosphates is restricted at the single cell level in rat cardiomyocytes.
- 2) Diffusion restrictions reported earlier on populations of cardiomyocytes are not caused by incomplete separation of cells in the measuring chamber or unstirred water layers around the cells.
- 3) Cardiomyocytes isolated from creatine-deficient mice and their unaltered littermates show similar kinetic behaviour and have no changes in mitochondrial organization in relaxed conditions. Cardiomyocytes from the both origins demonstrate the restriction of ADP diffusion from the solution into mitochondria.
- 4) Diffusion restrictions in rat cardiomyocytes are caused by equal contributions of VDACs on the mitochondrial outer membrane and cytosolic structures.
- 5) Only 2% of the VDACs on the mitochondrial outer membrane are available for the adenosine phosphate transport in relaxed cardiomyocytes.

The fact that diffusion restrictions occur in the healthy cardiomyocytes and diminish in pathological conditions makes them a perspective target for therapies of heart diseases.

REFERENCES

REFERENCES

- [1] R. Ventura-Clapier, A. Garnier, and V. Veksler. Energy metabolism in heart failure. *The Journal of Physiology*, 555(Pt 1):1–13, February 2004.
- [2] S. Neubauer. The Failing Heart - An Engine Out of Fuel. *New England Journal of Medicine*, 356(11):1140–1151, March 2007.
- [3] D. L. Mann and M. R. Bristow. Mechanisms and Models in Heart Failure. *Circulation*, 111(21):2837–2849, May 2005.
- [4] P. Ponikowski, S. D. Anker, K. F. AlHabib, M. R. Cowie, T. L. Force, S. Hu, T. Jaarsma, H. Krum, V. Rastogi, L. E. Rohde, U. C. Samal, H. Shimokawa, Budi S., K. Sliwa, and G. Filippatos. Heart failure: preventing disease and death worldwide. *ESC Heart Failure*, 1(1):4–25, September 2014.
- [5] N. Fillmore and G. D. Lopaschuk. Targeting mitochondrial oxidative metabolism as an approach to treat heart failure. *Biochimica et Biophysica Acta (BBA) - Molecular Cell Research*, 1833(4):857–865, April 2013.
- [6] P. A. Bottomley. NMR Spectroscopy of the Human Heart. In *eMagRes*. John Wiley & Sons, Ltd, 2007.
- [7] J. Lagarto, B. T. Dyer, C. Talbot, M. B. Sikkell, N. S. Peters, P. M.W. French, A. R. Lyon, and C. Dunsby. Application of time-resolved autofluorescence to label-free in vivo optical mapping of changes in tissue matrix and metabolism associated with myocardial infarction and heart failure. *Biomedical Optics Express*, 6(2):324–346, January 2015.
- [8] B. Unsold, H. Schotola, C. Jacobshagen, T. Seidler, S. Sossalla, J. Emons, S. Klede, R. Knoll, K. Guan, A. El-Armouche, W. A. Linke, H. Kogler, and G. Hasenfuss. Age-dependent changes in contractile function and passive elastic properties of myocardium from mice lacking muscle LIM protein (MLP). *European Journal of Heart Failure*, 14(4):430–437, April 2012.
- [9] K. Kjeldsen and H. Bundgaard. Myocardial Na,K-ATPase and digoxin therapy in human heart failure. *Annals of the New York Academy of Sciences*, 986:702–707, April 2003.

References

- [10] G. Olivetti, J. M. Capasso, L. G. Meggs, E. H. Sonnenblick, and P. Anversa. Cellular basis of chronic ventricular remodeling after myocardial infarction in rats. *Circulation Research*, 68(3):856–869, March 1991.
- [11] M. N. Sharikabad, J. M. Aronsen, E. Haugen, J. Pedersen, A. S. W. Moller, H. K. Mork, H. C. D. Aass, O. M. Sejersted, I. Sjaastad, and O. Brors. Cardiomyocytes from postinfarction failing rat hearts have improved ischemia tolerance. *American Journal of Physiology - Heart and Circulatory Physiology*, 296(3):H787–H795, March 2009.
- [12] P. Anversa, A. Malhotra, X. Zhang, P. Li, J. Scheuer, and J. M. Capasso. Long-term coronary stenosis in rats: cardiac performance, myocardial morphology, and contractile protein enzyme activity. *The American Journal of Physiology*, 263(1 Pt 2):H117–124, July 1992.
- [13] R. C. Gupta, H. Shimoyama, M. Tanimura, R. Nair, M. Lesch, and H. N. Sabbah. SR Ca(2+)-ATPase activity and expression in ventricular myocardium of dogs with heart failure. *The American Journal of Physiology*, 273(1 Pt 2):H12–18, July 1997.
- [14] J. S. Ingwall. *ATP and the Heart*. Springer US, Boston, MA, 2002.
- [15] S. Neubauer, M. Horn, M. Cramer, K. Harre, J. B. Newell, W. Peters, T. Pabst, G. Ertl, D. Hahn, J. S. Ingwall, and K. Kochsiek. Myocardial phosphocreatine-to-ATP ratio is a predictor of mortality in patients with dilated cardiomyopathy. *Circulation*, 96(7):2190–2196, October 1997.
- [16] R. C. Starling, D. F. Hammer, and R. A. Altschuld. Human myocardial ATP content and in vivo contractile function. *Molecular and Cellular Biochemistry*, 180(1-2):171–177, March 1998.
- [17] M. Beer, T. Seyfarth, J. Sandstede, W. Landschutz, C. Lipke, H. Kostler, M. von Kienlin, K. Harre, D. Hahn, and S. Neubauer. Absolute concentrations of high-energy phosphate metabolites in normal, hypertrophied, and failing human myocardium measured noninvasively with ³¹P-SLOOP magnetic resonance spectroscopy. *Journal of the American College of Cardiology*, 40(7):1267–1274, October 2002.
- [18] V. A. Saks, A. Kuznetsov, Z. A. Khuchua, E. V. Vasilyeva, J. O. Belikova, T. Kesvatera, and T. Tiivel. Control of cellular respiration in vivo by mitochondrial outer membrane and by creatine kinase. A new speculative hypothesis: possible involvement of mitochondrial-cytoskeleton interactions. *Journal of Molecular and Cellular Cardiology*, 27(1):625–645, January 1995.

- [19] M. Vendelin, N. Beraud, K. Guerrero, T. Andrienko, A. Kuznetsov, J. Olivares, L. Kay, and V. A. Saks. Mitochondrial regular arrangement in muscle cells: a "crystal-like" pattern. *American Journal of Physiology. Cell Physiology*, 288(3):C757–767, March 2005.
- [20] R. Birkedal, H. A. Shiels, and M. Vendelin. Three-dimensional mitochondrial arrangement in ventricular myocytes: from chaos to order. *AJP: Cell Physiology*, 291(6):C1148–C1158, December 2006.
- [21] T. Anmann, R. Guzun, N. Beraud, S. Pelloux, A. Kuznetsov, L. Kogerman, T. Kaambre, P. Sikk, K. Paju, N. Peet, E. Seppet, C. Ojeda, Y. Tourneur, and V. Saks. Different kinetics of the regulation of respiration in permeabilized cardiomyocytes and in HL-1 cardiac cells. Importance of cell structure/organization for respiration regulation. *Biochimica Et Biophysica Acta*, 1757(12):1597–1606, December 2006.
- [22] J. A. Hoerter, R. Ventura-Clapier, and A. Kuznetsov. Compartmentation of creatine kinases during perinatal development of mammalian heart. *Molecular and Cellular Biochemistry*, 133-134:277–286, May 1994.
- [23] T. Tiivel, L. Kadaya, A. Kuznetsov, T. Kaambre, N. Peet, P. Sikk, U. Braun, R. Ventura-Clapier, V. Saks, and E. K. Seppet. Developmental changes in regulation of mitochondrial respiration by ADP and creatine in rat heart in vivo. *Molecular and Cellular Biochemistry*, 208(1-2):119–128, May 2000.
- [24] N. Sokolova, M. Vendelin, and R. Birkedal. Intracellular diffusion restrictions in isolated cardiomyocytes from rainbow trout. *BMC Cell Biology*, 10(1):90, 2009.
- [25] H. Walter and D. E. Brooks. Phase separation in cytoplasm, due to macromolecular crowding, is the basis for microcompartmentation. *FEBS letters*, 361(2-3):135–139, March 1995.
- [26] L. Kay, V. A. Saks, and A. Rossi. Early alteration of the control of mitochondrial function in myocardial ischemia. *Journal of Molecular and Cellular Cardiology*, 29(12):3399–3411, December 1997.
- [27] C. E. Murry, R. B. Jennings, and K. A. Reimer. Preconditioning with ischemia: a delay of lethal cell injury in ischemic myocardium. *Circulation*, 74(5):1124–1136, November 1986.
- [28] M. Colombini. VDAC: the channel at the interface between mitochondria and the cytosol. *Molecular and Cellular Biochemistry*, 256-257(1-2):107–115, February 2004.

References

- [29] R. Guzun, M. Gonzalez-Granillo, M. Karu-Varikmaa, A. Grichine, Y. Usson, T. Kaambre, K. Guerrero-Roesch, A. Kuznetsov, U. Schlattner, and V. Saks. Regulation of respiration in muscle cells in vivo by VDAC through interaction with the cytoskeleton and MtCK within Mitochondrial Interactosome. *Biochimica Et Biophysica Acta*, 1818(6):1545–1554, June 2012.
- [30] V. Saks, A. Kuznetsov, T. Andrienko, Y. Usson, F. Appaix, K. Guerrero, T. Kaambre, P. Sikk, M. Lemba, and M. Vendelin. Heterogeneity of ADP Diffusion and Regulation of Respiration in Cardiac Cells. *Biophysical Journal*, 84(5):3436–3456, May 2003.
- [31] H. Ramay and M. Vendelin. Diffusion Restrictions Surrounding Mitochondria: A Mathematical Model of Heart Muscle Fibers. *Biophysical Journal*, 97(2):443–452, July 2009.
- [32] O. Kongas, T. L. Yuen, M. J. Wagner, J. H. G. M. van Beek, and K. Krab. High K_m of oxidative phosphorylation for ADP in skinned muscle fibers: where does it stem from? *AJP: Cell Physiology*, 283(3):C743–C751, September 2002.
- [33] T. Wallimann, M. Wyss, D. Brdiczka, K. Nicolay, and H. M. Eppenberger. Intracellular compartmentation, structure and function of creatine kinase isoenzymes in tissues with high and fluctuating energy demands: the 'phosphocreatine circuit' for cellular energy homeostasis. *Biochemical Journal*, 281(Pt 1):21–40, January 1992.
- [34] U. Schlattner, M. Forstner, M. Eder, O. Stachowiak, K. Fritz-Wolf, and T. Wallimann. Functional aspects of the X-ray structure of mitochondrial creatine kinase: a molecular physiology approach. *Molecular and Cellular Biochemistry*, 184(1-2):125–140, July 1998.
- [35] B. Chance and G. R. Williams. Respiratory enzymes in oxidative phosphorylation. I. Kinetics of oxygen utilization. *The Journal of Biological Chemistry*, 217(1):383–393, November 1955.
- [36] B. Chance and G. R. Williams. Respiratory enzymes in oxidative phosphorylation. III. The steady state. *The Journal of Biological Chemistry*, 217(1):409–427, November 1955.
- [37] B. Chance and G. R. Williams. Respiratory enzymes in oxidative phosphorylation. II. Difference spectra. *The Journal of Biological Chemistry*, 217(1):395–407, November 1955.

- [38] B. Chance and G. R. Williams. Respiratory enzymes in oxidative phosphorylation. IV. The respiratory chain. *The Journal of Biological Chemistry*, 217(1):429–438, November 1955.
- [39] S. Huang, A. A. Heikal, and W. W. Webb. Two-photon fluorescence spectroscopy and microscopy of NAD(P)H and flavoprotein. *Biophysical Journal*, 82(5):2811–2825, May 2002.
- [40] M. F. Galindo, J. Jordan, C. Gonzalez-Garcia, and V. Cena. Reactive oxygen species induce swelling and cytochrome *c* release but not transmembrane depolarization in isolated rat brain mitochondria. *British Journal of Pharmacology*, 139(4):797–804, June 2003.
- [41] Q. Yu and A. A. Heikal. Two-photon autofluorescence dynamics imaging reveals sensitivity of intracellular NADH concentration and conformation to cell physiology at the single-cell level. *Journal of Photochemistry and Photobiology. B, Biology*, 95(1):46–57, April 2009.
- [42] N. Ramanujam, M. F. Mitchell, A. Mahadevan, S. Warren, S. Thomsen, E. Silva, and R. Richards-Kortum. In vivo diagnosis of cervical intraepithelial neoplasia using 337-nm-excited laser-induced fluorescence. *Proceedings of the National Academy of Sciences of the United States of America*, 91(21):10193–10197, October 1994.
- [43] N. D. Kirkpatrick, C. Zou, M. A. Brewer, W. R. Brands, R. A. Drezek, and U. Utzinger. Endogenous fluorescence spectroscopy of cell suspensions for chemopreventive drug monitoring. *Photochemistry and Photobiology*, 81(1):125–134, February 2005.
- [44] S. Palmer, K. Litvinova, E. U. Rafailov, and G. Nabi. Detection of urinary bladder cancer cells using redox ratio and double excitation wavelengths autofluorescence. *Biomedical Optics Express*, 6(3):977, March 2015.
- [45] M. C. Skala, K. M. Ricking, D. K. Bird, A. Gendron-Fitzpatrick, J. Eickhoff, K. W. Eliceiri, P. J. Keely, and N. Ramanujam. In vivo multiphoton fluorescence lifetime imaging of protein-bound and free nicotinamide adenine dinucleotide in normal and precancerous epithelia. *Journal of Biomedical Optics*, 12(2):024014, April 2007.
- [46] J. H. Ostrander, C. M. McMahon, S. Lem, S. R. Millon, J. Q. Brown, V. L. Seewaldt, and N. Ramanujam. Optical Redox Ratio Differentiates Breast Cancer Cell Lines Based on Estrogen Receptor Status. *Cancer Research*, 70(11):4759–4766, June 2010.

References

- [47] A. T. Shah, K. E. Diggins, A. J. Walsh, J. M. Irish, and M. C. Skala. In Vivo Autofluorescence Imaging of Tumor Heterogeneity in Response to Treatment. *Neoplasia*, 17(12):862–870, December 2015.
- [48] D. Schaeue, J. A. Ratikan, and K. S. Iwamoto. Cellular Autofluorescence following Ionizing Radiation. *PLoS ONE*, 7(2):e32062, February 2012.
- [49] G. Papayan, N. Petrishchev, and M. Galagudza. Autofluorescence spectroscopy for NADH and flavoproteins redox state monitoring in the isolated rat heart subjected to ischemia-reperfusion. *Photodiagnosis and Photodynamic Therapy*, 11(3):400–408, September 2014.
- [50] R. C. I. Wust, M. Helmes, and G. J. M. Stienen. NADH and FAD kinetics reveal altered mitochondrial function in right ventricular heart failure. *European Heart Journal*, 34(suppl 1):P4199–P4199, August 2013.
- [51] H. Asfour, A. M. Wengrowski, R. Jaimes, Luther M. Swift, and Matthew W. Kay. NADH Fluorescence Imaging of Isolated Biventricular Working Rabbit Hearts. *Journal of Visualized Experiments*, (65), July 2012.
- [52] F. Sedlic, D. Pravdic, N. Hirata, Y. Mio, A. Sepac, A. K. Camara, T. Wakatsuki, Z. J. Bosnjak, and M. Bienengraeber. Monitoring mitochondrial electron fluxes using NAD(P)H-flavoprotein fluorometry reveals complex action of isoflurane on cardiomyocytes. *Biochimica Et Biophysica Acta*, 1797(10):1749–1758, October 2010.
- [53] M. C. Skala, K. M. Riching, A. Gendron-Fitzpatrick, J. Eickhoff, K. W. Eliceiri, J. G. White, and N. Ramanujam. In vivo multiphoton microscopy of NADH and FAD redox states, fluorescence lifetimes, and cellular morphology in precancerous epithelia. *Proceedings of the National Academy of Sciences*, 104(49):19494–19499, December 2007.
- [54] M. Matsubara, M. Ranji, B. G. Leshnowar, M. Noma, S. J. Ratcliffe, B. Chance, R. C. Gorman, and J. H. Gorman. In Vivo Fluorometric Assessment of Cyclosporine on Mitochondrial Function During Myocardial Ischemia and Reperfusion. *The Annals of Thoracic Surgery*, 89(5):1532–1537, May 2010.
- [55] P. Kosterin, G. H. Kim, M. Muschol, A. L. Obaid, and B. M. Salzberg. Changes in FAD and NADH fluorescence in neurosecretory terminals are triggered by calcium entry and by ADP production. *The Journal of Membrane Biology*, 208(2):113–124, November 2005.

- [56] W. S. Kunz and W. Kunz. Contribution of different enzymes to flavoprotein fluorescence of isolated rat liver mitochondria. *Biochimica Et Biophysica Acta*, 841(3):237–246, September 1985.
- [57] W. S. Kunz. Spectral properties of fluorescent flavoproteins of isolated rat liver mitochondria. *FEBS letters*, 195(1-2):92–96, January 1986.
- [58] A. K. Lam, P. N. Silva, S. M. Altamentova, and J. V. Rocheleau. Quantitative imaging of electron transfer flavoprotein autofluorescence reveals the dynamics of lipid partitioning in living pancreatic islets. *Integrative Biology*, 4(8):838, 2012.
- [59] T. R. Husson and N. P. Issa. Functional Imaging with Mitochondrial Flavoprotein Autofluorescence: Theory, Practice, and Applications. In Ron D. Frostig, editor, *In Vivo Optical Imaging of Brain Function*, Frontiers in Neuroscience. CRC Press/Taylor & Francis, Boca Raton (FL), 2nd edition, 2009.
- [60] J. V. Rocheleau, W. S. Head, and D. W. Piston. Quantitative NAD(P)H/Flavoprotein Autofluorescence Imaging Reveals Metabolic Mechanisms of Pancreatic Islet Pyruvate Response. *Journal of Biological Chemistry*, 279(30):31780–31787, July 2004.
- [61] L. Kummel. Ca, Mg-ATPase activity of permeabilised rat heart cells and its functional coupling to oxidative phosphorylation of the cells. *Cardiovascular Research*, 22(5):359–367, May 1988.
- [62] A. Kuznetsov, V. Veksler, F. N. Gellerich, V. Saks, R. Margreiter, and W. S. Kunz. Analysis of mitochondrial function in situ in permeabilized muscle fibers, tissues and cells. *Nature Protocols*, 3(6):965–976, 2008.
- [63] B. Chance and G. R. Williams. The respiratory chain and oxidative phosphorylation. *Advances in Enzymology and Related Subjects of Biochemistry*, 17:65–134, 1956.
- [64] M. Sepp, M. Vendelin, H. Vija, and R. Birkedal. ADP Compartmentation Analysis Reveals Coupling between Pyruvate Kinase and ATPases in Heart Muscle. *Biophysical Journal*, 98(12):2785–2793, June 2010.
- [65] A. Kaasik, V. Veksler, E. Boehm, M. Novotova, A. Minajeva, and R. Ventura-Clapier. Energetic crosstalk between organelles: architectural integration of energy production and utilization. *Circulation Research*, 89(2):153–159, July 2001.

References

- [66] R. Benz. Permeation of hydrophilic solutes through mitochondrial outer membranes: review on mitochondrial porins. *Biochimica Et Biophysica Acta*, 1197(2):167–196, June 1994.
- [67] V. Shoshan-Barmatz, V. De Pinto, M. Zweckstetter, Z. Raviv, N. Keinan, and N. Arbel. VDAC, a multi-functional mitochondrial protein regulating cell life and death. *Molecular Aspects of Medicine*, 31(3):227–285, June 2010.
- [68] S. Abu-Hamad, S. Sivan, and V. Shoshan-Barmatz. The expression level of the voltage-dependent anion channel controls life and death of the cell. *Proceedings of the National Academy of Sciences*, 103(15):5787–5792, April 2006.
- [69] S. P. Mathupala, Y. H. Ko, and P. L. Pedersen. The pivotal roles of mitochondria in cancer: Warburg and beyond and encouraging prospects for effective therapies. *Biochimica Et Biophysica Acta*, 1797(6-7):1225–1230, July 2010.
- [70] T. K. Rostovtseva, K. L. Sheldon, E. Hassanzadeh, C. Monge, V. Saks, S. M. Bezrukov, and D. L. Sackett. Tubulin binding blocks mitochondrial voltage-dependent anion channel and regulates respiration. *Proceedings of the National Academy of Sciences of the United States of America*, 105(48):18746–18751, December 2008.
- [71] C. Franzini-Armstrong. ER-mitochondria communication. How privileged? *Physiology (Bethesda, Md.)*, 22:261–268, August 2007.
- [72] R. Birkedal, M. Laasmaa, and M. Vendelin. The location of energetic compartments affects energetic communication in cardiomyocytes. *Frontiers in Physiology*, 5, September 2014.
- [73] A. G. Komarov, D. Deng, W. J. Craigen, and M. Colombini. New Insights into the Mechanism of Permeation through Large Channels. *Biophysical Journal*, 89(6):3950–3959, December 2005.
- [74] C. H. T. Quach, K. H. Jung, J. H. Lee, J. W. Park, S. H. Moon, Y. S. Cho, Y. S. Choe, and K. H. Lee. Mild Alkalinization Acutely Triggers the Warburg Effect by Enhancing Hexokinase Activity via Voltage-Dependent Anion Channel Binding. *PLOS ONE*, 11(8):e0159529, August 2016.
- [75] I. Biro, S. Pezeshki, H. Weingart, M. Winterhalter, and U. Kleinekathofer. Comparing the Temperature-Dependent Conductance of the Two Structurally Similar *E. coli* Porins OmpC and OmpF. *Biophysical Journal*, 98(9):1830–1839, May 2010.

- [76] G. Bathori, G. Csordas, C. Garcia-Perez, E. Davies, and G. Hajnoczky. Ca²⁺-dependent control of the permeability properties of the mitochondrial outer membrane and voltage-dependent anion-selective channel (VDAC). *The Journal of Biological Chemistry*, 281(25):17347–17358, June 2006.
- [77] H. Shimizu, J. Schredelseker, J. Huang, K. Lu, S. Naghdi, F. Lu, S. Franklin, H. D. G. Fiji, K. Wang, H. Zhu, C. Tian, B. Lin, H. Nakano, A. Ehrlich, J. Nakai, A. Z. Stieg, J. K. Gimzewski, A. Nakano, J. I. Goldhaber, T. M. Vondriska, G. Hajnoczky, O. Kwon, and J. N. Chen. Mitochondrial Ca²⁺ uptake by the voltage-dependent anion channel 2 regulates cardiac rhythmicity. *eLife*, 4, January 2015.
- [78] R. Guzun, N. Timohhina, K. Tepp, C. Monge, T. Kaambre, P. Sikk, A. Kuznetsov, C. Pison, and V. Saks. Regulation of respiration controlled by mitochondrial creatine kinase in permeabilized cardiac cells in situ. *Biochimica et Biophysica Acta (BBA) - Bioenergetics*, 1787(9):1089–1105, September 2009.
- [79] K. Imahashi, M. D. Schneider, C. Steenbergen, and E. Murphy. Transgenic expression of Bcl-2 modulates energy metabolism, prevents cytosolic acidification during ischemia, and reduces ischemia/reperfusion injury. *Circulation Research*, 95(7):734–741, October 2004.
- [80] V. A. Saks, T. Kaambre, P. Sikk, M. Eimre, E. Orlova, K. Paju, A. Piirsoo, F. Appaix, L. Kay, V. Regitz-Zagrosek, E. Fleck, and E. Seppet. Intracellular energetic units in red muscle cells. *The Biochemical Journal*, 356(Pt 2):643–657, June 2001.
- [81] E. Seppet, T. Kaambre, P. Sikk, T. Tiivel, H. Vija, M. Tonkonogi, K. Sahlin, L. Kay, F. Appaix, U. Braun, M. Eimre, and V. Saks. Functional complexes of mitochondria with Ca,MgATPases of myofibrils and sarcoplasmic reticulum in muscle cells. *Biochimica Et Biophysica Acta*, 1504(2-3):379–395, April 2001.
- [82] M. Vendelin, M. Eimre, E. Seppet, N. Peet, T. Andrienko, M. Lemba, J. Engelbrecht, Enn K. Seppet, and V. A. Saks. Intracellular diffusion of adenosine phosphates is locally restricted in cardiac muscle. *Molecular and Cellular Biochemistry*, 256-257(1-2):229–241, February 2004.
- [83] A. Illaste, M. Laasmaa, P. Peterson, and M. Vendelin. Analysis of Molecular Movement Reveals Latticelike Obstructions to Diffusion in Heart Muscle Cells. *Biophysical Journal*, 102(4):739–748, February 2012.

References

- [84] V. Eisner, G. Csordas, and G. Hajnoczky. Interactions between sarco-endoplasmic reticulum and mitochondria in cardiac and skeletal muscle - pivotal roles in Ca²⁺ and reactive oxygen species signaling. *Journal of Cell Science*, 126(14):2965–2978, July 2013.
- [85] R. M. Santer. Morphology and innervation of the fish heart. *Advances in Anatomy, Embryology, and Cell Biology*, 89:1–102, 1985.
- [86] M. Richards, O. Lomas, K. Jalink, K. L. Ford, R. D. Vaughan-Jones, K. Lefkimmiatis, and P. Swietach. Intracellular tortuosity underlies slow cAMP diffusion in adult ventricular myocytes. *Cardiovascular Research*, 110(3):395–407, 2016.

CURRICULUM VITAE

Curriculum Vitae

NATALJA JEPIHHINA

PERSONAL INFORMATION

Date of birth April 11, 1984
E-mail natalja@sysbio.ioc.ee

EDUCATION

2009 – 2017 Tallinn University of Technology (TUT)

Subject **PhD, Gene Technology**

Thesis Heterogeneity of diffusion restrictions in cardiomyocytes

Supervisor Dr. Marko Vendelin, *markov@sysbio.ioc.ee*
Head of Laboratory of Systems Biology, Department of Cybernetics, School of Science, TUT

2007 – 2009 Tallinn University of Technology

Subject **MSc, Gene Technology, cum laude**

Thesis Construction and characterization of recombinant luminescent bacterial sensors for evaluation of compounds causing oxidative stress

Supervisors Dr. Angela Ivask, *angela.ivask@kbfi.ee*
Senior Researcher of Laboratory of Environmental Toxicology at National Institute of Chemical Physics and Biophysics
Dr. Katrin Tomson, *katrin.tomson@ttu.ee*
Researcher of Department of Chemistry and Biotechnology, School of Science, TUT

2003 – 2007 University of Tartu (UT)

Subject **BSc, Gene Technology**

Thesis Study of *Erwinia carotovora* subsp. *carotovora* strain SC3193 *nip* gene regulation

Supervisor Kadri Tomasson, *tomasson@ut.ee*
PhD student of Institute of Molecular and Cell Biology at UT

RESEARCH EXPERIENCE

2009 – Department of Cybernetics at TUT

Laboratory of Systems Biology
PhD student

2007 – 2009 National Institute of Chemical Physics and Biophysics

Laboratory of Environmental Toxicology
MSc student

2003 – 2007 Institute of Molecular and Cell Biology at UT

BSc student

Curriculum Vitae

SPECIAL COURSES

- 2012** Federation of Laboratory Animal Science Associations (FELASA): C-category competence certificate

TEACHING

- 2011** Organization of practical course in Genetics of Bacteria
2009 – 2015 Seminars in bioenergetics and confocal microscopy for PhD students

SCHOLARSHIPS AND AWARDS

- 2010** Tallinn University of Technology Students research II prize
2009 Estonian Academy of Sciences Students research II prize

PUBLICATIONS

1. Simson P, **Jepihhina N**, Laasmaa, Peterson P, Birkedal R, and Vendelin M; **Restricted ADP movement in cardiomyocytes: Cytosolic diffusion obstacles are complemented with a small number of open mitochondrial voltage-dependent anion channels**, *Journal of Molecular and Cellular Cardiology*, 97, 197–203, 2016
2. Branovets J, Sepp M, Kotlyarova S, **Jepihhina N**, Sokolova N, Aksentijevic D, Lygate CA, Neubauer S, Vendelin M, Birkedal R; **Unchanged mitochondrial organization and compartmentation of high-energy phosphates in creatine-deficient GAMT^{-/-} mouse hearts**, *AJP-Heart and Circulatory Physiology*, 305(4), 506–520, 2013
3. **Jepihhina N**, Beraud N, Sepp M, Birkedal R, Vendelin M; **Permeabilized rat cardiomyocyte response demonstrates intracellular origin of diffusion obstacles**, *Biophysical Journal*, 101, 2112–2121, 2011
4. Ivask A, Bondarenko O, **Jepihhina, N**, Kahru A; **Profiling of the reactive oxygen species related ecotoxicity of CuO, ZnO, TiO₂, silver and fullerene nanoparticles using a set of recombinant luminescent *Escherichia coli* strains: differentiating the impact of particles and solubilised metals** *Analytical and Bioanalytical Chemistry*, 398:701–716, 2010

INTERNATIONAL CONFERENCE PRESENTATIONS

- 2015** **The Joint Meeting of the Federation of European Physiological Societies and the Baltic Physiological Societies (FEPS2015)**, Kaunas, Lithuania
Poster Jepihhina N, Simson P, Laasmaa M, Birkedal R, Vendelin M
The characterization of diffusion obstacles in rat cardiomyocytes
- 2015** **Biophysical Society 59th Annual Meeting**, Baltimore, Maryland, USA
Poster Jepihhina N, Simson P, Laasmaa M, Peterson P, Birkedal R, Vendelin M
The characterization of diffusion obstacles in rat cardiomyocytes
- 2012** **Biophysical Society 56th Annual Meeting**, San Diego, California, USA
Poster Jepihhina N, Beraud, N, Sepp, M, Birkedal, R, Vendelin M
Permeabilized Rat Cardiomyocyte Response Demonstrates Intracellular Origin of Diffusion Obstacles

EXTRAS

Languages Russian (mother tongue), Estonian (fluent), English (fluent)

Elulookirjeldus
NATALJA JEPHIHINA

ÜLDINFO

Sünniaeg 11. aprill, 1984
E-mail natalja@sysbio.ioc.ee

HARIDUS

2009 – 2016 Tallinna Tehnikaülikool (TTÜ)

Eriala **PhD, geenitehnoloogia**

Teema Difusioonitakistuste heterogeensus südamelihaskudedes

Juhendaja Dr. Marko Vendelin, *markov@sysbio.ioc.ee*
Süsteemibioloogia laboratooriumi juhataja, Süsteemibioloogia laboratoorium,
Küberneetika instituut, TTÜ

2007 – 2009 Tallinna Tehnikaülikool

Eriala **MSc, geenitehnoloogia, cum laude**

Teema Rekombinantsete luminesseeruvate sensorbakterite konstrueerimine ja
iseloomustamine ainete oksüdatiivse stressi potentsiaali hindamiseks

Juhendajad Dr. Angela Ivask, *angela.ivask@kbfi.ee*
Keskkonnatoksikoloogia laboratooriumi vanemteadur, Keemilise ja Bioloogilise Füüsika
Instituut

Dr. Katrin Tomson, *katrin.tomson@ttu.ee*
Teadur, Loodusteaduskonna Keemia ja biotehnoloogia instituut, TTÜ

2004 – 2007 Tartu Ülikool (TÜ)

Eriala **BSc, geenitehnoloogia**

Teema *Erwinia carotovora* alamli. *carotovora* SCC3193 *nip* geeni regulatsiooni uurimine

Juhendaja Kadri Tomasson, *tomasson@ut.ee*
Doktorant, Molekulaar- ja Rakubioloogia Instituut, TÜ

TEADUSTÖÖ KOGEMUS

2009 – TTÜ Küberneetika Instituut
Süsteemibioloogia laboratoorium
doktorant

2007 – 2009 Keemilise ja Bioloogilise Füüsika Instituut
Keskkonnatoksikoloogia laboratoorium
magistrant

2003 – 2007 TÜ Molekulaar- ja Rakubioloogia Instituut
bakalaureus

Elulookirjeldus

ÕPETUSTEGEVUS

- 2011** Bakterigenetika kursuse praktikumide läbiviimine
2009 – 2015 Bionergeetika, biofüüsika ja konfokaalmikroskoopia seminarid doktorantidele

TÄIENDÕPE

- 2012** Katseloomateaduse kursus (Federation of Laboratory Animal Science Associations): C-katekoria kompetents

STIPENDIUMID JA AUTASUD

- 2010** Tallinna Tehnikaülikooli üliõpilastööde II auhind
2009 Eesti Teaduste Akadeemia üliõpilastööde II auhind

PUBLIKATSIOONID

1. Simson P, **Jepihhina N**, Laasmaa, Peterson P, Birkedal R, and Vendelin M; **Restricted ADP movement in cardiomyocytes: Cytosolic diffusion obstacles are complemented with a small number of open mitochondrial voltage-dependent anion channels**, *Journal of Molecular and Cellular Cardiology*, 97, 197–203, 2016
2. Branovets J, Sepp M, Kotlyarova S, **Jepihhina N**, Sokolova N, Aksentijevic D, Lygate CA, Neubauer S, Vendelin M, Birkedal R; **Unchanged mitochondrial organization and compartmentation of high-energy phosphates in creatine-deficient GAMT^{-/-} mouse hearts**, *AJP-Heart and Circulatory Physiology*, 305(4), 506–520, 2013
3. **Jepihhina N**, Beraud N, Sepp M, Birkedal R, Vendelin M; **Permeabilized rat cardiomyocyte response demonstrates intracellular origin of diffusion obstacles**, *Biophysical Journal*, 101, 2112–2121, 2011
4. Ivask A, Bondarenko O, **Jepihhina, N**, Kahru A; **Profiling of the reactive oxygen species related ecotoxicity of CuO, ZnO, TiO₂, silver and fullerene nanoparticles using a set of recombinant luminescent *Escherichia coli* strains: differentiating the impact of particles and solubilised metals** *Analytical and Bioanalytical Chemistry*, 398:701–716, 2010

VALITUD ETTEKANDED RAHVUSVAHELISTELT KONVERENTSIDELT

- 2015** **The Joint Meeting of the Federation of European Physiological Societies and the Baltic Physiological Societies (FEPS2015)**, Kaunas, Lithuania
Poster Jepihhina N, Simson P, Laasmaa M, Birkedal R, Vendelin M
The characterization of diffusion obstacles in rat cardiomyocytes
- 2015** **Biophysical Society 59th Annual Meeting**, Baltimore, Maryland, USA
Poster Jepihhina N, Simson P, Laasmaa M, Peterson P, Birkedal R, Vendelin M
The characterization of diffusion obstacles in rat cardiomyocytes
- 2012** **Biophysical Society 56th Annual Meeting**, San Diego, California, USA
Poster Jepihhina N, Beraud, N, Sepp, M, Birkedal, R, Vendelin M
Permeabilized Rat Cardiomyocyte Response Demonstrates Intracellular Origin of Diffusion Obstacles

LISAD

Keeled Vene (emakeel), eesti (kõrgtase), inglise (kõrgtase)

APPENDIX

PUBLICATION I

Jepihhina N, Beraud N, Sepp M, Birkedal R, Vendelin M;
Permeabilized rat cardiomyocyte response demonstrates intracellular origin
of diffusion obstacles
Biophysical Journal, 101, 2112–2121, 2011

Permeabilized Rat Cardiomyocyte Response Demonstrates Intracellular Origin of Diffusion Obstacles

Natalja Jepihhina, Nathalie Beraud, Mervi Sepp, Rikke Birkedal, and Marko Vendelin*

Laboratory of Systems Biology, Institute of Cybernetics, Tallinn University of Technology, Tallinn, Estonia

ABSTRACT Intracellular diffusion restrictions for ADP and other molecules have been predicted earlier based on experiments on permeabilized fibers or cardiomyocytes. However, it is possible that the effective diffusion distance is larger than the cell dimensions due to clumping of cells and incomplete separation of cells in fiber preparations. The aim of this work was to check whether diffusion restrictions exist inside rat cardiomyocytes or are caused by large effective diffusion distance. For that, we determined the response of oxidative phosphorylation (OxPhos) to exogenous ADP and ATP stimulation in permeabilized rat cardiomyocytes using fluorescence microscopy. The state of OxPhos was monitored via NADH and flavoprotein autofluorescence. By varying the ADP or ATP concentration in flow chamber, we determined that OxPhos has a low affinity in cardiomyocytes. The experiments were repeated in a fluorometer on cardiomyocyte suspensions leading to similar autofluorescence changes induced by ADP as recorded under the microscope. ATP stimulated OxPhos more in a fluorometer than under the microscope, which was attributed to accumulation of ADP in fluorometer chamber. By calculating the flow profile around the cell in the microscope chamber and comparing model solutions to measured data, we demonstrate that intracellular structures impose significant diffusion obstacles in rat cardiomyocytes.

INTRODUCTION

When mitochondrial oxygen consumption is stimulated by exogenous ADP, mitochondria in situ in permeabilized fibers and cells from cardiac muscle have an affinity that is much lower than that of isolated mitochondria (1–3). The cause of this is still uncertain. Usually, the low affinity is attributed to intracellular diffusion restrictions that limit diffusion between the solution surrounding the cell and the mitochondrial inner membrane. As possible diffusion obstacles, limitation of permeability of voltage-dependent anion channel in mitochondrial outer membrane by tubulin (4) and intracellular structures such as sarcoplasmic reticulum and proteins associated with them (3,5–7) have been proposed. From two- and three-dimensional analysis of mitochondrial arrangement, it is clear that rat cardiomyocytes have a very high degree of order (8,9). In such ordered environment, intracellular diffusion obstacles associated with sarcoplasmic reticulum can be responsible for anisotropy in diffusion that was shown by extended raster image correlation spectroscopy (6).

As an alternative explanation, Kongas et al. (10) proposed that low affinity to ADP in permeabilized fibers and cells can be attributed to long diffusion pathways in the experiments: unstirred layers surrounding the cells and fibers may provide a significant restriction of ADP-diffusion rela-

tive to metabolism; fibers and cells in the oxygraph may form clumps, where outer cells restrict diffusion to the inner cells. Although analysis of the data in light of intracellular diffusion restrictions has been commonly used, the alternative explanation of the data by long diffusion distances in the experimental setup has not been tested. Our recent data from rainbow trout approached the long diffusion distance hypothesis (unstirred layers and clumping of cells). The data argued against diffusion restriction by unstirred layers (11). However, they did suggest that trout cardiac fibers were not completely separated and/or were clumping during oxygraph experiments, because the affinity (quantified by apparent K_M for exogenous ADP) of fibers was much lower (apparent K_M higher) than that of isolated cardiomyocytes (11). Note that apparent K_M for ADP was still larger in trout cardiomyocytes than in isolated mitochondria, indicating the existence of intracellular diffusion restrictions in trout cells.

The difference in the affinity of permeabilized trout cells and fibers is opposite to what has been reported for rat heart preparations, where the apparent K_M of permeabilized fibers is similar to that of cardiomyocytes (12). We have never observed cell aggregation in the oxygraph during experiments on rat cardiomyocytes, or under the microscope after experiments. However, it cannot be ruled out that temporary microscopic cell aggregates are formed, so that the diffusion distance from the medium to the mitochondria inside the cells is effectively much larger than the radius of a single cardiomyocyte (10). As a result, formation of aggregates in isolated cardiomyocyte preparation in solution cannot be ruled out based on observation of similar affinities to ADP of permeabilized rat cardiomyocytes and fibers.

Submitted June 15, 2011, and accepted for publication September 20, 2011.

*Correspondence: markov@ioc.ee

This is an Open Access article distributed under the terms of the Creative Commons-Attribution Noncommercial License (<http://creativecommons.org/licenses/by-nc/2.0/>), which permits unrestricted noncommercial use, distribution, and reproduction in any medium, provided the original work is properly cited.

Editor: Michael D. Stern.

© 2011 by the Biophysical Society
0006-3495/11/11/2112/10 \$2.00

doi: 10.1016/j.bpj.2011.09.025

This study was designed to check whether permeabilized rat cardiomyocytes exhibit low affinity to exogenous ADP at single cell level. We took advantage of the fact that changes in the autofluorescence of reduced nicotinamide adenine dinucleotide (NADH) and oxidized flavoproteins (FPs) reflect the redox state of the cell (13,14). NADH and FP autofluorescence has been used extensively to characterize the state of respiratory chain: for example, response of isolated mitochondria (13,15) or permeabilized fibers (16,17) to ADP stimulation; response of isolated cardiomyocytes to drugs (18,19); or monitoring mitochondrial function in vivo (20).

NADH autofluorescence is mainly of mitochondrial origin (21,22). FP autofluorescence comes from three groups of flavoproteins: α -lipoamide dehydrogenase, electron transfer flavoprotein, and a third group, which is likely to be acyl-CoA dehydrogenases (23–25). α -Lipoamide dehydrogenase is the catalytic subunit of pyruvate dehydrogenase, α -ketoglutarate dehydrogenase in the citric acid cycle, and the branched chain α -keto acid dehydrogenase complex involved in amino-acid metabolism. As NADH is a cofactor for these dehydrogenases, the redox state of the flavin moiety of α -lipoamide dehydrogenase is in equilibrium with that of mitochondrial NAD^+/NADH .

In this study, we recorded the autofluorescence of NADH and FP from single, permeabilized rat cardiomyocytes perfused with solution containing increasing concentrations of ADP and ATP. For comparison, the same experiment was performed on populations of permeabilized cardiomyocytes in a spectrofluorometer to mimic respiration kinetics experiments that have shown low affinity of mitochondrial respiration to exogenous ADP. From the analysis of the measured data by mathematical models, we demonstrate that the low affinity of mitochondrial respiration to exogenous ADP comes, in part, from intracellular diffusion obstacles in rat heart muscle cells.

MATERIALS AND METHODS

Adult outbred Wistar rats of both sexes weighing 300–500 g were used in the experiments. Animal procedures were approved by the Estonian National Committee for Ethics in Animal Experimentation (Estonian Ministry of Agriculture).

Before the experiments, animals were anesthetized with 0.5 mg/kg ketamine (Bioketan, Vetoquinol Biowet, Gorzów Wielkopolski, Poland) and 125 mg/kg dexmedetomidine (Dexdomitor; Orion, Espoo, Finland).

Isolation of cardiomyocytes

Calcium-tolerant cardiomyocytes were isolated as described in Sepp et al. (3). During isolation of cardiomyocytes, we used solutions from Sepp et al. (3) with slight modifications. Solutions are listed in the Supporting Material.

Fluorescence microscopy

Microscope experiments were performed on an inverted Nikon Eclipse Ti-U microscope (Nikon, Tokyo, Japan), described in the Supporting Mate-

rial. Immediately before each experiment, a new batch of cells were permeabilized for 5 min with gentle mixing in an Eppendorf tube with Mitomed solution (see the Supporting Material) containing 25 $\mu\text{g}/\text{mL}$ saponin and 50 μM ADP. A fraction of the permeabilized cells was put into a diamond-shaped fast-exchange chamber (15×6 mm, RC-24N; Warner Instruments, Harvard Apparatus, March-Hugstetten, Germany) on the microscope. They were allowed to sediment for 5–10 min before starting the superfusion with Mitomed solution containing different concentrations of ADP. Only those cells located in the middle of the chamber were used for measurements. According to the manufacturer, the geometry of the chamber provided laminar flow of solutions during experiments at the used flow rate of ~ 0.5 mL/min. The ADP concentration was increased stepwise from 50 to 100, 300, 500, 1000, and 2000 μM and the cells were superfused for at least 4.5 min at each step. The same experiment was done with ATP instead of ADP.

Spectrofluorometer recordings

Autofluorescence measurements on population level were performed in 4 mL plastic cuvettes (four-faced transparent cuvettes; Deltalab, Rubí, Spain) on a spectrofluorophotometer (Shimadzu RF-5301; Shimadzu Scientific Instruments, Kyoto, Japan). Autofluorescence spectra of flavoproteins and NADH were recorded using excitation and emission wavelengths similar to those used for microscope single cell studies: for NADH excitation was 340 nm, emission range 400–550 nm; for flavoproteins, excitation was 465 nm, emission range 500–600 nm. All spectra were taken three times to make sure that steady state was reached. The cell suspension was continuously stirred with magnetic stirrer bars (VWR, Wien, Austria) and before each measurement resuspended with a pipette to provide an homogeneous mixture. Autofluorescence of permeabilized cardiomyocytes was first recorded in substrate-free Mitomed solution in presence of 50 μM ADP or ATP, then substrates were added and cells were exposed to increasing concentrations of ADP or ATP, respectively. At the end of each titration, oligomycin and sodium cyanide were added to obtain the signal under fully reduced conditions. Spectra of cell suspension autofluorescence in substrate-free solution and in presence of oligomycin and cyanide were then used to normalize data of titration, as described below.

Analysis of fluorescence signal

Detailed description of analysis of fluorescence signal is given in the Supporting Material.

Statistics

The raw data were analyzed using homemade software. All results are shown as mean \pm SD.

Mathematical models

The experimental data were analyzed by several mathematical models. Description of the models is given in the Supporting Material.

RESULTS

Experimental results

The response of the permeabilized rat cardiomyocytes to changes in the surrounding solution was followed in fluorescence microscope. Two fluorescence signals were recorded from the same cell with the recorded signals corresponding to NADH and flavoproteins (FPs) fluorescence. In the

beginning of the experiment, the cells were permeabilized by saponin. After that, the solution in the imaging chamber was varied and the fluorescence of cells was observed. Representative fluorescence images of the cells are shown on Fig. 1. Note how increase of exogenous ADP leads to reduction in NADH fluorescence and increase of FP fluorescence.

To get the extremes in the levels of fluorescence, we subjected the cells to solutions that inhibit oxidative phosphorylation (solution containing oligomycin and cyanide, OL+CN) or an uncoupled mitochondrial respiratory chain by using the solution containing FCCP (Fig. 1). As it is demonstrated in Fig. 1, NADH fluorescence of nonrod-shaped cardiomyocytes was quite small (*right bottom corner* of images). The same was not true for FP fluorescence, with relatively high FP fluorescence observed in nonrod-shaped cardiomyocytes. Such level of autofluorescence in nonrod-shaped cells is consistent with earlier reports (21). For these cells, FP fluorescence either stayed relatively constant through the whole experiment or changed with the variation of ADP or ATP in solution similar to rod-shaped cardiomyocytes (results not shown).

We quantified the response of the cells to different solutions by calculating the average fluorescence of a cell and using the fluorescence levels recorded in presence of OL+CN and FCCP to normalize the data (see the [Supporting Material](#)). Representative traces with average fluorescence changes in a single cell during an experiment are shown in Fig. 2. As shown in Fig. 2, stimulation of respiration by exogenous ADP leads to a larger range of fluorescence changes in the cell than stimulation by exogenous ATP. When adding exogenous ATP, respiration is stimulated due to the hydrolysis of ATP by endogenous ATPases. Note that there is always a significant delay between the time-

moment at which the new solution started to enter the microscope imaging chamber (*dashed vertical lines* in Fig. 2) and the response of the cell. However, after a few images, the fluorescence of the cell is stable until the next change of solution.

To compare the single cell response to the response of a cell population, the experiments were repeated in a fluorometer. Rat cardiomyocyte suspension was added to the fluorometer cuvette and after permeabilization, increasing amounts of ADP or ATP was added. Fluorescence spectra were recorded to determine the level of NADH and FP fluorescence. As explained in the [Supporting Material](#), we had to avoid use of FCCP in the experiments in the fluorometer due to significant absorbance. For normalization of the fluorescence signal, the fluorescence of permeabilized cells was recorded before addition of substrates (but in the presence of low ADP or ATP). Sample spectra are shown in Fig. S1 in the [Supporting Material](#).

A comparison of fluorescence levels recorded in a microscope ($n = 8-13$) and a fluorometer ($n = 6$) are shown in Fig. 3. As it is evident from Fig. 3, A and C, NADH and FP fluorescence changes similarly on single cell and population level when exogenous ADP is varied. When respiration is stimulated by ATP, the autofluorescence response is larger in the fluorometer than in the microscope (Fig. 3, B and D). This difference is induced by the differences in response at lower ATP concentrations. At higher ATP concentrations, NADH and FP fluorescence measured in a fluorometer does not change significantly (compare fluorescence at ATP concentrations of 1 mM and 2 mM, Fig. 3, B and D). This saturation effect has not been observed in the single cell measurements. The difference in recorded fluorescence response to changes in ADP and ATP are demonstrated in Fig. 3, E and F. Note how the curve corresponding to NADH fluorescence response to exogenous ATP stimulation is shifted to the right from the curve corresponding to exogenous ADP stimulation. For FP, the corresponding shift is to the left.

Because fluorometer measurements were performed on populations of cardiomyocytes, we could relate changes in NADH and FP fluorescence to changes in respiration rate (VO_2). For that, VO_2 measured on populations of rat cardiomyocytes under similar conditions were used (data taken from Sepp et al. (3)). The relationship between fluorescence and VO_2 is shown in Fig. 4. Because VO_2 was not measured at all ADP and ATP concentrations used in this study, we had to omit several fluorescence measurements in Fig. 4. Note that the relationship between fluorescence and VO_2 is close to linear. This indicates that fluorescence changes follow similar kinetics as VO_2 . In addition, we observed that the fluorescence changes induced by exogenous ATP were larger than expected from VO_2 measurements. As a result, the relationship between NADH (or FP) fluorescence and VO_2 is not unique, but depends on the way the respiration is stimulated (Fig. 4, A and B).

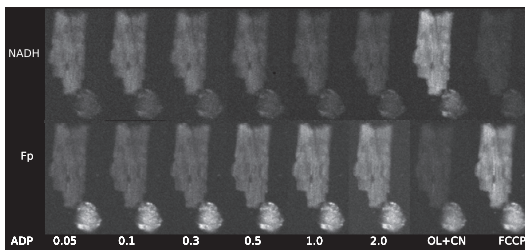


FIGURE 1 Example of the response of permeabilized cardiomyocytes to changes in solution. For demonstration, rod-shaped and nonrod-shaped cells are shown. Autofluorescence of the cells was recorded by fluorescence microscope with the fluorescence induced by 340 nm (*top row*) or 465 nm (*bottom row*) excitation. Note how gradual increase of ADP (concentration in mM shown below images) leads to changes in fluorescence with the maximal and minimal levels of fluorescence induced by oligomycin/cyanide (OL+CN) and FCCP. As it is clearly visible on the figure, fluorescence of nonrod-shaped cells (*bottom right corner* on all images) is relatively small in recordings of NADH fluorescence. However, the opposite was frequently true for recordings of fluorescence corresponding to flavo-protein (FP) signal.

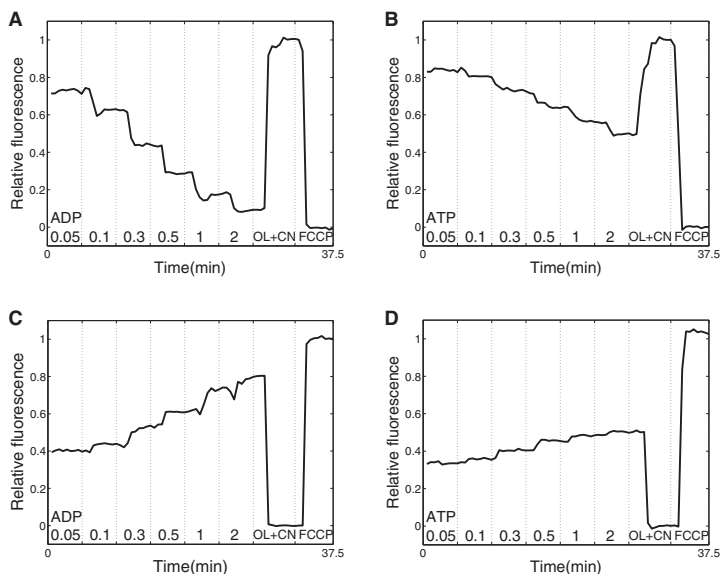


FIGURE 2 Average fluorescence of a single permeabilized cell exposed to the changes in solution denoted at the bottom. Fluorescence was recorded with excitation light of 340 nm (*top row*) or 465 nm (*bottom row*). The fluorescence was normalized by using the signal recorded in solutions OL+CN and FCCP as extreme values corresponding to relative fluorescence equal to 0 and 1 (see figure). The moment at which the change of solution was started by the experimenter is indicated (*dashed vertical line*). Note how stimulation of respiration by exogenous ADP (*A and C*) is able to change the fluorescence in a larger range than stimulation by exogenous ATP (*B and D*).

Differences in fluorometer and microscope measurements analyzed by compartmentalized model of a cardiomyocyte

We have shown that the fluorescence response to variation in exogenous ATP concentration was different in fluorometer and microscope (Fig. 3, *B and D*). To understand the cause of this difference, respiration stimulation by exogenous ATP can be analyzed by mathematical model of permeabilized rat cardiomyocytes (3). Because, in our experiments, 3 mM inorganic phosphate was present in solution, effects induced by phosphate supply to the cell should be negligible. Thus, we can focus in our analysis on ATP and ADP. When respiration is stimulated by exogenous ATP, endogenous ATPases hydrolyze it to the ADP that would stimulate respiration in mitochondria. In addition, ADP produced by endogenous ATPases can also leave the cell in solution if the concentration of ADP in solution is smaller than in the cell. In the fluorometer cuvette, solution is not exchanged and reaches the steady state relatively fast, as measured by HPLC in similar configuration (3).

In the microscope chamber, the solution is exchanged and ADP produced by upstream cells can be washed out. To track the ADP concentration in the microscope chamber, we have to distinguish between ADP present in prepared ATP solution and ADP produced by ATPases in the microscope chamber. In our conditions, ADP concentration was 1.5% of ATP concentration in prepared solution, as determined earlier by HPLC in solution without cells (3). To estimate ADP produced by all cells in the microscope chamber, we assumed that the ATPase rate can be described by the Michaelis-Menten equation with apparent $K_{m(ATP)}$ of

0.38 mM (3). Maximal ATPase activity of a cell (4.2 fmol/s) can be estimated from activity of ATP synthase (0.54 mM/s, see description of reaction-diffusion-convection model in the [Supporting Material](#)); stimulation of respiration by exogenous ATP relative to stimulation by ADP (25% (3)); and the volume of a cell (cylinder with 20- μ m diameter and 100- μ m length).

Taking into account the cell counts after isolation and series of dilutions made, we had ~1000 cells in a microscope chamber during experiments leading to 4 pmol/s maximal ATPase activity. When checked at all used concentrations of ATP by calculating ATPase rate using the Michaelis-Menten equation, the ADP concentration would increase by 8.1% (at 50 μ M ATP in solution) and 5.1% (300 μ M ATP) when compared with ADP contained in solution at a flow rate of 0.5 ml/min. Because a significant fraction of the cells is washed out at the beginning of the experiment, the effect of intracellular ATPases on the ADP concentration in the chamber is even smaller. Thus, in the microscope chamber, ADP produced by cells in the chamber has a minor effect and ADP in solution is mainly determined by ADP present in solution before entering the chamber.

To test further whether such differences in the solution surrounding the cells could cause the different fluorescence responses seen in Fig. 3 *B*, we calculated VO_2 . For comparison, a case with zero ADP in solution surrounding the cells is shown in Fig. 5. Note that in the case of zero ADP, there is still ATPase activity in the cell and some of the produced ADP stimulates respiration. As it is clear from the simulation results, ADP buildup during the measurements in the closed chamber configuration contributes significantly to VO_2 . From these simulation results, we conclude that the

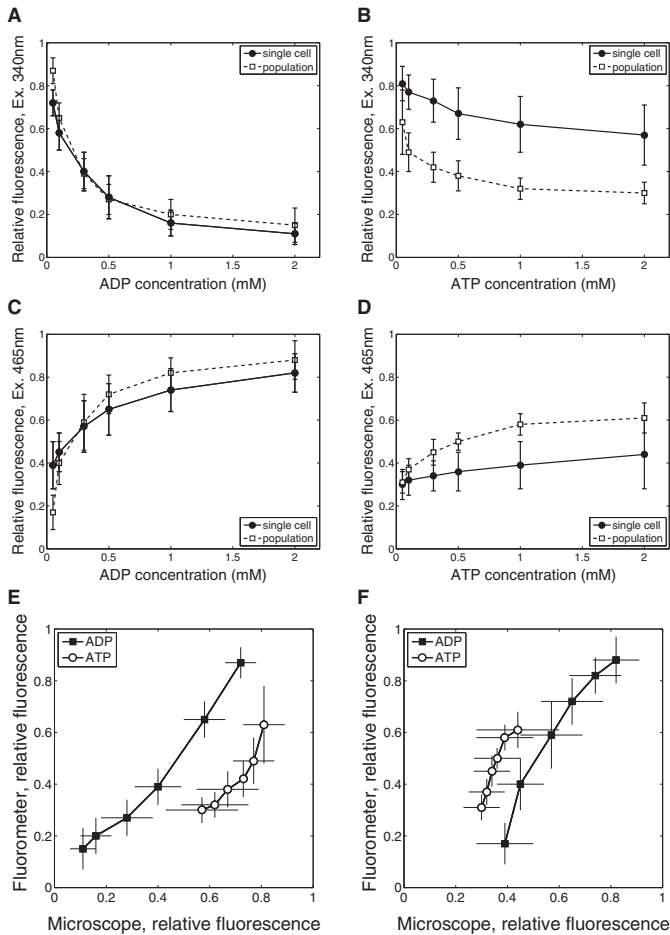


FIGURE 3 Comparison of fluorescence recordings performed on single cell level using fluorescence microscope with recordings on cell population level using fluorometer. The average fluorescence at different levels of exogenous ADP (A and C) and ATP (B and D) is shown for single cell and cell population recordings. Finally, average fluorescence recorded on single cell and population level is plotted against each other with fluorescence excited by 340 nm and 465 nm in E and F, respectively.

differences in NADH and FP fluorescence response to stimulation by endogenously generated ADP in fluorometer and microscope are caused by differences in the design of the corresponding measurement chambers.

Influence of unstirred water layers on the measurements

The low affinity of respiration, as evidenced by NADH and FP to changes in extracellular ADP, suggest significant intracellular diffusion restrictions. However, such low affinity can be also induced by large unstirred water layers surrounding the cells in the fluorometer or microscope chambers. Although analysis of unstirred water layers in the fluorometer chamber is not trivial due to the stirring and mixing of the cells in the experiments, the situation in the microscope chamber can be analyzed in detail. In our conditions, the flow in the chamber is laminar. By approximating the micro-

scope chamber by simplified geometry, we calculated the flow profile of the solution in the chamber (Fig. 6 A). The flow velocity was fastest near the inflow and outflow. In the center of the chamber, where the measurements were performed, the flow velocity reached $\sim 3100 \mu\text{m/s}$ at the surface of the solution. Near the cell, next to the cover glass, the flow is considerably slower. However, even $20 \mu\text{m}$ from the glass, the flow was $>100 \mu\text{m/s}$ in the central region of the chamber. Assuming that there is no flow of solution through the cell, the corrected flow profile in the cell surroundings was calculated. In those simulations, the flow profile in the middle of microscope chamber was taken into account. The flow in the cell surroundings is shown in Fig. 6 B by streamlines and arrows.

The calculated flow profile in the cell surroundings was used to analyze the influence of unstirred water layers on the measurements. For that, a reaction-diffusion-convection model was composed and we calculated the distribution of

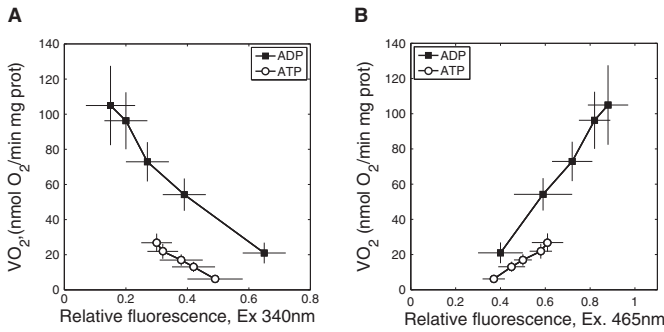


FIGURE 4 Relationship between fluorescence recorded in fluorometer (excitation 340 nm and 465 nm on A and B, respectively) and respiration rate. Note that the relationship is different for ADP and ATP stimulation.

ADP in solution and inside the cell taking into account mitochondrial respiration, diffusion, and convection of ADP. When 1 mM ADP is used in the solution entering the chamber, the model predicts significant diffusion gradients between the solution and parts of the cell next to the cover glass with the lowest ADP concentration equal to 0.67 mM (Fig. 6 B). In those simulations, it was assumed that apparent $K_{m(ADP)}$ of respiration was 0.015 mM, i.e., the same as for isolated mitochondria. To analyze how the supply of ADP influences VO₂ of the isolated cardiomyocyte, we calculated VO₂ of the cell in different conditions. Assuming that apparent $K_{m(ADP)}$ of mitochondria is 0.015 mM, we could see a large difference on calculated VO₂ when ADP was supplied by infinitely fast diffusion, diffusion as in water, and with the diffusion assisted by flow of solution (Fig. 6 C).

Note that when we take into account the flow surrounding the cell, the apparent affinity of VO₂ to ADP is considerably higher than the measured one (solid line in Fig. 6 C). Here,

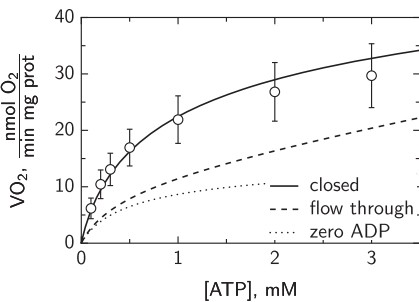


FIGURE 5 Calculated respiration rate VO₂ stimulated by exogenous ATP in permeabilized cardiomyocytes in the surroundings that mimic the situation in fluorometer (solid line) or microscope imaging chamber (dashed line). In fluorometer, measurements are performed in closed chamber whereas in microscope the solution is changed as it flows through the imaging chamber. As a result, ADP in solution can either accumulate (closed chamber) or will stay relatively low (flow through chamber). In simulations, flow through chamber had ADP concentration proportional to added ATP, in agreement with small ATP contamination by ADP. For comparison, VO₂ calculated with zero ADP concentration in solution surrounding the cell is shown (dotted line).

the VO₂ measured in an oxygraphy chamber for cell suspension (data from Sepp et al. (3)) is shown for comparison. Assuming that NADH and FP fluorescence is linearly related to VO₂ we estimated the relative VO₂ of a single cell from fluorescence measurements (Fig. 3, A and C). For that, fluorescence at zero ADP was taken into account in estimation of VO₂ by subtracting it. The fluorescence at zero ADP was found by fitting fluorescence measurements with a Michaelis-Menten-type relationship with the shift corresponding to fluorescence level at zero ADP. As it is clear from Fig. 6 C, to reproduce the experimental data, the affinity of mitochondrial respiration to ADP has to be reduced significantly by increasing apparent $K_{m(ADP)}$ of respiration to 0.15–0.45 mM. This demonstrates that low affinity of respiration is induced, in part, by intracellular diffusion restrictions.

DISCUSSION

According to our results, the fluorescence response to exogenous ADP and ATP stimulation was similar on single cell and population levels if we take into account the differences in experimental setups. On both studied levels, NADH and FP fluorescence varied when ADP was changed up to the millimolar range indicating a low affinity of mitochondrial oxidative phosphorylation to exogenous ADP. From the mathematical analysis of the measurements in microscope chamber, we demonstrated that low affinity of the respiration to exogenous ADP is in part induced by intracellular diffusion restrictions. To our knowledge, this is the first time the existence of intracellular diffusion restrictions for ADP has been demonstrated from experiments on single cells.

To study the autofluorescence of cardiomyocytes, we used a wide-field fluorescence microscope equipped with a sensitive camera. By using such setup and following a single isolated cardiomyocyte, we avoided complications that can occur in tissue preparations and in confocal imaging. In the studies on tissue or organ level, one has to compensate for organ motion, inhomogeneity of the cells, and absorption and scattering of excitation light and fluorescence by tissue.

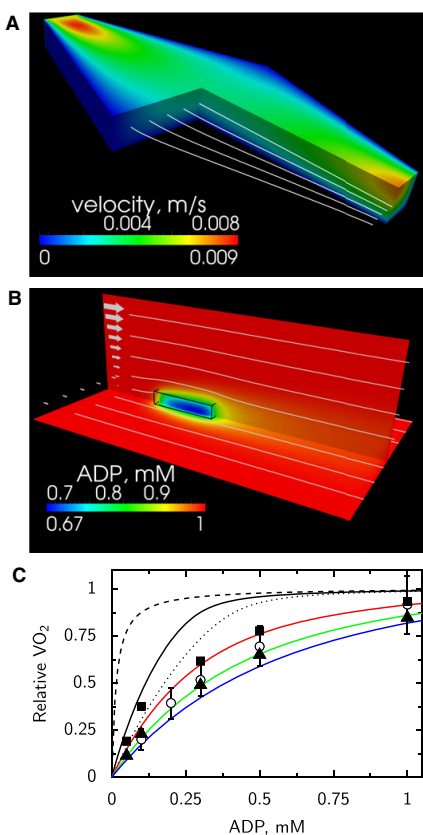


FIGURE 6 Analysis of single cell respiration in the microscope fast exchange chamber. (A) Flow profile in the microscope chamber found by the mathematical model. The flow profile is described by velocity magnitude (shown by color) and streamlines (white lines). At inflow (top left), the velocity is higher than at outflow (bottom right) due to the larger opening of the chamber at outflow. (B) Distribution of ADP (shown by color) predicted by the mathematical model around a cell situated in the middle of a chamber, attached to the glass. The location of the cell is outlined (black wire-frame) on the image. The flow in the box was calculated on basis of the flow distribution in the chamber taking into account the flow around the cell. The flow is indicated by the arrows (left) and streamlines (white lines). Note how flow of solution leads to asymmetric distribution of ADP next to the cell. (C) Influence of ADP mixing mechanisms on respiration rate of a cell in microscope chamber. Assuming that there are no intracellular diffusion restrictions, the calculated affinity of respiration to ADP is very high in the case of infinitely fast diffusion (dashed black line). If ADP is supplied just by diffusion, the affinity drops significantly (dotted black line). Taking into account flow distribution in the chamber, the predicted affinity of respiration to ADP (solid black line) is significantly higher than the one determined from experiments. For comparison, respiration rate dependency determined on the cell suspension in respiration chamber is shown (open dots) as well as respiration rate estimated from NADH (solid squares) and FP (solid triangles). Only by assuming significant intracellular diffusion restrictions modeled by increasing an apparent $K_{m(ADP)}$ of mitochondrial respiration to 0.15 mM (red line), 0.3 mM (green line), or 0.45 mM (blue line), is it possible to reproduce the measurements if the flow in the chamber is taken into account.

When confocal microscopy is used, small movement of the cell could lead to changes in focal plane that have to be taken into account. Due to the nature of the fluorescence microscope point-spread function, the signal is integrated through the whole thickness of the cell (point-spread function of our microscope has been published earlier in Laasmaa et al. (26)). As a result, small movements of the cell induced by changes in solution flow do not alter the measurements if the signal is averaged over the whole cell. In addition, use of a highly sensitive camera allowed us to reduce bleaching by attenuating the excitation light.

According to our results, changes in NADH and FP autofluorescence were linearly related to respiration rate (Fig. 4). Similar linear relationships were observed when respiration rates were varied by changes in substrates at different calcium levels (27). In our work, calcium, substrate, and inorganic phosphate levels were kept the same. As a result, regulation of respiration was rather simple and carried out by ADP in the vicinity of mitochondria. Such simple control probably resulted in the simple relationship between respiration rate, and NADH and FP autofluorescence.

The main result of this work is the demonstration of low ADP-affinity of mitochondrial respiration in single permeabilized cardiomyocytes. From the similar response of autofluorescence to stimulation of respiration by ADP and ATP on single cell and population level, we conclude that the analysis of intracellular diffusion on population of permeabilized cardiomyocytes is adequate and does not suffer from clumping of the cells in measurement solution. The differences in response of autofluorescence to stimulation by ATP (Fig. 3, B and D) were attributed to accumulation of ADP during measurements in the fluorometer chamber. As we have demonstrated earlier in similar setup by HPLC measurements (3), the ADP concentration increases from ~0.03 mM to ~0.06 mM during stimulation of respiration with 2 mM ATP. When oxidative phosphorylation is active, the ADP level stabilizes at 0.06 mM level. Note that the initial ADP was present as a small fraction in the injected ATP. This buildup of ADP in the surrounding solution leads to larger respiration rate, as demonstrated in Fig. 5 and can explain the larger autofluorescence response in fluorometer to stimulation of ATP compared to the measurements in microscope (Fig. 3, B and D).

Because single cell and cell populations results are similar, one can take advantage of both preparations in the studies. When larger population is used, it is possible to use macroscopical methods, such as following respiration rate by measuring oxygen concentration changes in solution, HPLC to determine dynamics of metabolite changes, and absorbance spectroscopy. Those methods have been applied in numerous studies (1,11,28), with our recent study applying a large set of them to analyze ADP compartmentation in permeabilized cardiomyocytes (3). Although macroscopical approaches are not possible on a single-cell level, there are clear advantages of using a single-cell preparation.

The main advantage is the ability to select a particular cell. As it is shown in Fig. 1, the response of a viable rod-shaped cardiomyocyte could be different from that of a contracted nonrod-shaped cell. In the microscope, we could choose the cells on the basis of their shape and response to external stimuli. This is not possible on a population level, because in population-level studies there is always a fraction of the cells that have been damaged during isolation. In addition, the single cell preparation allows us to study intracellular heterogeneity of the metabolism, such as metabolic oscillations (29–31). For regional analysis, confocal microscopy can be used (17) or image deconvolution algorithms to enhance fluorescence images. For deconvolution, several options exist with several open source deconvolution packages made available recently including end-user software packages or programming libraries (see Laasmaa et al. (32) and references within).

Although there are clear advantages in the use of single cell preparations, there is an important complication. Namely, to study the response of permeabilized cardiomyocytes to external stimuli, we are mainly limited to fluorescence-based methods. As we have done in this study, the response of mitochondrial oxidative phosphorylation was analyzed through autofluorescence of mitochondria. Unfortunately, we cannot yet relate that autofluorescence to respiration rate directly. In this work, we assumed that the linear relationships among VO_2 and NADH and FP fluorescence (Fig. 4) holds for the measurements in the microscope chamber as well. This is a phenomenological relationship and may not hold in all conditions.

As a part of the solution to the problem of relating VO_2 to fluorescence, mathematical models of oxidative phosphorylation can be used. Several detailed models are available that, with the proper calibration, could be applied to extract rates of the processes on the basis of fluorescence measurements. For example, mitochondrial respiration models developed by several groups (33–40) can be used as a starting point for development and calibration of the model that would be able to relate fluorescence measurements to respiration rate. Although all the details of regulation of oxidative phosphorylation are, to our knowledge, not yet known, and, consequently, none of the existing models is perfect, it should be possible to find a set of parameters that would reproduce the simpler experiments. For example, in our experiments, only ATP and ADP were varied and there was no variation of calcium, phosphate, and substrates leading to simple relationship between VO_2 and fluorescence (Fig. 4).

As one of the advantages of using single cell preparation, the influence of the unstirred water layer surrounding the cell can be quantified. Here, by using several mathematical models, we found the flow profile in the chamber and in the vicinity of the cell (Fig. 6, A and B). Knowing the flow profile, it is possible to find the influence of ADP or ATP supply from the solution in the cell and separate diffusion

gradients induced by intracellular structures from overall diffusion gradients in the system (Fig. 6, B and C). As it is clear from our simulations, intracellular diffusion restrictions are significant (compare *black* and *colored solid lines* in Fig. 6 C). In addition to intracellular diffusion restrictions, diffusion gradients induced by ADP supply in the chamber play a significant role as well (compare *dashed* and *solid lines* in Fig. 6 C). In our simulations, the cell was positioned along the flow.

We repeated the simulations with the cell positioned perpendicular to the flow and found that computed VO_2 -ADP relationships at different $K_{\text{m(ADP)}}$ were very close to the relationships found with the cell oriented along the flow (results not shown). This suggests that orientation of the cell positioned on the cover glass does not play a major role on the experimental outcome. However, on the basis of our analysis, we can recommend imaging the cell in the part of the chamber with the higher flow velocity (Fig. 6 A). This would reduce contribution of ADP supply in the overall gradients.

The demonstration that the diffusion restrictions are not induced by clumping of the cells in an oxygraph has important physiological consequences. As we have shown in this work, single permeabilized rat cardiomyocytes have a low affinity to exogenous ADP. From this, we conclude that there are significant diffusion restrictions between the solution surrounding the cell and the mitochondrial inner membrane. As we have shown earlier, on the basis of mathematical analysis of measurements performed on permeabilized rat heart muscle fibers and isolated cardiomyocytes, the mitochondrial outer membrane should lead to a diffusion gradient that is ≤ 0.16 mM (3,7) at half-maximal respiration rate with the rest of the gradient induced by some other intracellular structures. Those structures are not distributed uniformly, but are probably localized in certain areas of the cell, as demonstrated in analysis of respiration response kinetics to stimulation by ATP (5). When assuming that the rest of the diffusion gradient is induced by sarcoplasmic reticulum and proteins in its neighborhood, a very significant diffusion obstacle on that level was predicted by a three-dimensional reaction-diffusion model of rat heart muscle fiber (7).

The physiological role of such diffusion restrictions is still not clear, and is a subject of further studies. At present, we have not yet identified which intracellular structures are responsible for diffusion restrictions. As a result, we cannot predict whether those diffusion restrictions would influence intracellular energy fluxes in the heart leading to modulation of energy transfer depending on the workload (41). In addition, signaling, or response to pathological conditions can be influenced as well. However, what we have demonstrated in this work is that the diffusion restrictions that lower the affinity of mitochondrial respiration to exogenous ADP are localized within permeabilized rat cardiomyocytes.

SUPPORTING MATERIAL

Materials and Methods, Results, one figure, and references (42,43) are available at [http://www.biophysj.org/biophysj/supplemental/S0006-3495\(11\)01085-X](http://www.biophysj.org/biophysj/supplemental/S0006-3495(11)01085-X).

The authors thank Merle Mandel for technical assistance (Laboratory of Systems Biology, Institute of Cybernetics, Tallinn University of Technology, Estonia); Aivar Lõokene, Terje Robal, and Miina Lillepruun (Lipoprotein group, Bioorganic chemistry, Department of Chemistry, Tallinn University of Technology, Estonia) for providing access and help with fluorometer; Hena Ramay and Martin Laasmaa for help with analyzing the data (Laboratory of Systems Biology, Institute of Cybernetics, Tallinn University of Technology, Estonia).

This work was supported by the Wellcome Trust (Fellowship No. WT081755MA) and Estonian Science Foundation (grants 8041 and 7344, PhD stipends for N.J. and M.S., respectively).

REFERENCES

- Kümmel, L. 1988. Ca, Mg-ATPase activity of permeabilized rat heart cells and its functional coupling to oxidative phosphorylation of the cells. *Cardiovasc. Res.* 22:359–367.
- Veksler, V. I., A. V. Kuznetsov, ..., V. A. Saks. 1987. Mitochondrial respiratory parameters in cardiac tissue: a novel method of assessment by using saponin-skinned fibers. *Biochim. Biophys. Acta.* 892:191–196.
- Sepp, M., M. Vendelin, ..., R. Birkedal. 2010. ADP compartmentation analysis reveals coupling between pyruvate kinase and ATPases in heart muscle. *Biophys. J.* 98:2785–2793.
- Rostovtseva, T. K., K. L. Sheldon, ..., D. L. Sackett. 2008. Tubulin binding blocks mitochondrial voltage-dependent anion channel and regulates respiration. *Proc. Natl. Acad. Sci. USA.* 105:18746–18751.
- Vendelin, M., M. Eimre, ..., V. A. Saks. 2004. Intracellular diffusion of adenosine phosphates is locally restricted in cardiac muscle. *Mol. Cell. Biochem.* 256–257:229–241.
- Vendelin, M., and R. Birkedal. 2008. Anisotropic diffusion of fluorescently labeled ATP in rat cardiomyocytes determined by raster image correlation spectroscopy. *Am. J. Physiol. Cell Physiol.* 295:C1302–C1315.
- Ramay, H. R., and M. Vendelin. 2009. Diffusion restrictions surrounding mitochondria: a mathematical model of heart muscle fibers. *Biophys. J.* 97:443–452.
- Vendelin, M., N. Béraud, ..., V. A. Saks. 2005. Mitochondrial regular arrangement in muscle cells: a “crystal-like” pattern. *Am. J. Physiol. Cell Physiol.* 288:C757–C767.
- Birkedal, R., H. A. Shiels, and M. Vendelin. 2006. Three-dimensional mitochondrial arrangement in ventricular myocytes: from chaos to order. *Am. J. Physiol. Cell Physiol.* 291:C1148–C1158.
- Kongas, O., T. L. Yuen, ..., K. Krab. 2002. High K_m of oxidative phosphorylation for ADP in skinned muscle fibers: where does it stem from? *Am. J. Physiol. Cell Physiol.* 283:C743–C751.
- Sokolova, N., M. Vendelin, and R. Birkedal. 2009. Intracellular diffusion restrictions in isolated cardiomyocytes from rainbow trout. *BMC Cell Biol.* 10:90.
- Appaix, F., A. V. Kuznetsov, ..., V. Saks. 2003. Possible role of cytoskeleton in intracellular arrangement and regulation of mitochondria. *Exp. Physiol.* 88:175–190.
- Chance, B., and G. R. Williams. 1955. Respiratory enzymes in oxidative phosphorylation. III. The steady state. *J. Biol. Chem.* 217:409–427.
- Chance, B., B. Schoener, ..., Y. Nakase. 1979. Oxidation-reduction ratio studies of mitochondria in freeze-trapped samples. NADH and flavoprotein fluorescence signals. *J. Biol. Chem.* 254:4764–4771.
- Chance, B., and M. Baltscheffsky. 1958. Spectroscopic effects of adenosine diphosphate upon the respiratory pigments of rat-heart-muscle sarcosomes. *Biochem. J.* 68:283–295.
- Winkler, K., A. V. Kuznetsov, ..., W. S. Kunz. 1995. Laser-excited fluorescence studies of mitochondrial function in saponin-skinned skeletal muscle fibers of patients with chronic progressive external ophthalmoplegia. *Biochim. Biophys. Acta.* 1272:181–184.
- Kuznetsov, A. V., O. Mayboroda, ..., W. S. Kunz. 1998. Functional imaging of mitochondria in saponin-permeabilized mice muscle fibers. *J. Cell Biol.* 140:1091–1099.
- Huang, S., A. A. Heikal, and W. W. Webb. 2002. Two-photon fluorescence spectroscopy and microscopy of NAD(P)H and flavoprotein. *Biophys. J.* 82:2811–2825.
- Sedlic, F., D. Pravdic, ..., M. Bienengraeber. 2010. Monitoring mitochondrial electron fluxes using NAD(P)H-flavoprotein fluorometry reveals complex action of isoflurane on cardiomyocytes. *Biochim. Biophys. Acta.* 1797:1749–1758.
- Mayevsky, A., and E. Barbiro-Michaely. 2009. Use of NADH fluorescence to determine mitochondrial function in vivo. *Int. J. Biochem. Cell Biol.* 41:1977–1988.
- Eng, J., R. M. Lynch, and R. S. Balaban. 1989. Nicotinamide adenine dinucleotide fluorescence spectroscopy and imaging of isolated cardiac myocytes. *Biophys. J.* 55:621–630.
- Mayevsky, A., and G. G. Rogatsky. 2007. Mitochondrial function in vivo evaluated by NADH fluorescence: from animal models to human studies. *Am. J. Physiol. Cell Physiol.* 292:C615–C640.
- Kunz, W. S. 1986. Spectral properties of fluorescent flavoproteins of isolated rat liver mitochondria. *FEBS Lett.* 195:92–96.
- Kunz, W. S., and F. N. Gellerich. 1993. Quantification of the content of fluorescent flavoproteins in mitochondria from liver, kidney cortex, skeletal muscle, and brain. *Biochem. Med. Metab. Biol.* 50:103–110.
- Chorvat, Jr., D., J. Kirchnerova, ..., A. Chorvatova. 2005. Spectral unmixing of flavin autofluorescence components in cardiac myocytes. *Biophys. J.* 89:L55–L57.
- Laasmaa, M., M. Vendelin, and P. Peterson. 2011. Application of regularized Richardson-Lucy algorithm for deconvolution of confocal microscopy images. *J. Microsc.* 243:124–140.
- Territo, P. R., V. K. Mootha, ..., R. S. Balaban. 2000. Ca^{2+} activation of heart mitochondrial oxidative phosphorylation: role of the F_0F_1 -ATPase. *Am. J. Physiol. Cell Physiol.* 278:C423–C435.
- Saks, V. A., Y. O. Belikova, and A. V. Kuznetsov. 1991. In vivo regulation of mitochondrial respiration in cardiomyocytes: specific restrictions for intracellular diffusion of ADP. *Biochim. Biophys. Acta.* 1074:302–311.
- Romashko, D. N., E. Marban, and B. O’Rourke. 1998. Subcellular metabolic transients and mitochondrial redox waves in heart cells. *Proc. Natl. Acad. Sci. USA.* 95:1618–1623.
- Aon, M. A., S. Cortassa, and B. O’Rourke. 2004. Percolation and criticality in a mitochondrial network. *Proc. Natl. Acad. Sci. USA.* 101:4447–4452.
- Kurz, F. T., M. A. Aon, ..., A. A. Armondas. 2010. Spatio-temporal oscillations of individual mitochondria in cardiac myocytes reveal modulation of synchronized mitochondrial clusters. *Proc. Natl. Acad. Sci. USA.* 107:14315–14320.
- Laasmaa, M., M. Vendelin, and P. Peterson. 2011. Application of regularized Richardson-Lucy algorithm for deconvolution of confocal microscopy images. *J. Microsc.* 243:124–140.
- Jafri, M. S., S. J. Dudycha, and B. O’Rourke. 2001. Cardiac energy metabolism: models of cellular respiration. *Annu. Rev. Biomed. Eng.* 3:57–81.
- Korzeniewski, B. 1998. Regulation of ATP supply during muscle contraction: theoretical studies. *Biochem. J.* 330:1189–1195.
- Vendelin, M., O. Kongas, and V. Saks. 2000. Regulation of mitochondrial respiration in heart cells analyzed by reaction-diffusion model of energy transfer. *Am. J. Physiol. Cell Physiol.* 278:C747–C764.

36. Beard, D. A. 2005. A biophysical model of the mitochondrial respiratory system and oxidative phosphorylation. *PLoS Comput. Biol.* 1:e36.
37. Wu, F., F. Yang, ..., D. A. Beard. 2007. Computer modeling of mitochondrial tricarboxylic acid cycle, oxidative phosphorylation, metabolite transport, and electrophysiology. *J. Biol. Chem.* 282:24525–24537.
38. Nguyen, M.-H. T., S. J. Dudyca, and M. S. Jafri. 2007. Effect of Ca^{2+} on cardiac mitochondrial energy production is modulated by Na^{+} and H^{+} dynamics. *Am. J. Physiol. Cell Physiol.* 292:C2004–C2020.
39. Cortassa, S., M. A. Aon, ..., R. L. Winslow. 2006. A computational model integrating electrophysiology, contraction, and mitochondrial bioenergetics in the ventricular myocyte. *Biophys. J.* 91:1564–1589.
40. Bazil, J. N., G. T. Buzzard, and A. E. Rundell. 2010. Modeling mitochondrial bioenergetics with integrated volume dynamics. *PLoS Comput. Biol.* 6:e1000632.
41. Vendelin, M., J. A. Hoerter, ..., J. L. Mazet. 2010. Modulation of energy transfer pathways between mitochondria and myofibrils by changes in performance of perfused heart. *J. Biol. Chem.* 285:37240–37250.
42. Kushmerick, M. J., and R. J. Podolsky. 1969. Ionic mobility in muscle cells. *Science.* 166:1297–1298.
43. Bangerth, W., R. Hartmann, and G. Kanschat. 2007. Deal.II—a general purpose object oriented finite element library. *ACM Trans. Math. Softw.* 33:24.

Supporting material: Permeabilized rat cardiomyocyte response demonstrates intracellular origin of diffusion obstacles

Natalja Jepihhina, Nathalie Beraud, Mervi Sepp, Rikke Birkedal, and Marko Vendelin

Laboratory of Systems Biology, Institute of Cybernetics, Tallinn University of Technology, Akadeemia 21, 12618 Tallinn, Estonia

The supporting material includes detailed description of used solutions, mathematical models, and fluorescence spectra recorded in fluorometer.

MATERIALS AND METHODS

Experimental procedures

Solutions used in isolation of cardiomyocytes. Wash solution contained (in mM): 117 NaCl (Sigma-Aldrich, 71379), 5.7 KCl (Sigma-Aldrich, P5405), 4.4 NaHCO₃ (Sigma-Aldrich, S6014), 1.5 KH₂PO₄ (Sigma-Aldrich, P0662), 1.7 MgCl₂ (Sigma-Aldrich, 63068), 21 HEPES (Sigma-Aldrich, H3375), 20 Taurine (Sigma-Aldrich, 86329), 11.7 Glucose (Sigma-Aldrich, 158968), and pH was adjusted at 25°C to 7.4 with NaOH.

Digestion solution had the same composition as the wash solution with the addition of 3mg/ml BSA (Roche, 10 775 835 001), 0.375 mg/ml collagenase P (Roche). In some cases, 75 μM EGTA was added to the digestion solution due to high amounts of Ca²⁺ in the collagenase.

Sedimentation solution had the same composition as the wash solution with the addition of 2mg/ml BSA (Roche, 10 775 835 001), 10 μM leupeptine (Roche, 11 034 626 001), 2 μM soybean trypsin inhibitor (Fluka, 93619).

Fluorescence microscope. Microscope experiments were performed on an inverted Nikon Eclipse Ti-U microscope (Nikon, Japan) equipped with two tiers of motorized filter turrets for simultaneous acquisition of transmission and fluorescence images. For transmission images, light from the 100W halogen microscope lamp was passed through a 585/40 nm filter onto the specimen and through the dichroic filters in the turrets to a high-speed CCD camera (IPX-VGA210-LMCN, Imprx Inc., Florida, USA) mounted on the left port. For images of NADH and FP autofluorescence, respectively, light from a Prior Lumen 200 with a 200W metal halide lamp with

extended wavelength (Prior Scientific, Cambridge, United Kingdom) was passed via an optical fiber into the upper filter turret. For NADH recordings, the light was passed through a 340/26 nm excitation filter onto a 400 nm long pass dichroic mirror, which deflected the light onto the specimen. Light emitted from the specimen passed back through the upper filter cube to a 510 XR dichroic in the lower filter cube and reflected through a 460/80 nm emission filter to an Andor Ixon EMCCD camera (Andor Technologies, Belfast, United Kingdom). For FP recordings, the light was passed through a 465/30 nm excitation filter onto a 510 nm dichroic mirror, which deflected the light onto the specimen. Light emitted from the specimen passed back through the upper filter cube to a 560 XR dichroic in the lower filter cube and reflected through a 525/50 nm emission filter. All filters were purchased from AHF analysentechnik AG, Germany. Transmission images together with images of NADH or FP autofluorescence were acquired every 30 sec. To reduce photobleaching, a Uniblitz shutter (VCM-D1, Vincent Associates, Rochester, USA) timed the light exposure with the acquisition.

Analysis of fluorescence signal. Fluorescence signal intensity from microscope single cell experiments was analyzed using ImageJ software. Both cell containing and background regions were selected and corresponding average fluorescence signal intensities were determined with ImageJ plug-in “measure stack”. Then, background fluorescence was subtracted from cell fluorescence and data plotted on a time-scale. From the latter plot, average fluorescence was found for each condition to which the cell was exposed (ADP concentration, uncoupling or block of oxidative phosphorylation).

Data obtained from spectrofluorophotometer experiments was analyzed with home-made software written in Python. We integrated the recorded spectra in the ranges corresponding to the optical filters used in the fluorescence microscope: 420-500 nm and 500-550 nm for NADH and FP autofluorescence, respec-

tively.

Fluorescence signal recorded in microscope or fluorometer was normalized to the signal values in reduced and oxidized states. Mitochondria were reduced by oligomycin and cyanide (OL+CN); oxidized state was recorded either in the beginning of the experiment before addition of substrates in the presence of ADP or by adding FCCP at the end of the experiment. The following equations were used:

$$f_{NADH} = \frac{F - F_{OX}}{F_{RED} - F_{OX}},$$

$$f_{FP} = \frac{F - F_{RED}}{F_{OX} - F_{RED}},$$

where F was recorded fluorescence; F_{OX} and F_{RED} was fluorescence recorded in oxidized or reduced state, respectively.

Solutions. Substrate-free mitomed solution contained (in mM): 3.0 KH_2PO_4 (Sigma-Aldrich, P0662), 3.0 MgCl_2 (Sigma-Aldrich, 63068), 20 HEPES (Sigma-Aldrich, H3375), 0.5 EGTA (Sigma-Aldrich, 03778), 20 taurine (Sigma-Aldrich, 86329), 0.5 dithiothreitol (Sigma-Aldrich, D0632) and 60 lactobionate (Sigma-Aldrich, L2398). 5 glutamate (Sigma-Aldrich, 49449) and 2 malate (Sigma-Aldrich, M6413) were added as substrates together with 110 sucrose (Sigma-Aldrich, S1888), pH was adjusted at 25°C to 7.1 with KOH.

Concentrations of the uncoupler and respiration blockers were: FCCP (Carbonyl cyanide 4-(trifluoromethoxy)phenylhydrazone, 10 μM , Ascent Scientific, Asc-081), oligomycin A (10 μM , Teubio, 579-13-5), and sodium cyanide (5mM, Sigma-Aldrich, 205222).

Mathematical models

Compartmentalized model of rat cardiomyocyte energetics. The mathematical model of permeabilized rat cardiomyocyte was taken from (1). Among the models analyzed in (1), the models '3s' and '4s' were found to describe respiration and other measurements best. Here, the results obtained with the model '3s' are presented. Calculations with model '4s' led to almost the same results (results not shown). In short, the models consider permeabilized rat cardiomyocytes divided into several compartments: mitochondria, cytosol, and a small com-

partment inducing functional coupling between endogenous pyruvate kinase and fraction of ATPases. In addition, solution surrounding the cells is considered as well. All compartments are separated from each other by diffusion restrictions including the connection between solution and cytosolic compartment. As a result, concentrations of the metabolites are different in different compartment and could differ from the concentrations in surrounding solution. The concentrations and the rates of reactions are determined by relative activities of the enzymes and extent of diffusion restrictions. Model parameters were taken from (1).

Model of solution flow in microscope chamber and in the vicinity of the cell. To find the flow velocity profile in the fast exchange chamber and in the vicinity of the cell, Navier-Stokes equations for incompressible fluid were solved. Simulations were performed using *icoFoam* solver for laminar, isothermal, incompressible flow of Newtonian fluids from OpenFOAM toolbox (<http://www.openfoam.com>). The kinematic viscosity of fluid was taken equal to 10^{-6} m^2/s .

To find the flux velocity profile in microscope flow chamber, the geometry of the chamber was approximated by a diamond shape with the corners cut at in- and out-flow. The chamber was taken as 6 mm wide and 15 mm long. The openings were 1.33 mm wide for inflow and 2 mm for outflow and located 7 mm and 6 mm, respectively, from the center of the diamond. The chamber was modeled assuming 1 mm deep solution. As a boundary condition, non-flow condition (velocity was zero, normal gradient of pressure was zero) was specified for chamber walls. On the upper surface of solution, the solution was considered to move freely along that surface (*slip* boundary condition: normal gradient of pressure was zero, normal component of velocity was zero, gradient of tangential components of velocity were zero). On inflow, uniform velocity was assumed (0.00625m/s corresponding to 0.5ml/min) with normal gradient of pressure equal to zero. On outflow, pressure was assumed to be 0 Pa and normal gradient of velocity was set to zero.

To find the velocity profile in the vicinity of the cell, simulations were performed in a box with the sides of 600 μm along the flow (x -axis), 600 μm wide (y -axis) and 300 μm high (z -axis) that was considered

to be situated in the center of the diamond chamber. The cell (modeled as a box with the sides $100\ \mu\text{m}$ along the flow, $20\ \mu\text{m}$ wide and $20\ \mu\text{m}$ high) was positioned on the bottom of the simulation box and the no-flow conditions were given on the boundary of permeabilized cell (velocity zero, normal gradient of pressure zero). No-flow boundary conditions were applied on the bottom of the simulation box, as corresponding to the cover glass. In accordance with the simulation of the flow in the microscope chamber (see results), the flow surrounding the simulation box was considered to have only one non-zero velocity component (v_x), parallel to x -axis, that depend only on the distance from the glass z : $v_x = az^2 + bz$ (a and b were found by fitting the velocity profile calculated for the middle of a chamber). As a boundary condition, the velocity was given on the entrance into the simulation box and on the top wall (on those walls the normal gradient of pressure set to zero) and calculated assuming no normal gradient on the outflow wall (pressure set to zero). On the walls parallel to the flow, *slip* boundary condition was used.

The finite volume meshes for both cases were generated by using CUBIT tool suite (Sandia National Laboratories, New Mexico, USA, <http://cubit.sandia.gov>) with hexahedral element sizes of $50\ \mu\text{m}$ and $5\ \mu\text{m}$ for chamber and cell surroundings simulations, respectively. As an initial condition, pressure and velocity of the fluid was set to zero. Simulations were performed until solution stabilized (few seconds) with steady-state flow profile used in the further analysis.

Reaction-diffusion-convection model of cell surroundings. To quantify the influence of solution flow around the cell in the microscope chamber on measurements, we composed the mathematical model that took into account mitochondrial oxidative phosphorylation, diffusion of ADP in solution and the cell, and convection of ADP by flow of solution surrounding the cell. For simplicity, only ADP was followed and it was assumed that ADP is consumed by mitochondrial OxPhos only. Similar to bidomain approach in modeling electrophysiology, OxPhos reaction was given in continuum within the cell and reaction rate was described by Michaelis-Menten equation. Apparent $K_m(\text{ADP})$ of reaction was changed to reflect the influence of intracellular

diffusion obstacles from $0.015\ \text{mM}$ (no significant intracellular diffusion obstacles, same affinity as isolated mitochondria) to higher values (increased contribution of intracellular diffusion restrictions). The maximal mitochondrial ATP synthase activity in the cell was taken as $0.54\ \text{mM ATP/s}$, taking into account ADP/ O_2 ratio (6), maximal mitochondrial respiration rate ($13.5\ \mu\text{mol O}_2/\text{min}\cdot\text{g ww}$), wet weight to dry weight ratio (5), and volume to wet weight ratio ($0.5\ \text{ml/g ww}$), as in (2). This activity is somewhat higher than $0.41\ \text{mM/s}$ used by Kongas et al. (3). Diffusion coefficient of ADP in solution was taken equal to $397\ \mu\text{m}^2/\text{s}$ (3) and reduced to 41% of this value in the cell (4).

The simulation box was $450\ \mu\text{m}$ along the flow, $300\ \mu\text{m}$ wide, and $150\ \mu\text{m}$ high. The cell (same dimensions as in flow calculations above) was positioned on the bottom, $140\ \mu\text{m}$ from inflow into the simulation box. The flow velocity calculated by the other models was used to describe convection of ADP. As boundary conditions, no-flow (normal gradient of ADP was zero) was allowed on the bottom of the simulation box (corresponding to cover glass) and the ADP concentration on the other borders was set equal to the concentration used in experimental solution. For comparison, simulations with no convection were also performed. In those simulations, flow rate was set to zero and the simulation box was increased to $600\ \mu\text{m} \times 600\ \mu\text{m} \times 300\ \mu\text{m}$.

The finite element model solving partial derivative equation corresponding to reaction-diffusion-convection system was implemented in deal.II package (5). Finite element size was $2.5\ \mu\text{m}$. Integration was performed until steady-state was reached with the steady state solution used in the analysis to calculate respiration rate of the cell.

RESULTS

Fluorescence spectra recorded in fluorometer. In the first series of experiments ($n=7$), we used the same normalization of fluorescence signal as in the experiments performed in microscope chamber. However, use of FCCP in fluorometer resulted in alteration of recorded spectra that made it impossible to use. Namely, FCCP has a considerable absorbance in a wide range of wavelengths with a maximal absorbance at $\sim 380\ \text{nm}$. As it was evident from

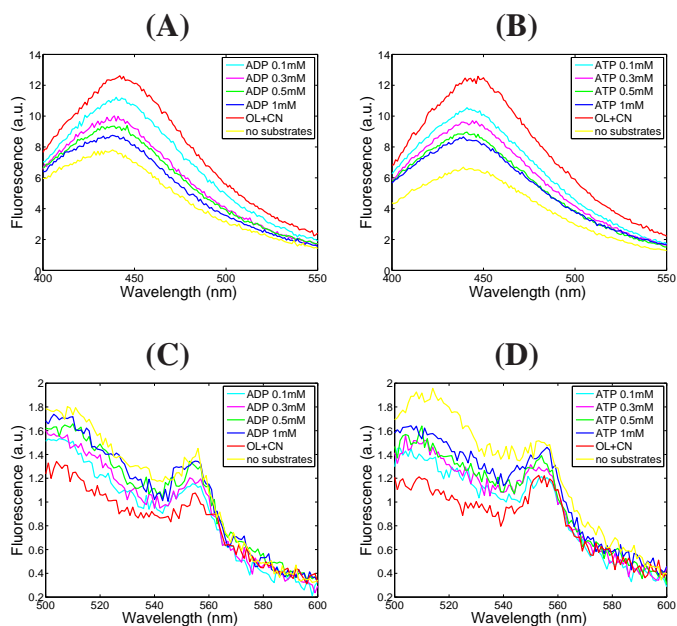


FIG. S1: Fluorescence spectra recorded with excitation light of 340nm (top row) or 465nm (bottom row). Solution with the permeabilized cardiomyocytes was exposed to different levels of exogenous ADP (left column) or ATP (right column) as well as OL+CN. In the beginning of the experiment, spectrum corresponding to oxidized state of mitochondria was recorded in the absence of substrates.

the shape of the NADH fluorescence spectrum when recorded in fluorometer, fluorescence was reduced at wavelengths below 450 nm. For recorded FP fluorescence the influence of FCCP was even larger: FP fluorescence in the presence of FCCP was smaller than fluorescence recorded in the presence of ADP or ATP. Note that this is opposite to expected fluorescence level and the results obtained on a single cell level in microscope. This effect of FCCP in fluorometer and the differences in recorded signal in microscope and fluorometer can be attributed to the optical pathways in those experiments. In the inverted microscope, the cells are recorded while sedimented to the cover glass. As a result, the microscope camera records the signal that comes from the cell, and passes the cover glass and microscope optics (objective, dichroic mirror, emission filter and tube lens). In the fluorometer, cells are in suspension and before excitation light can reach the cell it has to pass the solution. The same applies to the emitted light. While not a problem when cells are exposed to solution with low absorbance, the dif-

ference in optical pathways becomes important in solutions that have significant absorbance, as after addition of FCCP.

To avoid the influence of FCCP in the fluorometer recordings, we used for normalization the fluorescence of permeabilized cells recorded in the absence of substrates (but in the presence of low ADP or ATP). Due to the absence of substrates, mitochondria were in oxidized state leading to high FP and low NADH fluorescence. After recording of the spectra without substrates, spectra were recorded in the presence of different concentrations of ADP or ATP and, in the end of the experiment, in the presence of OL+CN. Representative spectra are shown in Fig. S1.

SUPPORTING REFERENCES

1. Sepp, M., M. Vendelin, H. Vija, and R. Birkedal, 2010. ADP compartmentation analysis reveals coupling between pyruvate kinase and ATPases in heart muscle. *Biophys J* 98:2785–2793.

2. Vendelin, M., M. Eimre, E. Seppet, N. Peet, T. Andrienko, M. Lemba, J. Engelbrecht, E. K. Seppet, and V. A. Saks, 2004. Intracellular diffusion of adenosine phosphates is locally restricted in cardiac muscle. *Mol Cell Biochem* 256-257:229–241.
3. Kongas, O., T. L. Yuen, M. J. Wagner, J. H. G. M. V. Beek, and K. Krab, 2002. High $K(m)$ of oxidative phosphorylation for ADP in skinned muscle fibers: where does it stem from? *Am J Physiol Cell Physiol* 283:C743–C751.
4. Kushmerick, M. J., and R. J. Podolsky, 1969. Ionic mobility in muscle cells. *Science* 166:1297–1298.
5. Bangerth, W., R. Hartmann, and G. Kanschat, 2007. deal.II — a General Purpose Object Oriented Finite Element Library. *ACM Transactions on Mathematical Software* 33:24.

PUBLICATION II

Branovets J, Sepp M, Kotlyarova S, **Jepihhina N**, Sokolova N, Aksentijevic D, Lygate CA, Neubauer S, Vendelin M, Birkedal R;

Unchanged mitochondrial organization and compartmentation of high-energy phosphates in creatine-deficient $GAMT^{-/-}$ mouse hearts

AJP-Heart and Circulatory Physiology, 305(4), 506–520, 2013

Unchanged mitochondrial organization and compartmentation of high-energy phosphates in creatine-deficient $\text{GAMT}^{-/-}$ mouse hearts

Jelena Branovets,¹ Mervi Sepp,¹ Svetlana Kotlyarova,¹ Natalja Jephihina,¹ Niina Sokolova,¹ Dunja Aksentijevic,² Craig A. Lygate,² Stefan Neubauer,² Marko Vendelin,¹ and Rikke Birkedal¹

¹Laboratory of Systems Biology, Institute of Cybernetics, Tallinn University of Technology, Tallinn, Estonia; and ²Department of Cardiovascular Medicine, Wellcome Trust Centre for Human Genetics, University of Oxford, Oxford, United Kingdom

Submitted 12 December 2012; accepted in final form 6 June 2013

Branovets J, Sepp M, Kotlyarova S, Jephihina N, Sokolova N, Aksentijevic D, Lygate CA, Neubauer S, Vendelin M, Birkedal R. Unchanged mitochondrial organization and compartmentation of high-energy phosphates in creatine-deficient $\text{GAMT}^{-/-}$ mouse hearts. *Am J Physiol Heart Circ Physiol* 305: H506–H520, 2013. First published June 21, 2013; doi:10.1152/ajpheart.00919.2012.—Disruption of the creatine kinase (CK) system in hearts of CK-deficient mice leads to changes in the ultrastructure and regulation of mitochondrial respiration. We expected to see similar changes in creatine-deficient mice, which lack the enzyme guanidinoacetate methyltransferase (GAMT) to produce creatine. The aim of this study was to characterize the changes in cardiomyocyte mitochondrial organization, regulation of respiration, and intracellular compartmentation associated with GAMT deficiency. Three-dimensional mitochondrial organization was assessed by confocal microscopy. On populations of permeabilized cardiomyocytes, we recorded ADP and ATP kinetics of respiration, competition between mitochondria and pyruvate kinase for ADP produced by ATPases, ADP kinetics of endogenous pyruvate kinase, and ATP kinetics of ATPases. These data were analyzed by mathematical models to estimate intracellular compartmentation. Quantitative analysis of morphological and kinetic data as well as derived model fits showed no difference between GAMT-deficient and wild-type mice. We conclude that inactivation of the CK system by GAMT deficiency does not alter mitochondrial organization and intracellular compartmentation in relaxed cardiomyocytes. Thus, our results suggest that the healthy heart is able to preserve cardiac function at a basal level in the absence of CK-facilitated energy transfer without compromising intracellular organization and the regulation of mitochondrial energy homeostasis. This raises questions on the importance of the CK system as a spatial energy buffer in unstressed cardiomyocytes.

creatinine shuttle; mitochondrial positioning; confocal imaging; intracellular diffusion barriers; respiration and ATPase kinetics; guanidinoacetate methyltransferase

CREATINE KINASE (CK) plays an important role as an energy buffer in several cell types, including heart, skeletal muscle, and brain. It catalyzes the phosphotransfer between creatine (Cr) and ATP. The importance of CK is highlighted by its strong regulation of local ATP concentration as shown by studies of sarcolemmal ATP-sensitive K^+ channels (1) and rigor formation in permeabilized fibers (55, 57). After induction of ischemia, contraction correlates with the phosphocreatine (PCr) level (14), and, after heart failure, the PCr-to-ATP ratio in the heart is a strong predictor of patient mortality (20). Additionally, a recent study (15) has shown that overexpress-

sion of cytosolic CK improves cardiac contractile function and viability after induced heart failure.

Cr deficiency inhibits the CK system. It may occur due to deficiency of the enzymes that synthesize Cr [L-arginine:glycine amidinotransferase (AGAT) and guanidinoacetate methyltransferase (GAMT)] or the Cr transporter (CrT or SLC6A8), which imports Cr across the sarcolemma. All three cases of Cr deficiency have been found in humans (8, 43), and all have been reproduced in mouse models ($\text{AGAT}^{-/-}$, $\text{GAMT}^{-/-}$, and $\text{CrT}^{-/-}$ mice). The $\text{GAMT}^{-/-}$ model is the most studied to date.

Considering the presumed importance of CK in the heart, it is remarkable that the baseline cardiac function of $\text{GAMT}^{-/-}$ mice is so little affected by the lack of a functional CK system. For example, ejection fraction is normal and only LV systolic pressure is slightly lower in $\text{GAMT}^{-/-}$ mice (19, 42). Furthermore, when the maximal exercise capacity and response to chronic myocardial infarction was compared in $\text{GAMT}^{-/-}$ and wild-type (WT) mice, no significant difference was observed (30). It is only under acute stress conditions that functional deficits are observed in both $\text{GAMT}^{-/-}$ and $\text{CK}^{-/-}$ hearts, e.g., reduced inotropic reserve and impaired recovery from ischemia-reperfusion injury (10, 19, 47). The near-normal basal cardiac performance in $\text{GAMT}^{-/-}$ mice could be due to extensive compensatory changes not identified in Ref. 30, similar to those described in the hearts of $\text{CK}^{-/-}$ mice, where the CK system is disabled by the lack of both cytosolic and mitochondrial muscle-specific CK isoforms. $\text{CK}^{-/-}$ hearts show only minor changes in performance (35), explained in part by cytoarchitectural changes that facilitate direct cross-talk between mitochondria and ATPases (23). Direct cross-talk between organelles is possible due to intracellular diffusion restrictions (60), as evidenced by a low apparent ADP affinity of mitochondrial respiration in permeabilized cardiomyocytes (27), which leads to the coupling of endogenous ATPases to mitochondria or glycolysis (44, 45) as well as anisotropy in diffusion (21, 51). In $\text{CK}^{-/-}$ mice, in the absence of Cr, the apparent ADP affinity of mitochondrial respiration was higher than in control experiments with WT mice (23). This suggests a reduction of the overall diffusion restriction between mitochondria and the surrounding solution (36). However, diffusion was sufficiently restricted for sarco(endo)plasmic reticulum Ca^{2+} -ATPase (SERCA) and myosin ATPase to preferentially use ATP generated in mitochondria as efficiently as in WT mice (23).

The aim of this study was to determine whether the hearts of $\text{GAMT}^{-/-}$ mice exhibit similar compensatory changes as those observed in the hearts of $\text{CK}^{-/-}$ mice. We used three approaches that we have previously applied to rat cardiomyo-

Address for reprint requests and other correspondence: M. Vendelin, Laboratory of Systems Biology, Institute of Cybernetics, Tallinn Univ. of Technology, Akadeemia 21, Tallinn 12618, Estonia (e-mail: markov@ioc.ee).

cytes. Using confocal microscopy, we quantified the three-dimensional (3-D) relative position of mitochondrial centers (as in Ref. 4). This allowed us to detect whether mitochondrial positioning is different in GAMT^{-/-} mice. On permeabilized cardiomyocytes, we recorded a full set of kinetic data to analyze the intracellular compartmentation of ADP/ATP using mathematical models. In rat cardiomyocytes, we discovered a strong functional coupling between pyruvate kinase (PK) and a fraction of ATPases (45). Because the activity of other phosphotransfer systems increases in CK^{-/-} mice (34) and because failing hearts experiencing a loss of CK (2), we speculated whether the coupling between PK and ATPases is upregulated in GAMT^{-/-} mice. Finally, we used fluorescence microscopy to record changes in NADH and flavoprotein (Fp) autofluorescence when permeabilized cardiomyocytes were exposed to increasing doses of ADP (as in Ref. 22). This would test whether the ADP kinetics of respiration, as recorded on a population level, also occurred on the single cell level.

MATERIALS AND METHODS

Animal procedures were approved by the Estonian National Committee for Ethics in Animal Experimentation (Estonian Ministry of Agriculture).

Animals. We received GAMT^{-/-} mice and WT littermates, which had been bred at The Wellcome Trust Centre for Human Genetics (Oxford, UK). Mice had been backcrossed on to a C57Bl/6J background for at least eight generations. Animals were kept in our local animal facility in cages with free access to water and food (vegetable-based, Cr-free chow, R70 from Lactamin). Mice of different genotypes were housed separately to prevent GAMT^{-/-} mice from taking up Cr via coprophagia of feces from WT littermates (41).

Cardiomyocytes were successfully isolated from eight GAMT^{-/-} mice (4 females and 4 males) and nine WT mice (5 females and 4 males) of similar age (female WT: 46.9 ± 4.9 wk and female GAMT^{-/-}: 45 ± 4.3 wk; male WT: 45.6 ± 1.5 wk and male GAMT^{-/-}: 45.9 ± 1.4 wk).

Genotyping. Knockout and WT mice were genotyped by PCR. Briefly, genomic DNA was extracted from tissue samples by SDS/proteinase K digestion followed by isopropanol precipitation. PCR amplification of the DNA fragments was performed using the following specific primers: 5'-CAGGCTCCCACCTTGA-3', 5'-AGGCCTACCCGCTTCCATTG-3', 5'-CCTCAGGCTCCCACCTTGG-3', and 5'-GGTCTCCCAACGCTCCATCACT-3'. PCRs were carried out in a 25- μ l volume containing 1 \times PCR buffer (Bioline Immobuffer), 0.5 mM dNTP mixture (Fermentas), 2 mM MgCl₂ (Bioline), 0.5–0.7 pmol of each primer (TAG Copenhagen), 5% DMSO (Sigma), 0.6 M betaine (Sigma), 0.06 U/ μ l IMMOLASE DNA polymerase (Bioline), and 5 μ l template DNA. After the initial denaturation step at 94°C for 5 min, nine cycles of PCR were carried out as follows: denaturation at 94°C for 60 s, annealing at 60°C for 60 s, and extension at 72°C for 30 s. In each cycle, the temperature was decreased by 0.5°C in each consequent annealing step. This was followed by 34 cycles of the following PCR: denaturation at 94°C for 60 s, annealing at 55°C for 60 s, and extension at 72°C for 30 s. This was done in a thermal cycler (Bio-Rad DNA Engine Peltier Thermal Cycler). PCR products were electrophoresed on a 1% agarose gel with ethidium bromide in 1 \times Tris-borate-EDTA. Amplification of a single 265-bp product or a 427-bp PCR product corresponded to WT GAMT (GAMT^{+/+}) or homozygous GAMT knockout (GAMT^{-/-}) genotype, respectively. Simultaneous amplification of a 265- and 427-bp fragments corresponded to a heterozygous GAMT (GAMT^{+/-}) genotype.

Total Cr content. The total Cr content was measured enzymatically from mouse hindlimb skeletal muscle. The metabolite extraction from tissue samples was done as follows. A 50- to 100-mg piece of tissue was homogenized in 2 ml of 0.6 M perchloric acid with 2 mM EDTA.

Water was added to provide a total volume of 10 ml, and the suspension was centrifuged at 10,000 g for 10 min at 4°C. The supernatant was neutralized with KOH, the precipitated salt was removed by centrifugation, and total Cr levels were assayed immediately from the resulting extract (pH 7.0–7.2) via coupled enzymatic reactions using a spectrofluorometer. The enzymatic reaction was performed in 500 μ l of 100 mmol/l potassium phosphate buffer (pH 7.5) containing 5 mmol/l MgCl₂, 16 kU/l CK, 8 mmol/l ADP, 16 kU/l hexokinase, 4 mM glucose, 40 kU/l creatinase, 20 kU/l sarcosine oxidase, 4 kU/l horseradish peroxidase, 10 μ mol/l Amplex red, and 6–40 μ l tissue extract. This mixture ensured that Cr and PCR were degraded by creatinase, which led to the production of H₂O₂ (which was later determined fluorescently using Amplex red conversion to resorufin). The blank mixture was identical except for the omission of creatinase. The reaction mixture was incubated for 30 min at room temperature. H₂O₂ was determined spectrofluorometrically in 2 ml of 100 mmol/l phosphate buffer containing 5 mmol/l MgCl₂. Fluorescence measurements were performed using 4-ml plastic cuvettes (four-faced transparent cuvettes, Deltalab, Rubí, Spain) in an RF-5301 PC spectrofluorometer (Shimadzu Scientific Instruments, Kyoto, Japan). The temperature was maintained at 25°C (Julabo F12-ED, JULABO Labortechnik). First, background fluorescence of the buffer without enzymes was measured, and 1 μ l of 5 mM Amplex red and 5 μ l of 100 U/ml horseradish peroxidase were then added to measure the contribution of Amplex red to fluorescence intensity. Finally, the fluorescence of the diluted reaction mixture was measured. At the end of each experiment, a calibration signal was generated with five additions of 1 μ l of 0.1 mM H₂O₂, each leading to a concentration increase of 50 nM. Measured fluorescence intensities (emission/excitation = 585/570 nm) were fitted assuming a linear relationship between fluorescence and the resorufin concentration in the cuvette, with the offset determined by the background fluorescence of the buffer. The fit was performed by minimizing the least-square difference between calculated and measured fluorescence through variation of the gain (fluorescence-to-resorufin concentration ratio), total Cr content, and resorufin contamination of Amplex red solution (proportional to the Amplex red concentration). Cr concentrations were expressed as nanomoles per milligram wet weight tissue. All measurements were repeated with three different dilutions, and a paired *t*-test between recordings with and without creatinase (sample vs. blank) was used to determine whether the total Cr content was identifiable by the method (a significance level of *P* < 0.05 was used).

Isolation of cardiomyocytes. Isolation of cardiomyocytes was carried out as previously described (45). Briefly, the heart was excised and immediately transferred to ice-cold wash solution (see composition below). It was cannulated via the aorta on a Langendorff perfusion system, which was thermostatted to 38.5°C (Julabo ED, JULABO Labortechnik). The heart was first perfused with wash solution at a constant pressure of 80 cmH₂O for at least 5 min. The flow rate under these conditions was 3.68 ± 1.68 ml/min (*n* = 17). After the heart was washed free of blood, the perfusion was switched to a digestion solution containing an additional 0.25 mg/ml collagenase P (Roche) and 3 mg/ml BSA. Perfusion was also switched to a constant flow of 1 ml/min until the pressure had decreased to 10–15% of the initial pressure at 80 cmH₂O and the heart was soft. After perfusion, the ventricles were isolated. They were cut into four pieces, which were incubated further in the digestion solution at 38.5°C with gentle shaking until the tissue started falling apart. Cells were further dissociated with a 5-ml pipette. Sedimentation solution (5 ml) was added before the cells were filtered into a glass tube. As a result, the cell suspension was a mix of isolated cardiomyocytes from the left and right ventricles. Cells were washed by sedimentation. First, extracellular Ca²⁺ was gradually increased to 1 mM to ensure Ca²⁺ tolerance of the cells (Ca²⁺ from a stock of 1 M CaCl₂ was added to the sedimentation solution). After this, extracellular Ca²⁺ was washed out again by washing the cells three times with 10 ml sedimentation solution.

Mitochondrial imaging. Freshly isolated cells kept in sedimentation solution were loaded with 1 μM TMRE (T-669, Molecular Probes, Life Technologies) for at least 15 min. A small fraction of the cells was added to 200 μl sedimentation solution in the chamber of a flexiPERM micro 12 reusable silicone cell culture chamber (Greiner Bio-One) attached to a coverslip. Confocal images were acquired on a Zeiss LSM 510 Duo built around an inverted Axio Observer Z1 microscope (Carl Zeiss) with a $\times 63/1.2$ numerical aperture (NA) water-immersion objective. The signal was acquired via a high-voltage single photomultiplier tube using 8-bit mode; the pinhole was set to one Airy disk. TMRE was excited with a 543-nm laser, and emission was recorded through a 575-nm long-pass filter. These experiments were carried out at room temperature.

Estimating the relative positioning of mitochondrial centers. Mitochondrial positioning was quantified by statistical analysis of the relative distances between neighboring mitochondrial centers, as in Ref. 4. In short, the following procedure was used. Each stack of confocal images was blurred by a 3-D Gaussian blur with a SD of 0.3 μm in all directions. The position of all mitochondrial centers was determined by finding local fluorescence maxima of the blurred 3-D stack of images. Subsarcolemmal mitochondria and mitochondria around the nucleus (perinuclear mitochondria) were filtered out as judged by the eye. A space around each mitochondrial center was divided into 14 sectors: 2 sectors in the y -direction along the myofibril, 2 sectors in the x -direction across the myofibril in the image plane, 2 sectors in the z -direction across the myofibril perpendicular to the image plane, 4 diagonal sectors in the xy -direction, and 4 diagonal sectors in the yz -direction (Fig. 1). For each mitochondrial center, we found the closest neighboring mitochondrial center in each of these sectors, as shown in Fig. 1. Finally, the relative position of these neighboring mitochondrial centers was analyzed by finding the probability density function and cumulative probability distribution, as in Ref. 4.

For statistical analysis, we found for each cell separately the cumulative distribution function for the nearest neighboring mitochondria in each direction. The averaged results of the distance at 25%, 50%, and 75% of the distribution function for R and R_{XZ}

(notation from Fig. 5) were compared for WT and GAMT^{-/-} cardiomyocytes, as detailed in the RESULTS.

Respirometer recordings. Respirometer recordings were used to determine 1) the respiration kinetics of permeabilized cells stimulated by stepwise increases in ADP or ATP and 2) the inhibition of ATP-stimulated respiration by a competitive assay consisting of phosphoenol pyruvate (PEP; 5 mM) and PK (20 IU/ml). For this, we used a Strathkelvin RC 650 respirometer equipped with six 1302 O₂ electrodes connected via a 929 Oxygen System interface (all from Strathkelvin Instruments) to a computer. The respirometer was thermostatted to 25°C (Julabo F12-ED, JULABO Labortechnik). The O₂ tension in each chamber was recorded by the software provided by Strathkelvin and our homemade software, which immediately calculated the rate of O₂ consumption as well. The latter is open-source software and is freely available at <http://code.google.com/p/iocbio/wiki/IOCBioStrathKelvin>.

For recordings of ADP kinetics, a 15- to 20- μl cell suspension was added to the respiration chamber containing 2 ml Cr and PCR-free respiration solution (see composition below). Cells were allowed at least 5 min to permeabilize before the steady-state basal respiration rate (V_0) was recorded. ADP was added to the respirometer chamber using a Hamilton syringe (801RN, Hamilton Bonaduz). The ADP concentration was increased in steps, and the respiration rate was allowed to reach steady state for at least 2 min before the addition of more ADP. Recordings of ATP kinetics were carried out in a similar way except that a 30- to 50- μl cell suspension was added to the chamber and ATP was added instead of ADP. To record how a competitive ADP-trapping assay consisting of PEP and PK competes with mitochondria for the consumption of ADP from ATPases, a 30- to 60- μl cell suspension was added to the respirometer chamber. After recording V_0 , 2 mM ATP was added to stimulate ATPases. Initially, this endogenously produced ADP was exclusively consumed by the mitochondria and stimulated respiration ($V_{2 \text{ mM ATP}}$). The addition of 5 mM PEP (no. P-7002, Sigma-Aldrich) activated endogenous PK to compete with mitochondria for the consumption of ADP and the lowered respiration rate (V_{PEP}). Further addition of 20 U/ml exogenous PK (no.

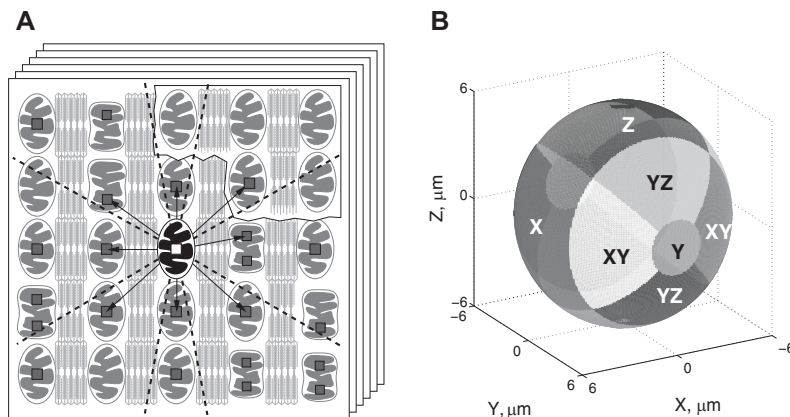


Fig. 1. Method used to analyze distribution of mitochondria in cardiomyocytes, taken from Ref. 4. *A*: first, a series of Z-stack confocal images of mitochondria in nonpermeabilized cardiomyocytes was acquired (scheme). Second, the local fluorescence maxima (small squares) were found. As indicated in the scheme, the maxima were not always on the same image in the stack. Note that sometimes two fluorescence maxima seem to be found per mitochondrion (as shown in *A*). Next, the closest neighbors were found for each mitochondrion, one per sector (the projections of the sector borders in two dimensions are shown by the dashed lines). In this scheme, the mitochondrion, in which neighbors are sought, is highlighted, and the closest neighbors to this mitochondrion are indicated by arrows. Note that the closest mitochondria in some sectors are not always from the same image in the stack. The relative coordinates of the closest neighbors, i.e., the coordinates relative to the highlighted mitochondrion, were stored and further analyzed. *B*: division of three-dimensional space into the sectors, with sectors shown by the different levels of gray. The mitochondrion for which neighbors are sought is positioned at the origin of coordinate system. Here, the coordinate y -axis corresponds to the fiber orientation. The sector names are shown in the scheme.

10109045001, Roche), lowered the respiration rate ($V_{PEP + PK}$) even more.

Spectrophotometer recordings. ATP kinetics of ATPases and ADP kinetics of endogenous PK were recorded using an Evolution 600 spectrophotometer (Thermo Fisher Scientific) equipped with a Peltier water-cooled cell changer (SPE 8 W, Thermo Fisher Scientific) to maintain temperature at 25°C. ADP production by ATPases in permeabilized cardiomyocytes was recorded in 2 ml respiration solution using a coupled assay consisting of 5 mM PEP (no. P-7002, Sigma-Aldrich), 0.3 mM NADH (no. 10128015001, Roche), 7.2 U/ml LDH (no. 61311, Sigma-Aldrich), and 20 U/ml PK (no. 10109045001, Roche). To avoid ADP consumption by mitochondria, respiration was inhibited by 5 mM NaCN (no. 205222, Sigma-Aldrich) and 10 μ M oligomycin (no. 75351, Sigma-Aldrich). The basal ATPase rate was first recorded in the absence of ATP and then at increasing concentrations of ATP. Rates were recorded for 3 min after each addition, and steady state was verified for each step. NADH was replenished as needed to keep absorbance between 1.7 and 0.7 (the linear range of NADH consumption as verified by preliminary experiments; data not shown). The ADP kinetics of endogenous PK were recorded using the same coupled assay (where only 5 mM NaCN, 10 μ M oligomycin, 5 mM PEP, 0.3 mM NADH, and 7.2 U/ml LDH were added), and PK activity was recorded at increasing ADP concentrations.

For normalization, the protein content was measured with a Nano-drop 2000 (Thermo Fisher Scientific).

Mathematical model. For a detailed description of the model, see Ref. 45. In brief, models of different complexity were considered (Fig. 2). All models included three separate compartments: extracellular solution, cytoplasm, and intermembrane space (IMS). *Models 3* and *4* also included a fourth compartment (*compartment 4*) with PK and ATPase to describe coupling between glycolysis and ATPases, as described in Ref. 45. The processes considered in the models were diffusion between compartments restricted by diffusion barriers, the reactions of ATPases, oxidative phosphorylation, and the reactions of endogenous PK. The models containing two groups of ATPases (2, 3, and 4) were also considered in a simplified form (2s, 3s, and 4s) with both groups of ATPases having the same affinities for ATP and ADP.

For simplicity, ATP synthesis in mitochondria was described by the simple phenomenological Michaelis-Menten-type equation involving the concentrations of ATP and ADP only in the IMS, as shown in Fig. 2. Note that this approach is possible due to high concentrations of P_i , oxygen, and substrates, as used in our experiments. This simplification allowed us to simulate diffusion and reactions in the intracellular compartments only (cytoplasm, IMS, and *compartment 4*) and thus allowed us to ignore the details of the reactions involved in the respiratory chain. The same approach has been applied by us earlier and used to estimate the compartmentation of ATPases and intracel-

lular diffusion restrictions in two dimensions (52), three dimensions (36), and simplified multicompartment (45) analysis of the intracellular environment.

To compare the models, the goodness of fit was evaluated using Akaike information criteria (AIC), corrected AIC (AIC_c), and Bayesian information criteria (BIC), which were calculated for each model. For all three criteria, the best-fitting model is the one with the minimum criterion value. Those criteria take into account the goodness of fit and number of parameters in the model. Using AIC_c and BIC, a larger number of parameters is penalized more than in AIC. Multiple goodness criteria were used to ensure that the conclusions would not depend on the selection of one particular criterion.

In addition, models were compared by an *F*-test for nested models, which allows comparison of *models 1* and *2* with *model 3* as well as *models 1* and *2* with *model 4*. The *F*-test takes the number of parameters into account so that statistical significance indicates that the more complicated model fits the data better irrespective of the number of parameters.

Next, the *F*-test was used to evaluate confidence intervals for each of the fitted model parameters. Confidence intervals were calculated using an *F*-test and show the range where the fit is worse than an optimal fit but with a *P* value larger than 0.05 (in terms of extra sum of squares), as in Ref. 45.

Finally, to test whether the data recorded in WT and GAMT^{-/-} cardiomyocytes were significantly different from each other, the data were fit either separately for different types of cardiomyocytes or by fitting both sets with the same model parameters (pooled data set). The *F*-test was applied to test whether an increased number of parameters induced by fitting the experiments separately was justified or whether the better fits were due to chance. For this test, a fit of pooled data by a single set of model parameters can be considered as a simplified version of fitting the data separately using two sets of model parameters: one for WT cardiomyocytes and one for GAMT^{-/-} cardiomyocytes.

For a detailed model description, numeric methods, and statistical analysis, see Ref. 45.

Recordings of NADH and Fp autofluorescence. Recordings of NADH and Fp autofluorescence were performed as described in Ref. 22. In brief, micro-scope experiments were performed on an inverted Nikon Eclipse Ti-U microscope (Nikon, Tokyo, Japan; objective CFI Super Plan Fluor ELWD $\times 20/0.45$ NA) equipped with two tiers of motorized filter turrets for simultaneous acquisition of transmission and fluorescence images. For images of NADH and Fp autofluorescence, respectively, light from a Prior Lumen 200 with a 200-W metal halide lamp with extended wavelength (Prior Scientific, Cambridge, UK) was passed via an optical fiber into the upper filter turret. For NADH recordings, the light was passed through a 340/26-nm excita-

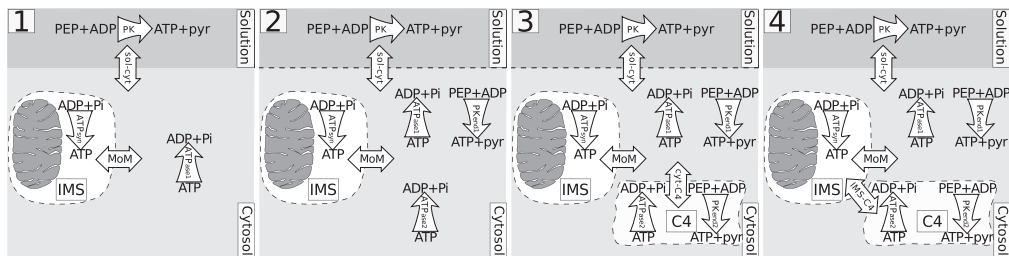


Fig. 2. Schematic diagrams of *models 1–4*. Compartments are indicated by dashed lines, reactions by single-headed curved arrows, and exchange between compartments by double-headed straight arrows. All models have compartments representing the solution, cytosol, and mitochondrial intermembrane space (IMS). *Models 3* and *4* include a fourth compartment (C4). The reactions considered are mitochondrial ATP synthesis in the mitochondrial matrix leading to the conversion of ADP to ATP in the mitochondrial IMS (ATP_{syn}), ATP consumption by ATPases (ATPase1 and ATPase2), and ATP synthesis by endogenous pyruvate kinase (PK; PKend1 and PKend2) and exogenous PK. The following exchanges between compartments were calculated: solution and cytosol (sol-cyt), IMS and cytosol through the outer mitochondrial membrane (MoM), cytosol and C4 (cyt-C4), and IMS and C4 (IMS-C4). PEP, phosphoenol pyruvate.

tion filter onto a 400-nm long-pass dichroic mirror, which deflected the light onto the specimen. Light emitted from the specimen passed back through the upper filter cube to a 510 XR dichroic in the lower filter cube and reflected through a 460/80-nm emission filter to an Andor Ixon EMCCD camera (Andor Technologies, Belfast, UK). For Fp recordings, the light was passed through a 465/30-nm excitation filter onto a 510-nm dichroic mirror, which deflected the light onto the specimen. Light emitted from the specimen passed back through the upper filter cube to a 560 XR dichroic in the lower filter cube and reflected through a 525/50-nm emission filter. All filters were purchased from AHF Analysetechnik. For each filter, the first number describes the mode wavelength and the second number describes the total bandwidth at half-maximum transparency (half-minimum optical density). This means that a 340/26-nm filter mainly passes light between 327 and 356 nm. Filter specifications, including plots of their optical density at different wavelengths, can be found on the suppliers website (<http://www.ahf.de>). Transmission images together with images of NADH or Fp autofluorescence were acquired every 30 s. To reduce photobleaching, a Uniblitz shutter (VCM-D1, Vincent Associates, Rochester, NY) timed the light exposure with the acquisition.

Immediately before each experiment, a new batch of cells was permeabilized for 5 min with gentle mixing in an Eppendorf tube with respiration solution containing 25 µg/ml saponin and 50 µM ADP. A fraction of the permeabilized cells was put into a diamond-shaped fast-exchange chamber (15 × 6 mm, RC-24N, Warner Instruments, Harvard Apparatus, March-Hugstetten, Germany) on the microscope. Cells were allowed to sediment for 5–10 min before the superfusion was started with respiration solution containing different concentrations of ADP. Only cells located in the middle of the chamber were used for measurements. According to the manufacturer, the geometry of the chamber provided laminar flow of solutions during experiments at the used flow rate of ≈0.5 ml/min and was laminar in our conditions, as confirmed by mathematical model of the flow (22). The ADP concentration was increased stepwise from 50 to 100, 300, 500, 1,000, and 2,000 µM, and cells were superfused for at least 4.5 min at each step.

Fluorescence signal intensity from microscope single cell experiments was analyzed using ImageJ software. Both regions containing each cell and background regions were selected, and corresponding average fluorescence signal intensities were determined with the ImageJ plug-in “measure stack.” Background fluorescence was then subtracted from cell fluorescence, and the data were plotted on a timescale. From the latter plot, average fluorescence was found for each condition to which the cell was exposed (ADP concentration, uncoupling or block of oxidative phosphorylation). To enable comparison between cells, signals were normalized to maximum and

minimum fluorescence recorded under fully reduced (respiration inhibited with oligomycin and cyanide) or oxidized (mitochondria uncoupled with FCCP) conditions.

Solutions. The wash solution consisted of (in mM) 117 NaCl (no. 71379, Sigma-Aldrich), 5.7 KCl (no. P-5405, Sigma-Aldrich), 1.5 KH₂PO₄ (no. P-0662, Sigma-Aldrich), 4.4 NaHCO₃ (no. S-6014, Sigma-Aldrich), 1.7 MgCl₂ (no. 63068, Sigma-Aldrich), 21 HEPES (no. H-3375, Sigma-Aldrich), 20 taurine (no. 86329, Sigma-Aldrich), and 11.7 glucose (no. 158968, Sigma-Aldrich). pH was adjusted to 7.4 with NaOH.

For the collagenase solution, 0.25 mg/ml collagenase P (no. 11213873001, Roche) and 3 mg/ml BSA (no. 10775835001, Roche) was added to 40 ml of the wash solution.

For the sedimentation solution, 2 mM pyruvate (no. P-2256, Sigma-Aldrich), 10 µM leupeptin (no. 11034626001, Roche), 2 µM soybean trypsin inhibitor (no. 93619, Sigma-Aldrich), and 3 mg/ml BSA (no. 10775835001, Roche) were added to 60 ml of the wash solution.

The respiration solution contained (in mM) 110 sucrose (no. S-1888, Sigma-Aldrich), 60 K-lactobionic acid (no. L-2398, Sigma-Aldrich), 3 KH₂PO₄ (no. P-0662, Sigma-Aldrich), 3 MgCl₂ (no. 63068, Sigma-Aldrich), 20 HEPES (no. H-3375, Sigma-Aldrich), 20 taurine (no. 86329, Sigma-Aldrich), 0.5 EGTA (no. 71379, Sigma-Aldrich), 0.5 DTT (no. D-0632, Sigma-Aldrich), 2 malate (no. M-6413, Sigma-Aldrich), and 5 glutamate (no. 49449, Sigma-Aldrich). pH was adjusted to 7.1 with KOH. Immediately before use, 5 mg/ml BSA (no. 10775835001, Roche) and 20 µg/ml saponin (no. 47036, Sigma-Aldrich) were added.

The ADP stock solution contained 200 mM ADP (no. A-2754, Sigma-Aldrich) and 60 mM MgCl₂ (no. 63068, Sigma-Aldrich). pH was adjusted to 7.1 with KOH.

The ATP stock solution contained (in mM) 200 ATP (no. 10127531001, Roche), 200 Mg-acetate (no. M-5661, Sigma-Aldrich), and 20 HEPES (no. H-3375, Sigma-Aldrich). pH was adjusted to 7.1 with KOH.

Concentrations of the uncoupler and respiration blockers were as follows: FCCP (10 µM, no. Asc-081, Ascent Scientific), oligomycin A (10 µM, no. 579-13-5, Tebu-bio), and sodium cyanide (5 mM, no. 205222, Sigma-Aldrich).

Statistics. Raw data were analyzed using homemade software. Values are given as means ± SD.

RESULTS

Characteristics of WT and GAMT^{-/-} mice. Genotypes of the mice were confirmed by PCR. The results are shown in Fig. 3.

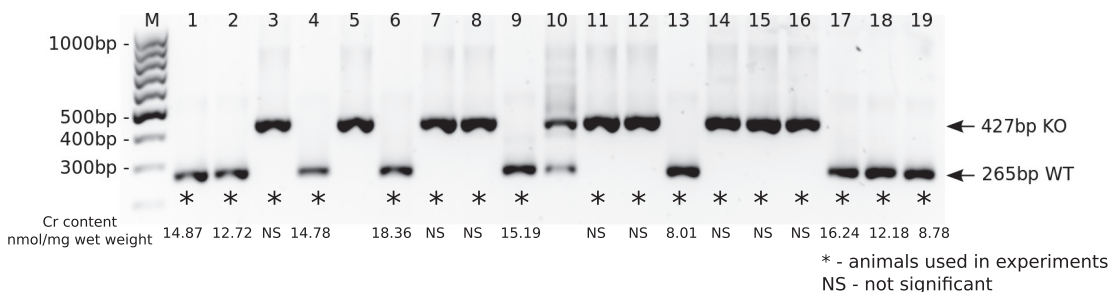


Fig. 3. Genotyping of guanidinoacetate methyltransferase (GAMT)-deficient (GAMT^{-/-}) mice by PCR. After PCR amplification, samples were analyzed on 1% agarose gel stained with ethidium bromide along with a DNA ladder (lane M: GeneRuler 100-bp DNA Ladder). The 265- and 427-bp-long PCR products corresponded to wild-type (WT) GAMT (GAMT^{+/+}) or homozygous GAMT knockout (GAMT^{-/-} KO) genotypes, respectively. *Animals that were used in experiments. Total skeletal muscle creatine (Cr) content (expressed as nmol/mg wet wt) is shown under each mouse used in the experiments, respectively. The levels of Cr in GAMT^{-/-} mice were statistically not significant (NS).

GAMT^{-/-} mice had a lower body weight than their WT littermates [female WT: 24.2 ± 3.8 g vs. female GAMT^{-/-}: 17.5 ± 2.6 g ($P < 0.05$); male WT: 34.5 ± 5.3 g vs. male GAMT^{-/-}: 23.0 ± 2.7 g ($P < 0.01$)]. In female mice, tibial length was also shorter in GAMT^{-/-} than WT mice [female WT: 21.8 ± 0.2 mm vs. female GAMT^{-/-}: 21.1 ± 0.6 mm ($P < 0.05$); male WT: 22.6 ± 0.6 mm vs. male GAMT^{-/-}: 21.7 ± 0.8 mm ($P = 0.1330$)]. This is in agreement with previous observations (19, 41).

Total Cr content was measured enzymatically in GAMT^{-/-} and WT mice used in the experiments. Skeletal muscle Cr content was 13.46 ± 3.40 nmol/mg wet wt in WT control mice ($n = 9$) and undetectable in GAMT^{-/-} mice ($n = 8$) (Fig. 3). This was confirmed statistically with a paired *t*-test showing no significant difference in the Cr content between the GAMT^{-/-} sample and the corresponding blank ($P > 0.05$) and a signif-

icant difference between the WT sample and the corresponding blank ($P < 0.05$).

Mitochondrial positioning. Visual inspection of the confocal images showed similar mitochondrial distribution in GAMT^{-/-} and WT cardiomyocytes. This was confirmed by quantitative analysis of the relative positioning of the mitochondrial centers (Figs. 4 and 5). Figure 4 shows the probability densities of the closest mitochondrial centers found in the different sectors. There was no difference between GAMT^{-/-} and WT cardiomyocytes. Figure 5 shows plots of the cumulative distribution functions. The graphs for WT and GAMT^{-/-} cardiomyocytes were overlapping or were very close in all directions (Fig. 5).

For statistical analysis, we found the averaged distances R and R_{YZ} (notation from Fig. 5) at 25%, 50%, and 75% of the cumulative distribution function (Table 1). There was no significant

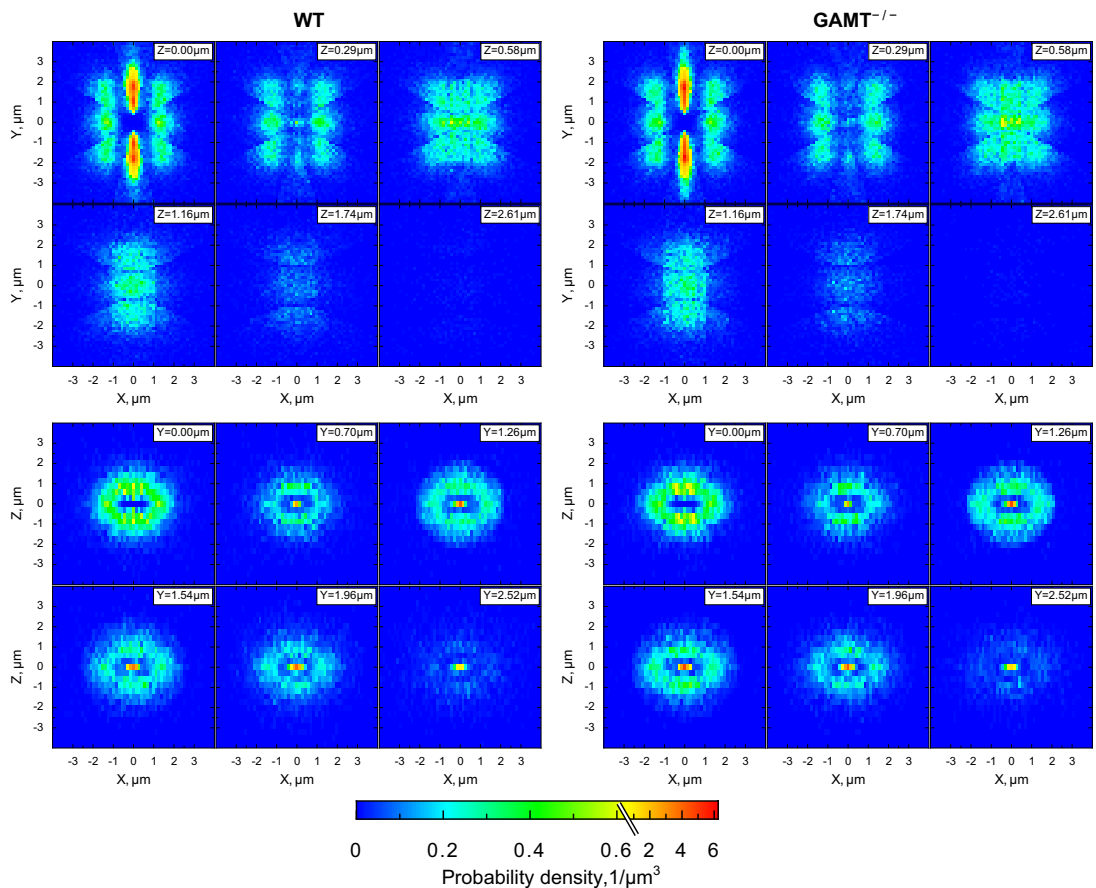


Fig. 4. Probability density of the closest mitochondrial centers in each of the directions in WT (left) and GAMT^{-/-} (right) cardiomyocytes. A total of 24,588 (WT) and 23,405 (GAMT^{-/-}) mitochondria from 6 cells were analyzed. Each mitochondrial center was considered to be in the origin (0, 0). The space around was divided into 14 sectors, and the distribution of the closest mitochondrial centers in each sector was analyzed. Results from sectors with the same direction were pooled. Here, and in the following analysis, the *y*-direction was taken along the myofibrils and *x*- and *z*-directions were transversal directions at and perpendicular to the image planes, respectively. The *xy*- and *yz*-directions were diagonal directions. Two-dimensional probability density is shown at different planes perpendicular to the *z*-axis (*XY*-planes; top) or the *y*-axis (*XZ*-planes; bottom) at different distances from the origin as indicated at the top right corner of each plane. Note how similar the mitochondrial distributions were in GAMT^{-/-} and WT cardiomyocytes.

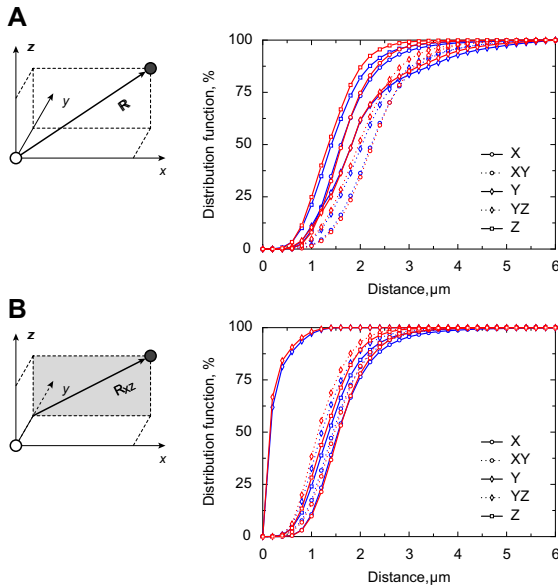


Fig. 5. Cumulative distribution function of the distance between centers of neighboring mitochondria in different directions. The distribution functions for the following distances were calculated: distance (*R*) from the origin to the nearest mitochondrion in each direction (A) and distance (*R_{XZ}*) from the y-axis through the origin to the nearest mitochondrion in each direction (B). The differences in the corresponding distances are highlighted on the schemes shown in A and B, left. If the rows of mitochondria were parallel, *R_{XZ}* would be the same in the X- and XY-directions and Z- and YZ-directions. Indeed, their distribution functions were very close. For parallel rows, *R_{XZ}* in the Y-sector would be 0. Note in both A and B that the distribution functions for the WT (blue) and GAMT^{-/-} (red) groups were either overlapping or very close to each other.

difference in the distances between WT and GAMT^{-/-} cardiomyocytes as analyzed with mixed-design ANOVA. In this statistical test, the between-subject variables were mouse genotypes (2 levels: WT or GAMT^{-/-}) and the within-subject variables were directions for *R* and *R_{XZ}* (5 directions for each, 10 levels in total) and percentile points (3 levels). On the basis of ANOVA, we concluded that there was no significant main

effect of genotype, *P* = 0.28. No significant differences in the distances were found when we compared the distances obtained at all directions and all percentile points for WT and GAMT^{-/-} cardiomyocytes using Welch's *t*-test and correcting for multiple comparisons using the Šidák correction.

From this analysis, we conclude that the distances between mitochondrial centers in WT and GAMT^{-/-} cardiomyocytes were not significantly different. Furthermore, we did not observe any compensation in mitochondrial positioning to the lack of a functional CK shuttle in GAMT^{-/-} cardiomyocytes.

Kinetic recordings. In the respirometer, we recorded the kinetics of ADP- and ATP-stimulated respiration in permeabilized cardiomyocytes. ADP directly stimulates respiration, whereas ATP is first hydrolyzed by ATPases to ADP, which diffuses to the mitochondria and stimulates respiration (Fig. 6, A and B). In addition, we recorded how ATP-stimulated respiration is affected by a competitive ADP-trapping system consisting of PEP activating endogenous PK and PEP activating additional 20 U/ml exogenous PK (Table 2). The respiration data were complemented by spectrophotometric recordings of the kinetics of ATP-stimulated ATPase activity and ADP-stimulated endogenous PK activity using a coupled assay (Fig. 6, C and D).

Analysis of kinetic data by mathematical models. The experimental data were fitted by several mathematical models with different levels of compartmentation (Fig. 2). The model fits were compared with the measurements shown in Fig. 6 and Table 2. To analyze the data obtained from WT and GAMT^{-/-} mouse cardiomyocytes, we first fitted the data separately. The data were then pooled together and fitted (parameters shown in Table 3). As expected, the fit was better when the models were allowed to fit the WT and GAMT^{-/-} data separately (quantified by sum of squares in least-squares fitting). However, according to the extra sum-of-squares *F*-test (*F*-test), the increased number of parameters induced by fitting the experiments separately was not justified, and the better fits were due to chance (depending on the model, *P* was from 0.37 to 0.99). From this, we concluded that the kinetic recordings in WT and GAMT^{-/-} mouse cardiomyocytes were not significantly different and that the two cases could be described by a single set of a model parameters.

Table 1. Distances at 25%, 50%, and 75% of the distribution function for *R_{XYZ}* and *R_{XZ}*

Direction	25%		50%		75%	
	WT	GAMT ^{-/-}	WT	GAMT ^{-/-}	WT	GAMT ^{-/-}
<i>R_{XYZ}</i>						
X	1.28 ± 0.04	1.31 ± 0.08	1.61 ± 0.04	1.64 ± 0.07	2.07 ± 0.09	2.06 ± 0.09
XY	1.81 ± 0.08	1.88 ± 0.12	2.25 ± 0.07	2.29 ± 0.11	2.76 ± 0.10	2.78 ± 0.13
Y	1.35 ± 0.15	1.39 ± 0.18	1.83 ± 0.08	1.82 ± 0.09	2.56 ± 0.29	2.39 ± 0.15
YZ	1.61 ± 0.08	1.57 ± 0.10	2.08 ± 0.11	2.01 ± 0.11	2.65 ± 0.23	2.48 ± 0.11
Z	1.07 ± 0.05	0.99 ± 0.08	1.43 ± 0.08	1.35 ± 0.08	1.89 ± 0.19	1.75 ± 0.08
<i>R_{XZ}</i>						
X	1.23 ± 0.03	1.27 ± 0.08	1.55 ± 0.04	1.58 ± 0.07	2.00 ± 0.09	2.00 ± 0.10
XY	1.12 ± 0.03	1.17 ± 0.07	1.45 ± 0.02	1.50 ± 0.08	1.88 ± 0.05	1.90 ± 0.10
Y	0.08 ± 0.01	0.07 ± 0.02	0.16 ± 0.03	0.12 ± 0.04	0.32 ± 0.09	0.24 ± 0.06
YZ	0.92 ± 0.04	0.86 ± 0.07	1.23 ± 0.05	1.14 ± 0.08	1.68 ± 0.15	1.54 ± 0.10
Z	1.03 ± 0.05	0.95 ± 0.08	1.38 ± 0.08	1.29 ± 0.08	1.82 ± 0.20	1.68 ± 0.09

Values (in μm) are means ± SD; *n* = 6 wild-type (WT) cardiomyocytes and 6 guanidinoacetate methyltransferase (GAMT)-deficient (GAMT^{-/-}) cardiomyocytes. *R_{XYZ}*, distance from the origin to the nearest mitochondrion; *R_{XZ}*, distance from the y-axis through the origin to the nearest mitochondrion.

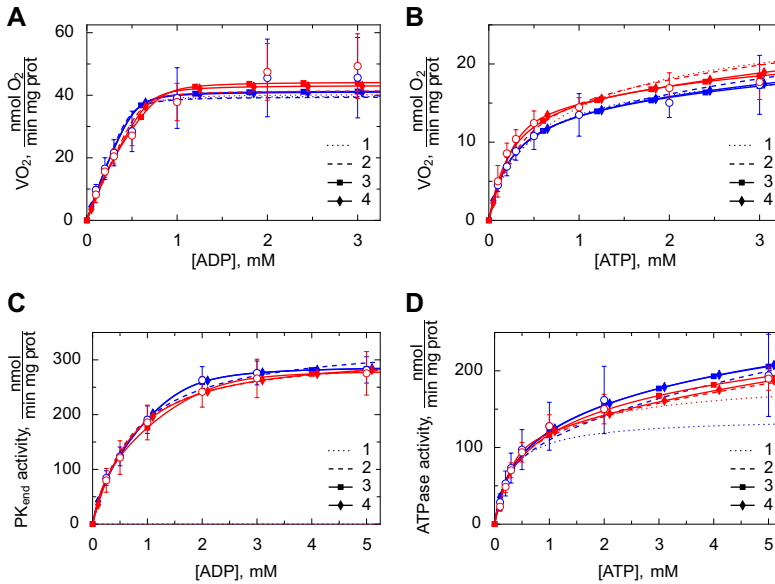


Fig. 6. Kinetic analysis of permeabilized cardiomyocytes from WT (blue) and GAMT^{-/-} (red) mice. Measurements were performed in respiration solution containing 2 mM malate and 5 mM glutamate to support ADP-stimulated respiration. The experimental results are shown as means ± SD (open circles). These were compared with the solutions from *models 1–4*. Fits from simplified *model 2s, 3s, and 4s* were excluded for simplicity. *A*: respiration rate as a function of the ADP concentration added to the respirometer chamber (*n* = 6 and 5 for WT and GAMT^{-/-} cardiomyocytes, respectively). *B*: respiration rate as a function of ATP (*n* = 7 and 5 for WT and GAMT^{-/-} cardiomyocytes, respectively). *C*: endogenous PK activity in the spectrophotometer cuvette (*n* = 8 and 7 for WT and GAMT^{-/-} cardiomyocytes, respectively). *D*: ATPase activity as a function of ATP in the spectrophotometer cuvette (*n* = 9 and 7 for WT and GAMT^{-/-} cardiomyocytes, respectively). Note that the fits from *models 3 and 4* were either very close or overlapping in all cases. VO₂, O₂ consumption.

As previously found for rat cardiomyocytes (45), the fits obtained by *models 1, 2, and 2s* were considerably worse than the fits with the other models, as shown by statistical analysis using an F-test of the nested models (Table 4). However, when information criteria were used, only *model 1* was considerably worse than the other models (AIC_c and BIC). By comparing the results from multiple goodness-of-fit criteria, we can conclude that solutions of all models, except for *model 1*, can be considered reasonable. The main difference between *model 2* and *models 3, 3s, 4, and 4s* is the introduction of a coupling between a part of endogenous PK and ATPases. Thus, while the F-test strongly suggests that a part of endogenous PK is coupled to ATPases (*P* < 0.05), the information criteria analysis was not conclusive, and further studies are needed. In addition, considerable diffusion restriction was identified at the level of the mitochondrial outer membrane and at the level of

intracellular diffusion restrictions separating mitochondria from the surrounding solution.

As explained above, when analyzing the model parameters obtained by fitting the data, we have to consider the pooled case only (Table 3). In the models, all reaction rates were simulated using Michaelis-Menten kinetics with the apparent kinetic constants *V*_{max} and *K*_m. ATPases were considered to be inhibited competitively by ADP (where *K*_{iATPase} is the apparent inhibition constant). The diffusion restrictions are described via exchange coefficients between the compartments (where *C*_{compartment 1-compartment 2} is the exchange coefficient between *compartment 1* and *compartment 2*). Table 3 shows the parameters used for each model. According to our simulation results using the pooled data set, the diffusion restrictions that separate the surrounding solution from mitochondria were similar to the diffusion restrictions

Table 2. *V*_{2 mM ATP}, *V*_{PEP}, and *V*_{PEP + PK} for experimental data and the various models

	Experimental Data	Models						
		1	2	2s	3	3s	4	4s
WT								
<i>V</i> _{2 mM ATP}	14.48 ± 4.24	15.98	16.14	16.72	15.71	15.33	15.79	15.51
<i>V</i> _{PEP}	11.15 ± 3.73	17.23	11.45	11.73	8.88	11.15	9.1	11.53
<i>V</i> _{PK + PEP}	4.84 ± 2.02	5.53	4.42	5.68	6.5	6.87	6.15	6.43
GAMT^{-/-}								
<i>V</i> _{2 mM ATP}	14.07 ± 3.02	18.12	17.97	19.08	17.14	16.58	17.14	17
<i>V</i> _{PEP}	10.86 ± 2.53	19.69	12.36	12.82	9.81	11.29	11.52	13.07
<i>V</i> _{PK + PEP}	5.21 ± 2.18	8.16	7.16	7.62	9.22	9.9	6.46	10.43
Pooled								
<i>V</i> _{2 mM ATP}	14.30 ± 3.64	17.66	17.31	18.4	16.6	16.04	16.5	16.55
<i>V</i> _{PEP}	11.02 ± 3.16	19.06	12.06	12.69	9.19	11.07	11.26	12.25
<i>V</i> _{PK + PEP}	5.00 ± 2.03	7.13	6.04	7.07	8.4	8.95	5.61	9.01

Values are in nmol·min⁻¹·mg protein⁻¹; *n* = 8 WT cardiomyocytes, 7 GAMT^{-/-} cardiomyocytes, and 15 pooled cardiomyocytes. Experimental data were compared with simulation results obtained by *models 1–4* and their simplified versions (*models 2s, 3s, and 4s*). *V*_{2 mM ATP}, ATP-stimulated respiration rate; *V*_{PEP}, inhibition of ATP-stimulated respiration rate by endogenous pyruvate kinase (PK); *V*_{PEP + PK}, inhibition of ATP-stimulated respiration rate by endogenous PK; PEP, phosphoenol pyruvate.

Table 3. Model parameters found by fitting the pooled data obtained from WT and GAMT^{-/-} cardiomyocytes

	Models						
	1	2 s	2	3 s	3	4 s	4
$V_{\max\text{ATPsyn}}$, nmol·min ⁻¹ ·mg protein ⁻¹							
Optimal value	233	248	243	257	262	255	254
Confidence intervals	62–720	174–335	172–330	191–332	193–344	182–338	190–327
$C_{\text{sol-cyt}}$, nmol·mM ⁻¹ ·min ⁻¹ ·mg protein ⁻¹							
Optimal value	1,461	1,017	1,295	409	299	493	1,234
Confidence intervals	175 to >10 ⁵	562–2031	606–3,062	249–651	199–426	273–893	635–2,464
C_{MOM} , nmol·mM ⁻¹ ·min ⁻¹ ·mg protein ⁻¹							
Optimal value	646	676	612	1,132	2,362	950	517
Confidence intervals	222–2,231	530–875	481–791	786–1,788	1,264–7,394	662–1,479	425–635
$C_{\text{IMS-C4}}$, nmol·mM ⁻¹ ·min ⁻¹ ·mg protein ⁻¹							
Optimal value						8.39	366
Confidence intervals						1.72–16	261–544
$C_{\text{cyto-C4}}$, nmol·mM ⁻¹ ·min ⁻¹ ·mg protein ⁻¹							
Optimal value				0.005	156		
Confidence intervals				0.003–0.009	81–343		
$V_{\max\text{ATPase1}}$, nmol·min ⁻¹ ·mg protein ⁻¹							
Optimal value	181	177	614	119	89	105	742
Confidence intervals	90–298	156–198	322–954	108–130	79–99	93–117	474–1,045
K_{mATPase1} , mM							
Optimal value	0.21	0.271	10	0.235	0.201	0.201	10
Confidence intervals	0.06–0.834	0.206–0.358	≥10	0.187–0.294	0.147–0.276	0.143–0.279	6.91 to >10
K_{IATPase1} , mM							
Optimal value	0.051	0.102	0.05	9.62	10	10	0.051
Confidence intervals	0.05 to >10	0.056–0.228	0.05 to >10	0.208 to >10	≥10	0.229 to >10	0.05–0.09
$V_{\max\text{ATPase2}}$, nmol·min ⁻¹ ·mg protein ⁻¹							
Optimal value			107	119	278	127	95
Confidence intervals			92–122	75–169	186–391	42–4,500	82–108
K_{mATPase2} , mM							
Optimal value			0.194		3.77		0.051
Confidence intervals			0.131–0.286		2.47–6.26		0.05–0.1
K_{IATPase2} , mM							
Optimal value			10		0.053		10
Confidence intervals			0.142 to >10		0.05–0.147		0.166 to >10
$V_{\max\text{PKend1}}$, nmol·min ⁻¹ ·mg protein ⁻¹							
Optimal value		322	327	235	68	284	327
Confidence intervals		282–362	287–368	204–267	42–94	244–325	293–361
K_{mPKend1} , mM							
Optimal value		0.546	0.621	0.33	0.05	0.596	0.616
Confidence intervals		0.366–0.809	0.424–0.904	0.208–0.502	0.05–0.112	0.414–0.852	0.448–0.845
$V_{\max\text{PKend2}}$, nmol·min ⁻¹ ·mg protein ⁻¹							
Optimal value				356	217	47	0.118
Confidence intervals				111–7199	180–258	23–72	0.053–29

induced by mitochondrial outer membrane. This is clear from a comparison of the exchange coefficients $C_{\text{sol-cyt}}$ and C_{MOM} for all the models that provided reasonable fits (Table 3). Namely, while for some models (*models 2, 2s, and 4*) the diffusion restriction induced by the mitochondrial outer membrane was larger than the one separating the surrounding solution from mitochondria, the opposite was true for the other models (*models 3, 3s, and 4s*). However, we should note that for all models, with the exception of *model 3*, those diffusion restrictions were of the same order of magnitude, suggesting that they are similar. Note that the description of ATPases and endogenous PK interaction in *compartment 4* is a phenomenological one and that all the model parameters obtained for this compartment, including the exchange coefficient, are phenomenological coefficients and may not represent the interaction between ATPases and PK in a mechanistic way (as discussed in Ref. 45). As such, the

obtained low exchange coefficient for *compartment 4* is a part of a general description of coupling between PK and ATPases and cannot be compared directly with the other exchange coefficients found by the model.

Autofluorescence of single, permeabilized cardiomyocytes during ADP titration. To verify that diffusion restrictions were not due to clumping of the cells, we recorded NADH and Fp autofluorescence responses to the change in ADP at the single cell level (Fig. 7). The mainly mitochondrial origin of NADH and Fp fluorescence signals allowed us to relate fluorescence to the state of oxidative phosphorylation. NADH and Fp signals decreased and increased, respectively, as the concentration of ADP in the surrounding solution was increased (Fig. 7). We compared the normalized NADH and Fp fluorescence at each ADP concentration and found no statistically significant difference between cardiomyocytes from WT and GAMT^{-/-} mice (P from 0.09 to 0.95 by Welch's t -test; Fig. 7, *C* and *D*).

Table 4. Statistical analysis of the fits

	AIC	AIC _c	BIC	F-Tests					
				Model 2s	Model 2	Model 3s	Model 3	Model 4s	Model 4
WT cardiomyocytes									
Model 1	98.39	102.2	590.48	<0.0001	<0.0001	<0.0001	<0.0001	<0.0001	<0.0001
Model 2s	-23.1	-15.9	34.47		0.124	<0.05	<0.05	<0.05	<0.05
Model 2	-26.13	-10.61	42.56			<0.05	<0.05	<0.05	<0.05
Model 3s	-32.68	-17.15	41.44				0.113		
Model 3	-36.58	-12.32	47.13						
Model 4s	-30.43	-14.9	41.8						<0.05
Model 4	-37.7	-13.44	47.0						
GAMT ^{-/-} cardiomyocytes									
Model 1	77.59	81.41	298.61	<0.0001	<0.0001	<0.0001	<0.0001	<0.0001	<0.0001
Model 2s	7.75	14.95	48.76		0.139	<0.01	<0.01	<0.05	<0.001
Model 2	5.14	20.67	53.25			<0.01	<0.01	<0.01	<0.001
Model 3s	-11.33	4.2	46.23				0.583		
Model 3	-9.28	14.98	52.37						
Model 4s	0.55	16.08	50.88						<0.01
Model 4	-16.84	7.43	50.4						
Pooled WT and GAMT ^{-/-} cardiomyocytes									
Model 1	167.94	169.59	877.59	<0.0001	<0.0001	<0.0001	<0.0001	<0.0001	<0.0001
Model 2s	-15.07	-12.13	66.43		<0.01	<0.0001	<0.0001	<0.001	<0.0001
Model 2	-27.04	-21.3	69.56			<0.0001	<0.0001	<0.001	<0.0001
Model 3s	-47.47	-41.73	62.17				0.052		
Model 3	-51.09	-42.82	68.14						
Model 4s	-33.13	-27.4	67.08						<0.0001
Model 4	-54.96	-46.68	67.15						

Fits were analyzed by calculating Akaike information criteria (AIC), corrected AIC (AIC_c), and Bayesian information criteria (BIC). For all three criteria, the best-fitting model was the one with the minimum criterion value. Note that for AIC_c and BIC, a larger number of parameters is penalized more than in AIC. *F*-tests of the nested models are shown, with the simpler model (rows) compared with the nested, more complicated model (columns). The analysis was performed for fits of the data recorded from WT and GAMT^{-/-} mouse cardiomyocytes separately as well as for pooled data.

Because no statistically significant difference was found when we performed multiple comparisons separately, no additional correction for multiple tests or ANOVA analysis was required to check whether the difference in autofluorescence between cardiomyocytes from WT and GAMT^{-/-} mice was significant. Thus, on the basis of our results, diffusion from the solution to the mitochondrial inner membrane is restricted to the same extent.

DISCUSSION

The present study shows that inactivation of the CK system by GAMT deficiency due to lack of Cr is not associated with any changes in cardiomyocyte mitochondrial organization or stimulated respiration or its regulation by exogenous and endogenous ADP-supply. In addition, according to our modeling results, there was no change in intracellular compartmentation when cells were in a relaxed state. This indicates that inactivation of the CK system by GAMT deficiency does not induce cytoarchitectural changes.

The CK system is considered an important temporal and spatial energy buffer in the heart. In all muscle types, CK is present near sites of ATP consumption and sites of ATP production. In white, glycolytic skeletal muscle, CK is present near the myofibrillar I-band and functionally coupled to glycolytic enzymes (26). In oxidative skeletal muscle and the heart, mitochondrial CK is bound to the outer side of the inner mitochondrial membrane (25) and functionally coupled to respiration (59). Cytosolic CK is localized at the myofibrillar M-band, which is favorable for the regeneration of ATP for myosin ATPase (58). Also, it is bound near and functionally coupled to SERCA (33), sarcolemmal ATP-sensitive K⁺ chan-

nels (9), and Na⁺-K⁺-ATPase (13). The “spatial energy buffer” or “energy transport” function of CK has mainly been ascribed to tissues such as the heart, where a relatively large fraction of the CK activity is of mitochondrial origin (56, 59). Mitochondrial CK activity is tissue specific and relates to oxidative capacity (56). This relationship can also be observed during cardiac maturation (12, 16). Facilitation of ADP/ATP transport may seem particularly important in oxidative muscles, where ADP/ATP diffusion is restricted (28, 40, 56) and mitochondrial energy production, although more efficient than glycolysis, is more distant and physically separated from ATPases by the mitochondrial membranes. In terms of energy transport, the CK system provides a parallel energy circuit between sites of production and consumption. PCr and Cr are smaller molecules than ATP and ADP and thus diffuse faster (32). Another advantage is that they are present in higher concentrations, allowing the build up of larger gradients of Cr than ADP. For example, whereas the Cr concentration is in the order of 10 mM, the ADP concentration is ~50 μM. Since diffusion is driven by the absolute difference in concentration, the same gradient for ADP would require 10 mM/50 μM = 20 × larger relative difference in concentration than for Cr.

The importance of CK has been the subject of debate for a long time, with sometimes vague hypotheses used to define the role of CK, precluding testing of the hypotheses using a strong inference approach (3). An alternative view has been proposed that the high transport via PCr and Cr is simply a consequence of the CK reaction being close to equilibrium (32). After making some assumptions on the relative concentrations of ATP, ADP, PCr, and Cr, it has been shown that CK is expected to facilitate energy transfer, leading to most of the energy

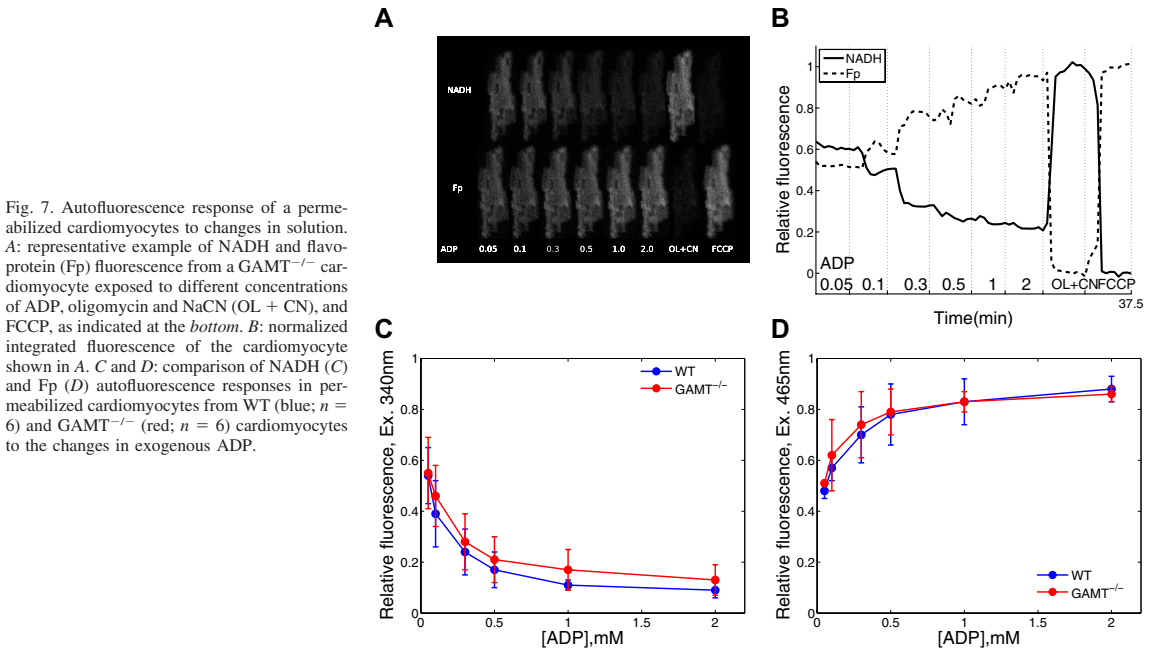


Fig. 7. Autofluorescence response of a permeabilized cardiomyocyte to changes in solution. *A*: representative example of NADH and flavo-protein (Fp) fluorescence from a $GAMT^{-/-}$ cardiomyocyte exposed to different concentrations of ADP, oligomycin and NaCN (OL + CN), and FCCP, as indicated at the bottom. *B*: normalized integrated fluorescence of the cardiomyocyte shown in *A*. *C* and *D*: comparison of NADH (*C*) and Fp (*D*) autofluorescence responses in permeabilized cardiomyocytes from WT (blue; $n = 6$) and $GAMT^{-/-}$ (red; $n = 6$) cardiomyocytes to the changes in exogenous ADP.

transfer to occur through PCr and Cr diffusion. In addition, for small diffusion distances, such as in cardiac muscle, the absence of an active CK system should not have any significant functional consequences (32). The latter was demonstrated assuming that there are no significant diffusion restrictions on the diffusion path of molecules between ATPases and mitochondria. Recently, on the basis of analysis of raster image correlation spectroscopy recordings, we (21) suggested that rat cardiomyocytes are split into smaller compartments with lattice-like barriers. The location of the barriers and the intracellular structures forming them are still unknown and would have different physiological consequences depending on whether the barriers are between ATPases and mitochondria or not. The lack of adaptation to inactive CK reported by us is in agreement with the mechanism of CK operation suggested by Meyer et al. (32) in their analysis.

If we assume the importance of the CK system as an additional energy transport system in the heart, it seems intuitive that disruption of this shuttle by genetic knockout of cytosolic and mitochondrial CK would lead to changes in the ultrastructure and regulation of mitochondrial respiration. In cardiomyocytes from $CK^{-/-}$ mice, rows of myofilaments were split into thinner myofilaments by mitochondria wedging into the branching points, as if to compensate for a lack of energy transfer by diminishing intracellular diffusion distances (23). In addition, permeabilized fibers from $CK^{-/-}$ mice have a higher ADP affinity of respiration than WT control mice, indicating smaller intracellular diffusion restrictions imposed on the molecules (23). Such changes in morphology and ADP affinity were consistent with the viewpoint that CK regulates the local ATP-to-ADP ratio and “compensatory mechanisms should be operating in $CK^{-/-}$ mouse heart to overcome dif-

fusion limitation and to preserve cardiac function at least at moderate levels of activity” (23). It was therefore surprising to find no difference between cardiomyocytes from $GAMT^{-/-}$ and their WT littermates. Both had parallel rows of mitochondria with the same distances between mitochondrial centers (Figs. 4 and 5 and Table 1). In permeabilized cardiomyocytes, ADP sensitivity was similar at the population level (Fig. 6) as well as at the single cell level (Fig. 7). Finally, intracellular compartmentation, as assessed by kinetic measurements and mathematical modeling, was found to be the same in both WT and $GAMT^{-/-}$ cardiomyocytes. These findings are in agreement with and extend the observations of a recent study (30) that failed to identify any adaptational changes when left ventricular proteomes, adenylate kinase activity, or mitochondrial respiration were compared.

The difference between our results and those from $CK^{-/-}$ mice might be explained by differences in the genetic background ($CK^{-/-}$ mice on a mixed C57BL/6 and S129 background were compared with WT C57BL/6 mice) and genetic drift. This has been shown to play a role in a study (31) of mice deficient in mitochondrial CK (Mt- $CK^{-/-}$ mice). In the present study, we compared $GAMT^{-/-}$ mice with their WT littermates. Alternatively, the different outcomes may be the result of different genetic modifications. Indeed, CK is a structural as well as catalytic protein. Muscle-type CK is an integral part of the myofibrillar M-band (17, 18, 49), where it serves as an efficient ATP-regenerating system for myosin ATPase located on both sides of the M-band (58). Mt-CK in the mitochondria seems to play a structural role in addition to ADP regeneration. It has been suggested that the octameric form induces the formation of contact sites between the inner and outer mitochondrial membranes (46), where it is involved in lipid transfer

between the two membranes (11). In another study (29), the structural role of Mt-CK has been demonstrated by finding that it stabilizes specific contact sites between inner and outer mitochondrial membranes. It must be noted that these findings are not from cardiac muscle. It remains to be verified whether the lack of Mt-CK in cardiac muscle affects mitochondrial organization. However, an increase citrate synthase activity does suggest an increased mitochondrial volume in cardiac muscle of Mt-CK^{-/-} mice (31). As CK is expressed to the same extent in GAMT^{-/-} mice as in WT mice (19), these other roles of (especially) Mt-CK are preserved in GAMT^{-/-} mice, and our results reflect only the catalytic role of CK.

It is tempting to speculate that guanidinoacetate (GA) may be used by CK in a similar manner as Cr. Indeed, although GAMT^{-/-} mice have undetectable levels of total Cr, as shown in Fig. 3, they have a considerable amount of phosphorylated (p-)GA. In the heart, the p-GA concentration in a GAMT^{-/-} mouse is ~2/3 of the PCr concentration in a WT mouse (19). However, phosphotransfer from ATP to p-GA was undetectable in GAMT^{-/-} mice (29), and it has been shown that the reactivity of muscle-type CK with GA is ~100 times smaller than with Cr (5). This reactivity is sufficient to dephosphorylate p-GA at the induction of ischemia (24) or cyanide inhibition of oxidative phosphorylation (5). However, for energy transfer between mitochondria and ATPases, Mt-CK must convert ATP into PCr or its analog. When ATP-stimulated respiration on isolated mitochondria or on permeabilized fibers was analyzed, Mt-CK reactivity in the presence of GA was negligible and ADP synthesis from GA and ATP was not able to stimulate respiration (5). Taking into account the inability of Mt-CK to react with GA as well as undetectable levels of total Cr, the contribution of the CK shuttle to energy transfer is expected to be negligible in GAMT^{-/-} cardiomyocytes. Thus, in contrast to the suggestion cited above from Ref. 23, the present results suggest that disruption of CK shuttle does not necessarily lead to compensatory changes in mitochondrial arrangement and intracellular compartmentation.

Applied methods and study limitations. In this study, we used confocal microscopy to estimate the intracellular mitochondrial positioning in WT and GAMT^{-/-} cardiomyocytes. The analysis was based on a method that we have previously applied on rat and trout cardiomyocytes (4, 50). Compared with traditional electron microscopy, there are several differences that ought to be considered when interpreting the data obtained by our method. Analysis of confocal images allowed us to use live cells. Thus, there are no histological artifacts that may be introduced by the fixation and dehydration of cells during their preparation for electron microscopy (38). In addition, the distances between the centers of mitochondria estimated by our method can be analyzed in three dimensions (Fig. 1) with an estimation based on a large number of mitochondria. In this study, >20,000 mitochondria were analyzed for each of the genotypes. Collecting a similar amount of data using electron microscopy is possible but would probably not be feasible when time and monetary costs are considered. Taking into account that most of the SDs of the percentile points shown in Table 1 are below 100 nm, the method can be considered precise and should be able to identify subtle changes in mitochondrial positioning. Note that those deviations include variability between cells as well. Such precision can be attributed to sub-Airy disk accuracy in finding centers of

the objects in optical microscopy. However, in contrast to electron microscopy, confocal microscopy images do not allow us to determine relative distances between the borders of the objects, such as the distance between membranes of neighboring mitochondria, due to the limits induced by diffraction. As a result, in our study, such distances cannot be analyzed accurately and have not been reported. A further consideration is the isolation procedure, which is of great importance in obtaining a high yield of viable cardiomyocytes with unaltered morphological characteristics. The dissociation of a heart into a single cell suspension involves several critical factors such as excision and cannulation for perfusion, collagenase quality and activity, the length of enzyme digestion, and the Ca²⁺ concentration in the perfusion solution. To control for these variables, we used several criteria to check the quality of the isolation procedure, for example, contraction of cardiomyocytes upon electrical field stimulation, indicating that cells are Ca²⁺ tolerant, and checking for the prevalence of rod-shaped cells with clear striations and well-delineated membranes. However, even with those tests, we cannot exclude a possibility that there are some morphological changes introduced during the isolation procedure that may influence the analysis of mitochondrial positioning.

It is important to keep in mind the limitations of this study. For the functional assays, we studied cardiomyocytes with the sarcolemma permeabilized by saponin. Because the surrounding solution contained low free Ca²⁺, cells were kept in a resting state. We stimulated mitochondrial respiration and endogenous PK and ATPases by adding ADP or ATP to the solution outside the cells. Thus, these compounds had to cross an unstirred layer around the cells (22) as well as the intracellular diffusion obstacles, which partition cardiomyocytes into smaller compartments (21, 23, 45), before reaching the mitochondria. In contrast, in intact, working cells, there is a circuit of ADP/ATP between adjacent ATPases and mitochondria significantly reducing the diffusion distances and obstacles that influence the energy transfer if compared with the permeabilized cardiomyocyte experiments. In addition, the level of intracellular compartmentation induced by diffusion restrictions is not known in working heart muscle cells. While an analysis of raster image correlation spectroscopy measurements on relaxed rat cardiomyocytes suggested lattice-like intracellular diffusion barriers separating the cardiomyocytes into smaller compartments (21), it is not clear whether such compartmentation persists in the contracting cell. Mitochondrial respiration was stimulated to the maximal rate by very high concentrations of ADP in the presence of a high concentration of P_i, which is also an important regulator of mitochondrial respiration (7, 39, 61). Thus, the changes induced by GAMT deficiency have not been probed in the same conditions as in vivo experiments. However, on the basis of our analysis, we can conclude that the mitochondrial organization and intracellular compartmentation, as observed in our experiments, are unchanged in GAMT^{-/-} mice.

Disruption of the CK system may be compensated for by other mechanisms that were not measured in this study. For example, upregulation of alternative phosphotransfer systems, such as adenylate kinase, has been observed in CK^{-/-} mice (34), and upregulation of other glycolytic enzymes is observed after heart failure (2). Upregulation of these alternative phosphotransfer systems may serve to compensate for both the

temporal and spatial buffer functions of the CK system. However, the change after heart failure may also simply reflect a change of phenotype induced by reverting to a fetal gene expression (37). Metabolically, this includes an upregulation of glycolytic enzymes and a downregulation of mitochondrial enzymes (48, 54). Clearly, further studies are needed to determine how disruption of the CK system by GAMT deficiency affects the cardiac phenotype.

Our kinetic recordings, such as mitochondrial respiration and ATPase activities, were performed in the absence of Cr in solution. This was done to determine whether intracellular compartmentation and mitochondrial respiration capacity changed during adaptation of the cells to Cr deficiency in GAMT^{-/-} mice. As we have previously demonstrated (45), this information can be obtained using kinetic recordings without Cr. Thus, while we know on the basis of earlier studies that the total Cr content is too low to be determined in GAMT^{-/-} mice leading to inactivation of the CK shuttle system in GAMT^{-/-} mice, the kinetic properties of CK isoforms, their distribution, and coupling to mitochondrial respiration is not known and cannot be predicted on the basis of our measurements.

Physiological implications. The lack of compensatory changes in GAMT^{-/-} mice prompts a careful consideration of the role of the CK system in cardiomyocytes. At the whole heart level, both CK^{-/-} and GAMT^{-/-} mice show almost no changes in basal contractile performance (6, 42), but they fail to perform at inotropically stimulated high workload and are more susceptible to ischemia-reperfusion injury (10, 19, 47). Clearly, the CK system is indispensable when the heart is exposed to a severe energetic challenge. But how important is it as an energy transport system? It is well established that a significant fraction of energy transport occurs via the CK system in the heart, and this is severely diminished in the failing heart (20). However, Meyer et al. (32) suggested that CK-facilitated energy transfer is merely a consequence of the existence of the CK system and is not required for cardiac function, if the diffusion distances are taken into account. Its main role is to buffer temporal fluctuations in the ADP-to-ATP ratio during situations, when energy demand is higher than energy production (32). A recent analysis of ³¹P NMR data suggested that the contribution of the CK shuttle to overall energy transfer between mitochondria and ATPases can depend on the workload and could reduce with an increase in workload or in pathological conditions (53). While our results are by no means conclusive, they raise questions regarding the importance of CK as an energy transport system at low and moderate workloads.

In conclusion, our results suggest that the healthy heart is able to preserve cardiac function at a basal level in the absence of CK-facilitated energy transfer without compromising intracellular organization and the regulation of mitochondrial energy homeostasis.

ACKNOWLEDGMENTS

The authors acknowledge Prof. Dirk Isbrandt (University of Hamburg, Hamburg, Germany) for generating the strain of GAMT-deficient mice as well as Merle Mandel and Adele Puusalu (Institute of Cybernetics, Tallinn University of Technology, Tallinn, Estonia) for technical assistance.

GRANTS

This work was funded by The Wellcome Trust Fellowship WT081755MA, the European Union through the European Regional Development Fund, Estonian Science Foundation Grant ETF8041 (PhD stipends for J. Branovets, N. Jephina, and N. Sokolova), and British Heart Foundation Grant RG/10/002/28187.

DISCLOSURES

No conflicts of interest, financial or otherwise, are declared by the author(s).

AUTHOR CONTRIBUTIONS

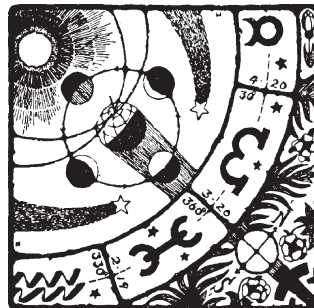
Author contributions: J.B., S.K., N.J., N.S., and D.A. performed experiments; J.B., M.S., S.K., N.J., and M.V. analyzed data; J.B., M.S., M.V., and R.B. interpreted results of experiments; J.B., M.S., and M.V. prepared figures; C.A.L., S.N., M.V., and R.B. conception and design of research; C.A.L., S.N., M.V., and R.B. edited and revised manuscript; C.A.L., S.N., M.V., and R.B. approved final version of manuscript; R.B. drafted manuscript.

REFERENCES

1. Abraham MR, Selivanov VA, Hodgson DM, Pucar D, Zingman LV, Wieringa B, Dzeja PP, Alekseev AE, Terzic A. Coupling of cell energetics with membrane metabolic sensing. *J Biol Chem* 277: 24427–24434, 2002.
2. Aksentijevic D, Lygate CA, Makinen K, Zervou S, Sebag-Montefiore L, Medway D, Barnes H, Schneider JE, Neubauer S. High-energy phosphotransfer in the failing mouse heart: role of adenylate kinase and glycolytic enzymes. *Eur J Heart Fail* 12: 1282–1289, 2010.
3. Beard DA, Kushmerick MJ. Strong Inference for Systems Biology. *PLoS Comput Biol* 5: e1000459, 2009.
4. Birkedal R, Shiels HA, Vendelin M. Three-dimensional mitochondrial arrangement in ventricular myocytes: from chaos to order. *Am J Physiol Cell Physiol* 291: C1148–C1158, 2006.
5. Boehm EA, Radda GK, Tomlin H, Clark JF. The utilisation of creatine and its analogues by cytosolic and mitochondrial creatine kinase. *Biochim Biophys Acta* 1274: 119–128, 1996.
6. Bonz AW, Kniesch S, Hofmann U, Küllmer S, Bauer L, Wagner H, Ertl G, Spindler M. Functional properties and [Ca²⁺]_i metabolism of creatine kinase–KO mice myocardium. *Biochem Biophys Res Commun* 298: 163–168, 2002.
7. Bose S, French S, Evans FJ, Joubert F, Balaban RS. Metabolic network control of oxidative phosphorylation. *J Biol Chem* 278: 39155–39165, 2003.
8. Braissant O, Henry H, Béard E, Uldry J. Creatine deficiency syndromes and the importance of creatine synthesis in the brain. *Amino Acids* 40: 1315–1324, 2011.
9. Crawford RM, Ranki HJ, Botting CH, Budas GR, Jovanovic A. Creatine kinase is physically associated with the cardiac ATP-sensitive K⁺ channel in vivo. *FASEB J* 16: 102–104, 2002.
10. Crozatier B, Badoual T, Boehm E, Ennezat PV, Guenoun T, Su J, Veksler V, Hittinger L, Ventura-Clapier R. Role of creatine kinase in cardiac excitation-contraction coupling: studies in creatine kinase-deficient mice. *FASEB J* 16: 653–660, 2002.
11. Epand RF, Schlattner U, Wallimann T, Lacombe ML, Epand RM. novel lipid transfer property of two mitochondrial proteins that bridge the inner and outer membranes. *Biophys J* 92: 126–137, 2007.
12. Fischer A, ten Hove M, Sebag-Montefiore L, Wagner H, Clarke K, Watkins H, Lygate CA, Neubauer S. Changes in creatine transporter function during cardiac maturation in the rat. *BMC Dev Biol* 10: 70, 2010.
13. Grosse R, Spitzer E, Kupriyanov VV, Saks VA, Repke KR. Coordinate interplay between (Na⁺ + K⁺)-ATPase and creatine phosphokinase optimizes (Na⁺/K⁺)-antiport across the membrane of vesicles formed from the plasma membrane of cardiac muscle cell. *Biochim Biophys Acta* 603: 142–156, 1980.
14. Gudbjarnason S, Mathes P, Ravens KG. Functional compartmentation of ATP and creatine phosphate in heart muscle. *J Mol Cell Cardiol* 1: 325–339, 1970.
15. Gupta A, Akki A, Wang Y, Leppo MK, Chacko VP, Foster DB, Caceres V, Shi S, Kirk JA, Su J, Lai S, Paolocci N, Steenbergen C, Gerstenblith G, Weiss RG. Creatine kinase-mediated improvement of function in failing mouse hearts provides causal evidence the failing heart is energy starved. *J Clin Invest* 122: 291–302, 2012.

16. Hoerter JA, Ventura-Clapier R, Kuznetsov A. Compartmentation of creatine kinases during perinatal development of mammalian heart. *Mol Cell Biochem* 133–134: 277–286, 1994.
17. Hornemann T, Kempa S, Himmel M, Hayek K, Fürst DO, Wallimann T. Muscle-type creatine kinase interacts with central domains of the M-band proteins myomesin and M-protein. *J Mol Biol* 332: 877–887, 2003.
18. Hornemann T, Stolz M, Wallimann T. Isoenzyme-specific interaction of muscle-type creatine kinase with the sarcomeric M-line is mediated by NH₂-terminal lysine charge-clamps. *J Cell Biol* 149: 1225–1234, 2000.
19. Hove ten M, Lygate CA, Fischer A, Schneider JE, Sang AE, Hulbert K, Sebag-Montefiore L, Watkins H, Clarke K, Isbrandt D, Wallis J, Neubauer S. Reduced inotropic reserve and increased susceptibility to cardiac ischemia/reperfusion injury in phosphocreatine-deficient guanidinoacetate-N-methyltransferase-knockout mice. *Circulation* 111: 2477–2485, 2005.
20. Ten Hove M, Neubauer S. MR spectroscopy in heart failure—clinical and experimental findings. *Heart Fail Rev* 12: 48–57, 2007.
21. Illuste A, Laasmaa M, Peterson P, Vendelin M. Analysis of molecular movement reveals lattice-like obstructions to diffusion in heart muscle cells. *Biophys J* 102: 739–748, 2012.
22. Jephthina N, Beraud N, Sepp M, Birkedal R, Vendelin M. Permeabilized rat cardiomyocyte response demonstrates intracellular origin of diffusion obstacles. *Biophys J* 101: 2112–2121, 2011.
23. Kaasik A, Veksler V, Boehm E, Novotova M, Minajeva A, Ventura-Clapier R. Energetic crosstalk between organelles: architectural integration of energy production and utilization. *Circ Res* 89: 153–159, 2001.
24. Kan HE, Renema WKJ, Isbrandt D, Heerschap A. Phosphorylated guanidinoacetate partly compensates for the lack of phosphocreatine in skeletal muscle of mice lacking guanidinoacetate methyltransferase. *J Physiol* 560: 219–229, 2004.
25. Karo J, Peterson P, Vendelin M. Molecular dynamics simulations of creatine kinase and adenine nucleotide translocase in mitochondrial membrane patch. *J Biol Chem* 287: 7467–7476, 2012.
26. Kraft T, Hornemann T, Stolz M, Nier V, Wallimann T. Coupling of creatine kinase to glycolytic enzymes at the sarcomeric I-band of skeletal muscle: a biochemical study in situ. *J Muscle Res Cell Motil* 21: 691–703, 2000.
27. Kümmel L. Ca, Mg-ATPase activity of permeabilized rat heart cells and its functional coupling to oxidative phosphorylation of the cells. *Cardiovasc Res* 22: 359–367, 1988.
28. Kuznetsov AV, Tiivel T, Sikk P, Kaambre T, Kay L, Daneshrad Z, Rossi A, Kadaja L, Peet N, Seppet E, Saks VA. Striking differences between the kinetics of regulation of respiration by ADP in slow-twitch and fast-twitch muscles in vivo. *Eur J Biochem* 241: 909–915, 1996.
29. Lenz H, Schmidt M, Welge V, Kueper T, Schlattner U, Wallimann T, Elsässer HP, Wittern KP, Wenck H, Staeb F, Blatt T. Inhibition of cytosolic and mitochondrial creatine kinase by siRNA in HaCat- and HeLaS3-cells affects cell viability and mitochondrial morphology. *Mol Cell Biochem* 306: 153–162, 2007.
30. Lygate CA, Aksentijevic D, Dawson D, ten Hove M, Phillips D, de Bono JP, Medway DJ, Sebag-Montefiore L, Hunyor I, Channon KM, Clarke K, Zervou S, Watkins H, Balaban RS, Neubauer S. Living without creatine: unchanged exercise capacity and response to chronic myocardial infarction in creatine-deficient mice. *Circ Res* 112: 945–955, 2013.
31. Lygate CA, Hunyor I, Medway D, de Bono JP, Dawson D, Wallis J, Sebag-Montefiore L, Neubauer S. Cardiac phenotype of mitochondrial creatine kinase knockout mice is modified on a pure C57BL/6 genetic background. *J Mol Cell Cardiol* 46: 93–99, 2009.
32. Meyer RA, Sweeney HL, Kushmerick MJ. A simple analysis of the “phosphocreatine shuttle”. *Am J Physiol Cell Physiol* 246: C365–C377, 1984.
33. Minajeva A, Ventura-Clapier R, Veksler V. Ca²⁺ uptake by cardiac sarcoplasmic reticulum ATPase in situ strongly depends on bound creatine kinase. *Pflügers Arch* 432: 904–912, 1996.
34. Momken I, Lechêne P, Koulmann N, Fortin D, Mateo P, Doan BT, Hoerter J, Bigard X, Veksler V, Ventura-Clapier R. Impaired voluntary running capacity of creatine kinase-deficient mice. *J Physiol* 565: 951–964, 2005.
35. Nahrendorf M, Streif JU, Hiller KH, Hu K, Nordbeck P, Ritter O, Sosnovik D, Bauer L, Neubauer S, Jakob PM, Ertl G, Spindler M, Bauer WR. Multimodal functional cardiac MRI in creatine kinase-deficient mice reveals subtle abnormalities in myocardial perfusion and mechanics. *Am J Physiol Heart Circ Physiol* 290: H2516–H2521, 2006.
36. Ramay HR, Vendelin M. Diffusion restrictions surrounding mitochondria: a mathematical model of heart muscle fibers. *Biophys J* 97: 443–452, 2009.
37. Razeghi P, Young ME, Alcorn JL, Moravec CS, Frazier OH, Taegtmeier H. Metabolic gene expression in fetal and failing human heart. *Circulation* 104: 2923–2931, 2001.
38. Roy RR, Pierotti DJ, Edgerton VR. Skeletal muscle fiber cross-sectional area: effects of freezing procedures. *Acta Anat (Basel)* 155: 131–135, 1996.
39. Saks VA, Kongas O, Vendelin M, Kay L. Role of the creatine/phosphocreatine system in the regulation of mitochondrial respiration. *Acta Physiol Scand* 168: 635–641, 2000.
40. Saks V, Kuznetsov A, Andrienko T, Usson Y, Appaix F, Guerrero K, Kaambre T, Sikk P, Lemba M, Vendelin M. Heterogeneity of ADP diffusion and regulation of respiration in cardiac cells. *Biophys J* 84: 3436–3456, 2003.
41. Schmidt A, Marescau B, Boehm EA, Renema WK, Peco R, Das A, Steinfeld R, Chan S, Wallis J, Davidoff M, Ullrich K, Waldschutz R, Heerschap A, De Deyn PP, Neubauer S, Isbrandt D. Severely altered guanidino compound levels, disturbed body weight homeostasis and impaired fertility in a mouse model of guanidinoacetate N-methyltransferase (GAMT) deficiency. *Hum Mol Genet* 13: 905–921, 2004.
42. Schneider JE, Stork LA, Bell JT, Hove ten M, Isbrandt D, Clarke K, Watkins H, Lygate CA, Neubauer S. Cardiac structure and function during ageing in energetically compromised guanidinoacetate N-methyltransferase (GAMT)-knockout mice—a one year longitudinal MRI study. *J Cardiovasc Magn Reson* 10: 9, 2008.
43. Schulze A. Creatine deficiency syndromes. *Mol Cell Biochem* 244: 143–150, 2003.
44. Seppet EK, Kaambre T, Sikk P, Tiivel T, Vija H, Tonkonogi M, Sahlin K, Kay L, Appaix F, Braun U, Eimre M, Saks VA. Functional complexes of mitochondria with Ca, MgATPases of myofibrils and sarcoplasmic reticulum in muscle cells. *Biochim Biophys Acta* 1504: 379–395, 2001.
45. Sepp M, Vendelin M, Vija H, Birkedal R. ADP compartmentation analysis reveals coupling between pyruvate kinase and ATPases in heart muscle. *Biophys J* 98: 2785–2793, 2010.
46. Speer O, Bäck N, Buerklen T, Brdiczka D, Koretsky A, Wallimann T, Eriksson O. Octameric mitochondrial creatine kinase induces and stabilizes contact sites between the inner and outer membrane. *Biochem J* 385: 445, 2005.
47. Spindler M, Meyer K, Strömer H, Leupold A, Boehm E, Wagner H, Neubauer S. Creatine kinase-deficient hearts exhibit increased susceptibility to ischemia-reperfusion injury and impaired calcium homeostasis. *Am J Physiol Heart Circ Physiol* 287: H1039–H1045, 2004.
48. Taegtmeier H, Wilson CR, Razeghi P, Sharma S. Metabolic energetics and genetics in the heart. *Ann NY Acad Sci* 1047: 208–218, 2005.
49. Turner DC, Wallimann T, Eppenberger HM. A protein that binds specifically to the M-line of skeletal muscle is identified as the muscle form of creatine kinase. *Proc Natl Acad Sci USA* 70: 702–705, 1973.
50. Vendelin M, Béraud N, Guerrero K, Andrienko T, Kuznetsov AV, Olivares J, Kay L, Saks VA. Mitochondrial regular arrangement in muscle cells: a “crystal-like” pattern. *Am J Physiol Cell Physiol* 288: C757–C767, 2005.
51. Vendelin M, Birkedal R. Anisotropic diffusion of fluorescently labeled ATP in rat cardiomyocytes determined by raster image correlation spectroscopy. *Am J Physiol Cell Physiol* 295: C1302–C1315, 2008.
52. Vendelin M, Eimre M, Seppet E, Peet N, Andrienko T, Lemba M, Engelbrecht J, Seppet EK, Saks VA. Intracellular diffusion of adenosine phosphates is locally restricted in cardiac muscle. *Mol Cell Biochem* 256–257: 229–241, 2004.
53. Vendelin M, Hoerter JA, Mateo P, Soboll S, Gillet B, Mazet JL. Modulation of energy transfer pathways between mitochondria and myofibrils by changes in performance of perfused heart. *J Biol Chem* 285: 37240–37250, 2010.
54. Ventura-Clapier R, Garnier A, Veksler V. Energy metabolism in heart failure. *J Physiol* 555: 1–13, 2004.
55. Ventura-Clapier R, Kuznetsov AV, d’Albis A, Deursen van J, Wieringa B, Veksler VI. Muscle creatine kinase-deficient mice. I. Alterations in myofibrillar function. *J Biol Chem* 270: 19914–19920, 1995.

56. **Ventura-Clapier R, Kuznetsov A, Veksler V, Boehm E, Anfous K.** Functional coupling of creatine kinases in muscles: species and tissue specificity. *Mol Cell Biochem* 184: 231–247, 1998.
57. **Ventura-Clapier R, Mekhfi H, Vassort G.** Role of creatine kinase in force development in chemically skinned rat cardiac muscle. *J Gen Physiol* 89: 815–837, 1987.
58. **Wallimann T, Schlosser T, Eppenberger HM.** Function of M-line-bound creatine kinase as intramyofibrillar ATP regenerator at the receiving end of the phosphorylcreatine shuttle in muscle. *J Biol Chem* 259: 5238–5246, 1984.
59. **Wallimann T, Wyss M, Brdiczka D, Nicolay K, Eppenberger H.** Intracellular compartmentation, structure and function of creatine kinase isoenzymes in tissues with high and fluctuating energy demands: the “phosphocreatine circuit” for cellular energy homeostasis. *Biochem J* 281: 21–40, 1992.
60. **Weiss JN, Korge P.** The cytoplasm: no longer a well-mixed bag. *Circ Res* 89: 108–110, 2001.
61. **Wu F, Zhang EY, Zhang J, Bache RJ, Beard DA.** Phosphate metabolite concentrations and ATP hydrolysis potential in normal and ischaemic hearts. *J Physiol* 586: 4193–4208, 2008.



PUBLICATION III

Simson* P, **Jepihhina*** N, Laasma M, Peterson P, Birkedal R, and Vendelin M;
**Restricted ADP movement in cardiomyocytes: Cytosolic diffusion obstacles
are complemented with a small number of open mitochondrial voltage-dependent
anion channels**

Journal of Molecular and Cellular Cardiology, 97, 197–203, 2016

** authors contributed equally*



Contents lists available at ScienceDirect

Journal of Molecular and Cellular Cardiology

journal homepage: www.elsevier.com/locate/yjmcc

Original article

Restricted ADP movement in cardiomyocytes: Cytosolic diffusion obstacles are complemented with a small number of open mitochondrial voltage-dependent anion channels

Päivo Simson¹, Natalja Jepihhina¹, Martin Laasmaa, Pearu Peterson, Rikke Birkedal, Marko Vendelin^{*}

Laboratory of Systems Biology, Institute of Cybernetics, Tallinn University of Technology, Akadeemia Rd 21, 12618 Tallinn, Estonia

ARTICLE INFO

Article history:

Received 31 March 2016

Accepted 19 April 2016

Available online 31 May 2016

Keywords:

Oxidative phosphorylation

Regulation

Rat cardiomyocytes

Voltage-dependent anion channel VDAC

Intracellular diffusion obstacles

ABSTRACT

Adequate intracellular energy transfer is crucial for proper cardiac function. In energy starved failing hearts, partial restoration of energy transfer can rescue mechanical performance. There are two types of diffusion obstacles that interfere with energy transfer from mitochondria to ATPases: mitochondrial outer membrane (MOM) with voltage-dependent anion channel (VDAC) permeable to small hydrophilic molecules and cytoplasmic diffusion barriers grouping ATP-producers and -consumers. So far, there is no method developed to clearly distinguish the contributions of cytoplasmic barriers and MOM to the overall diffusion restriction. Furthermore, the number of open VDACS *in vivo* remains unknown. The aim of this work was to establish the partitioning of intracellular diffusion obstacles in cardiomyocytes. We studied the response of mitochondrial oxidative phosphorylation of permeabilized rat cardiomyocytes to changes in extracellular ADP by recording 3D image stacks of NADH auto-fluorescence. Using cell-specific mathematical models, we determined the permeability of MOM and cytoplasmic barriers. We found that only ~2% of VDACS are accessible to cytosolic ADP and cytoplasmic diffusion barriers reduce the apparent diffusion coefficient by 6–10×. In cardiomyocytes, diffusion barriers in the cytoplasm and by the MOM restrict ADP/ATP diffusion to similar extents suggesting a major role of both barriers in energy transfer and other intracellular processes.

© 2016 Elsevier Ltd. All rights reserved.

1. Introduction

The intracellular environment in the heart muscle is highly compartmentalized with not only intracellular organelles determining the compartments, but a high level of compartmentalization in the cytosol as well [1]. In this compartmentalized environment, energy transfer between ATPases and ATP-producing mitochondria plays a vital role in cardiac function. In failing hearts, energy transfer is compromised and the resulting energy starvation limits cardiac performance [2].

Several mechanisms of energy transfer have been proposed. Based on diffusion coefficients measured in frog skeletal muscle [3], direct ATP/ADP and P_i diffusion between ATPases and mitochondria seems to be sufficient to cover short diffusion distances [4,5]. To facilitate direct diffusion, the creatine kinase shuttle may form a parallel energy transfer

system [6]. Furthermore, on the basis of a study of skeletal muscle, it has been proposed that diffusion distances required by energy transfer systems can be minimized by formation of a mitochondrial reticulum [7]. Such a reticulum would provide proton-motive force conduction from cell periphery to the cell interior leading to the reduction of diffusion distances for oxygen and substrates. The importance of adequate energy transfer is obvious in failing hearts and hearts injured by ischemia-reperfusion, where the overexpression of muscle creatine kinase increases energy transfer via the creatine kinase system and is able to rescue mechanical performance [8].

In cardiomyocytes, adequate energy transfer seems to be intimately connected to the compartmentation of the intracellular environment. The formation of a mitochondrial reticulum throughout the cell [7], local mitochondrial networks [9], and the existence of intracellular compartments in the cytosol [10–14] suggests that there are barriers causing significant restriction of diffusion and forming compartments of variable size in oxidative muscle cells. The origin of this diffusion restriction is, however, not fully understood. In the studies of heart energetics, there are two types of experiments demonstrating restricted movement of ATP/ADP in cardiomyocytes. First, it has been demonstrated that 20× larger ADP concentration is required to

Abbreviations: CK, creatine kinase; DC, diffusion coefficient; GAMT, GuanidinoAcetate MethylTransferase; MOM, mitochondrial outer membrane; VDAC, voltage-dependent anion channel.

^{*} Corresponding author.

E-mail address: markov@ioc.ee (M. Vendelin).

¹ Authors contributed equally to this work.

stimulate respiration in permeabilized cardiomyocytes and fibers to reach parity of respiration in isolated mitochondria [15–17]. This indicates that there are significant diffusion restrictions on the way of ADP from solution, through the cytosol of the permeabilized cell, to the mitochondrial inner membrane where it is picked up by the adenine nucleotide translocase. Earlier, we have shown that these diffusion restrictions are of intracellular nature [18,19]. The second type of experiments demonstrate strong coupling between ATPases and ATP synthesis by mitochondria [20–22] or glycolysis [23]. Crucially, coupling between ATP synthesis in mitochondria and ATPases shows that there is a diffusion obstacle grouping mitochondria and ATPases together [24,25].

The compartmentalization of cardiomyocytes is expected to play a major role in regulation of energy transfer and, possibly, in other processes such as signaling and apoptosis in the healthy and diseased heart. There is a clear link between the level of compartmentalization and the state of cardiomyocytes. In pathological conditions, diffusion restrictions were severely reduced after acute ischemia and chronic heart failure when assessed by analyzing respiration kinetics [26–28]. On the other hand, preconditioning the heart with a brief period of ischemia reduced this effect and kept the sensitivity of respiration to ADP in permeabilized fibers low [29]. Such correlation between the state of the heart muscle and diffusion restrictions suggests that these restrictions play an important role in the regulation of intracellular processes and could be a target of therapies in the treatment of heart disease.

The overall diffusion restriction identified on the basis of respiration kinetics measurements has been suggested to be due to restricted permeability of mitochondrial outer membrane, MOM [30–33]. MOM permeability to ADP can be regulated by modulation of VDAC permeability by voltage, or by external factors, such as tubulin, for example. Indeed, on single channel experiments, tubulin has been demonstrated to reduce permeability for ADP [30]. In certain conditions, and in the presence of tubulin, a fraction of mitochondria showed a reduced apparent affinity to ADP similar to the reduction in the affinity demonstrated in permeabilized cardiomyocytes [30]. However, while tubulin can reduce VDAC permeability, to our knowledge, it has never been established what MOM permeability in cardiomyocytes is. Note that the tubulin-dependent closure of VDAC to ADP would not lead to the coupling between ATPases and mitochondrial ATP synthesis demonstrated in the absence of creatine [20–22]. To reproduce this type of experiment, diffusion restrictions surrounding ATPases and mitochondria are required [34]. Shielding of the MOM by sarcoplasmic reticulum wrapping around the mitochondria could also explain the restricted diffusion of exogenous ADP and would be in agreement with the coupling between sarcoplasmic reticulum Ca^{2+} -ATPase and mitochondria [35]. Intriguingly, this second type of diffusion restriction is consistent with the intracellular diffusion barriers forming a lattice in the cardiomyocytes, as indicated on the basis of raster image correlation microscopy data analysis [36] and 3D mathematical model of cardiomyocytes [37].

While two types of diffusion restrictions have been shown, to our knowledge, there has been no experimental method that would allow to simultaneously quantify both diffusion restrictions in a single cell. The aim of this work is to establish the partitioning of intracellular diffusion obstacles in the heart muscle. In particular, we determine the number of VDACS that allow movement of ADP through MOM and the apparent diffusion coefficient (DC) in cardiomyocytes.

2. Methods

2.1. Experimental procedures

Adult outbred Wistar rats of both sexes weighing 250–500 g were used in the experiments. Animal procedures were approved by the Estonian National Committee for Ethics in Animal Experimentation (Estonian Ministry of Agriculture). Before the experiments, animals were anesthetized with 0.5 mg/kg ketamine (Bioketan, Vetoquinol Biowet,

Gorzów Wielkopolski, Poland) and 125 mg/kg dexmedetomidine (Dexdomitor; Orion, Espoo, Finland).

2.2. Cell isolation and measurements

Cardiomyocytes were isolated as described in [38]. Cardiomyocytes were put into a diamond-shaped fast-exchange chamber (15×6 mm, RC-24N; Warner Instruments, Harvard Apparatus, March-Hugstetten, Germany) on the fluorescence microscope. Cells were allowed to sediment (5–10 min) and then they were permeabilized with Mitomed solution containing 100 $\mu\text{mol/L}$ ADP and 25 $\mu\text{g/mL}$ of saponin. Then ADP concentration was increased stepwise from 100 to 300, 500, 1000, and 2000 $\mu\text{mol/L}$. The cells were superfused for at least 5 min at each step. Next, 3D image of a cell was taken. At the end of each experiment, the precise geometry of each cell was determined by a z-stack with the step size of 1 μm in the presence of 10 $\mu\text{mol/L}$ oligomycin and 5 mmol/L sodium cyanide. Next, the cell was exposed to the uncoupler FCCP (Carbonyl cyanide 4-(trifluoromethoxy) phenylhydrazone) to determine the baseline fluorescence. Note that the experiment was performed in the flow chamber with solutions in each condition flowing through chamber to ensure the replacement of the solution used in the previous condition. Only those cells located in the middle of the chamber were used for measurements. According to the manufacturer and our simulations [18], the geometry of the chamber provided laminar flow of solutions during experiments at the used flow rate of 0.5 mL/min. For detailed descriptions of cardiomyocyte isolation, used solutions, and the fluorescence microscope see Supporting Information

2.3. Mathematical model

The mathematical model was composed to describe reaction-diffusion system with ADP/ATP diffusion inside the cardiomyocyte, and two reactions: ATPase and ATP synthase. For each studied cardiomyocyte, the 3D geometry was constructed. Boundary contours for the cell and for the nuclei were found manually from recorded image stacks and custom made software was used to generate three-dimensional surfaces representing the shape of the cell and the shapes of the nuclei. Netgen mesh generator [39] was then used to create the finite element mesh for numerical calculations. External ADP concentration was considered constant and the outer boundary of the cell was assumed to be permeable to ADP. The model equations included five parameters in total: ADP/ATP diffusion coefficient D in cytosolic and myofibrillar compartments (cytosolic for short), reaction rates $V_1 \equiv V_{\max}(\text{ATPsyn})$, $V_2 \equiv V_{\max}(\text{ATPase})$ and Michaelis constants $K_1 \equiv K_m(\text{ADP})$, $K_2 \equiv K_m(\text{ATP})$ for ATP synthase and ATPase respectively. Here K_1 is an apparent Michaelis constant for mitochondrial ATP synthesis in respect to local cytosolic ADP. In calculations we assumed the reaction rates V_1 , V_2 and the Michaelis constant K_2 to be known and varied the diffusion constant D and the apparent Michaelis constant K_1 . If looked from the point of view of the ADP/ATP diffusion restrictions, D describes the cytosolic part and K_1 the mitochondrial outer membrane part of the restrictions. The stationary state solutions were calculated numerically for various external ADP concentrations using finite element software package FEniCS [40]. As a result, ADP and ATP concentration fields inside the modeled cardiomyocyte were obtained. A linear relation between the respiration rate VO_2 and NADH fluorescence intensity was assumed, as an approximation to the measured relationship [18]. Since the respiration rate is linearly related to ATP synthase activity, we could directly link ADP concentration to local NADH fluorescence. To simulate widefield microscope imaging the theoretical fluorescence field was convolved with experimentally measured point spread function [41]. By analyzing the results for various D and K_1 combinations, the best fit for experimental data was found. See Supporting Information for formal description of the model.

2.4. Data fitting

A detailed description of image processing and data fitting is given in Supporting Information. Data is shown as mean \pm SEM.

2.5. Relationship between apparent mitochondrial affinity and VDAC permeability

The apparent Michaelis constant K_1 of mitochondrial ATP synthesis is closely related to the mitochondrial outer membrane permeability and therefore to the number of open VDACs during the experiment. This relation can be estimated from the balance of the mean ATP synthase rate inside the mitochondrion to the ADP flow through the mitochondrial outer membrane (see Supporting Information for detailed calculations). The total number of VDACs on the mitochondrial outer membrane was estimated from general data available for intracellular water and dry mass distribution in intact rat heart [42], mitochondrial positioning [43], VDAC fraction among mitochondrial proteins [44], and VDAC molecular weight [45], as shown in Supporting Information.

3. Results

To establish the distribution of intracellular diffusion obstacles in the cardiomyocytes, we turned to analysis of the response of permeabilized cardiomyocytes to variation of extracellular ADP. Earlier, we have demonstrated that the NADH-induced autofluorescence is linearly related to respiration rate of cardiomyocytes in our conditions [18]. Note that this linear relationship (see Fig. S1) was found in the conditions used in our experiments and is not an universal property of the mitochondrial respiration in the heart. Here, we assumed that by determining local NADH autofluorescence in cardiomyocytes, we can estimate respiration rate in that part of the cell. In our study we considered the following processes: ADP diffusion from extracellular solution into the permeabilized cardiomyocyte, mitochondrial oxidative phosphorylation, and endogenous ATPase activity (Fig. 1A and B). As a reporter of mitochondrial oxidative phosphorylation activity, we recorded NADH-induced fluorescence under a fluorescence microscope. As expected, variation of ADP concentration induced changes in fluorescence (Fig. 1C). The fluorescence was normalized by exposing cells to oligomycin and

cyanide (blocking oxidative phosphorylation, maximal NADH fluorescence) or uncoupling mitochondria by FCCP (all NADH oxidized, minimal fluorescence). By recording 3D image stacks under the microscope, we obtained the distribution of intracellular fluorescence (Fig. 1D). To analyze the experimental data obtained from a single cell, we composed a mathematical model that took into account the geometry of a particular cell. For that, a 3D image stack recorded in the presence of oligomycin and cyanide were used to manually mark the boundary of the cell as well the location of the nuclei (Fig. 1E) allowing us to generate a finite element mesh (Fig. 1F). By solving reaction-diffusion equations, we determined the distribution of ADP in the cell (Fig. 1G), local respiration rate, and, taking into account the relationship between NADH-induced fluorescence and respiration as well as the microscope point spread function, we calculated the distribution of intracellular fluorescence predicted by the model (Fig. 1H).

In general, measured NADH fluorescence distribution heterogeneity is induced by the heterogeneity of the mitochondrial response, cell geometry (thickness of the cell) and mitochondrial distribution (see example in Supporting Information, Fig. S3). To study the intracellular heterogeneity of the mitochondrial response and reduce the effects induced by cell geometry on measured fluorescence, we normalized the fluorescence at each location to the fluorescence recorded in the same location in the presence of oligomycin and cyanide. This normalization was performed after subtracting the fluorescence recorded in the uncoupled case (in the presence of FCCP). As it is clear from the comparison of normalized fluorescence, in the experiment (Fig. 2, left column) and in the simulations taking into account the diffusion restrictions induced by MOM and cytoplasmic obstacles, there is a similar heterogeneity within the cell (Fig. 2, middle column). In contrast, when we assumed that the intracellular diffusion in cytosolic and myofibrillar compartments is fast as in [3], the normalized fluorescence was homogeneous (Fig. 2, right column). Thus, we can conclude that closure of VDAC in the MOM is not the only diffusion obstacle leading to a high apparent K_m of mitochondrial respiration in permeabilized cardiomyocytes.

To determine the distribution of diffusion obstacles between cytoplasm and MOM, we found the least square residual between the normalized measured fluorescence and the calculated images. The diffusion restriction induced by MOM was simulated by increasing

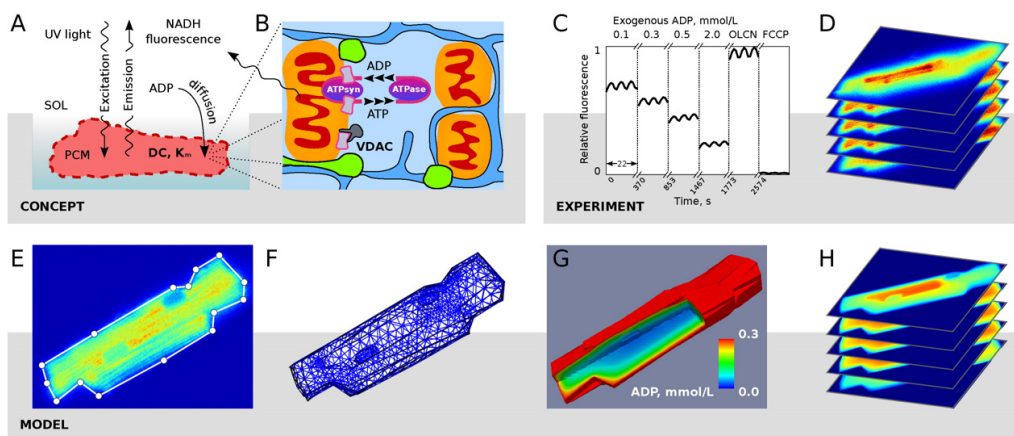


Fig. 1. Overall design of the study. To determine the DC and the number of open VDACS for ADP in mitochondrial outer membrane, we permeabilized the cardiomyocytes (PCM) and recorded NADH-induced fluorescence (A). The distribution of fluorescence in PCM is expected to be influenced by the distance of mitochondria from the permeabilized sarcolemma, intracellular DC, mitochondrial ATP synthase exposure to cytosol through open VDACS, and intracellular ATPases (B). The heterogeneity of the fluorescence was determined by recording images at different focal planes (D) for several extracellular ADP concentrations (C). Several image stacks were recorded in each condition and normalized by maximal and minimal fluorescence obtained in the presence of oligomycin and cyanide (OLCN) and FCCP, respectively (C). The experimental data obtained from PCM was analyzed by constructing cell-specific finite element model. Geometry of PCM was found manually from recorded image stacks (E) and mesh was generated (F). For given parameter set, the model calculated ADP concentration distribution within the cell (G) and corresponding NADH-induced fluorescence (H). By fitting the calculated (H) to the measured (D) fluorescence images, the DC and apparent K_m of mitochondria was found. On the basis of the apparent K_m , number of open VDACS was calculated.

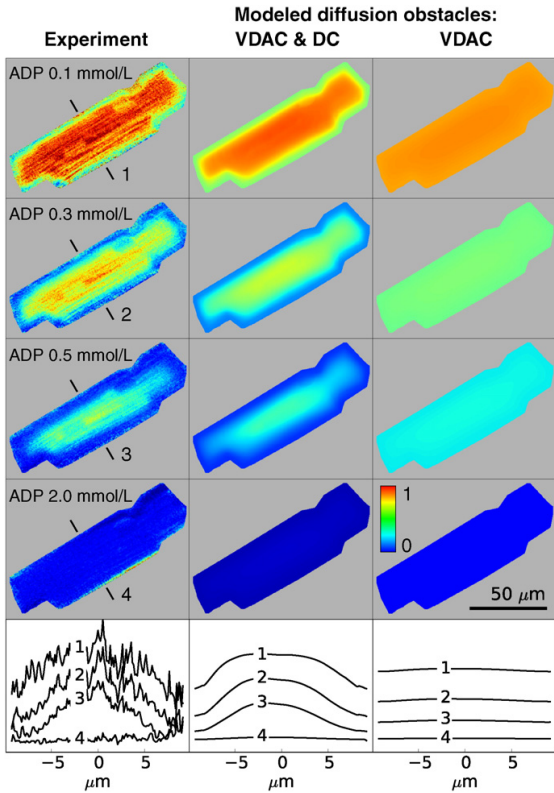


Fig. 2. NADH autofluorescence of a single permeabilized cardiomyocyte was varied by changing extracellular ADP concentrations. The fluorescence images recorded by a camera and normalized in each location by maximal fluorescence obtained in the presence of mitochondrial respiration inhibitors, oligomycin and cyanide (left column), are compared with the images calculated by the model (middle and right columns). The normalized fluorescence intensity is encoded by color, as shown on the bar. Model results are shown here for two cases: diffusion restriction between extracellular solution and mitochondrial inner membrane is either partitioned between cytosolic diffusion obstacles and mitochondrial outer membrane (middle column, $DC = 15 \mu\text{m}^2/\text{s}$, $K_m(\text{ADP}) = 0.1 \text{ mmol/L}$) or exclusively induced by closure of VDAC in mitochondrial outer membrane (right column, $DC = 200 \mu\text{m}^2/\text{s}$, $K_m(\text{ADP}) = 0.28 \text{ mmol/L}$). Note the similar intracellular heterogeneity in experiment and simulation results in the middle column. This is in sharp contrast with the results in the right column that show no significant gradients in relative autofluorescence, compared to the experimental data.

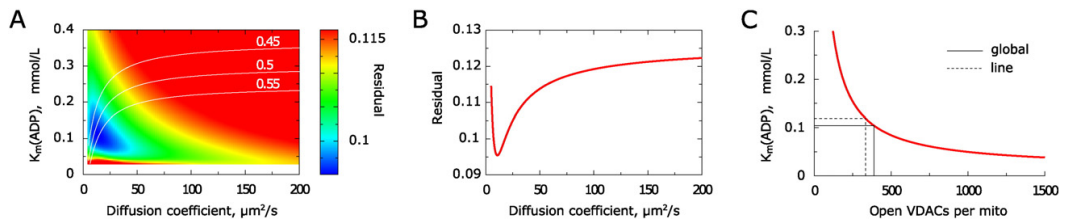


Fig. 3. Representative analysis of the model fit against the measurements. A: The least square residual (encoded in color) of the model fit for different combinations of cytosolic diffusion coefficient and apparent mitochondrial $K_m(\text{ADP})$. The white lines correspond to the relationship between the DC and K_m that would lead to respiration rate of 0.45, 0.5, or 0.55 times smaller than the maximal respiration rate in the presence of 0.3 mmol/L ADP in extracellular solution. Note that the minimum of the residual is next to the relationship corresponding to apparent $K_m(\text{ADP})$ of 0.3 mmol/L of a permeabilized cell. B: The least square residual of the fit found along the line in A corresponding to apparent $K_m(\text{ADP})$ of 0.3 mmol/L of a permeabilized cell (line marked by 0.5). C: Relationship between apparent $K_m(\text{ADP})$ of mitochondria and number of open VDACS. According to simulations performed in this case, there are 400–450 VDACS open for ADP per mitochondrion, marked by lines corresponding to the global minimum (as in A) or minimum found along the line (as in B).

apparent K_m of mitochondrial respiration to ADP in vicinity of the mitochondria [$\text{Mito } K_m(\text{ADP})$]. In the example shown in the Fig. 3A, there is a global minimum in residual at cytosolic DC $14.8 \mu\text{m}^2/\text{s}$ and $\text{Mito } K_m(\text{ADP})$ 0.108 mmol/L. This minimum is close to the line depicting the relationship between the cytosolic DC and $\text{Mito } K_m(\text{ADP})$ corresponding to the apparent K_m of permeabilized cell respiration to ADP in solution equal to 0.3 mmol/L. The corresponding relationship is shown in Fig. 3A by a white line marked with 0.5. When we calculate the residual along this relationship (i.e. along the line), the constrained minimum is at the DC equal to $10.8 \mu\text{m}^2/\text{s}$ and $\text{Mito } K_m(\text{ADP})$ equal to 0.120 mmol/L (Fig. 3B). The summary of performed experiments is shown in Table 1 with the results obtained using global minima (as in Fig. 3A) or the minima found along the relationship corresponding to the cellular $K_m(\text{ADP})$ of 0.3 mmol/L (as in Fig. 3B). As it is clear from Fig. 3C and Table 1, roughly a half of the apparent K_m of permeabilized cell respiration (0.3 mmol/L to extracellular ADP) is caused by closure of VDAC ($\sim 0.16 \text{ mmol/L}$, Table 1) with the second half contributed by cytoplasmic diffusion obstacles.

To estimate the number of open VDACS in MOM, we found the relationship between MOM permeability and $\text{Mito } K_m(\text{ADP})$. For that, we related the permeability of a single VDAC to ADP [46] to respiration rate of a single mitochondria assuming that the flux through MOM is in balance with ATP synthesis (see Supporting Information). As shown in Fig. 3C, in that example, there are about 400 VDACS accessible to ADP from cytosol in each mitochondria. On average, we found that the number of VDACS open for cytosolic ADP is approximately 300 per mitochondrion, $n = 7$. When compared to the total amount of VDACS in the membrane (around 14,000 per mitochondrion, see Supporting Information), the number of VDACS open for ADP is rather small, about 2% from all VDACS.

4. Discussion

The main result of our work is that we demonstrate and quantify two significant intracellular diffusion restrictions in cardiomyocytes. As suggested earlier on the basis of tubulin-VDAC interaction [30], we demonstrate that a significant number of VDACS are closed in cardiomyocytes and create a large diffusion obstacle for ADP diffusion through MOM. However, reduction of open VDAC by interaction with tubulin [30] or some other mechanism, such as wrapping by sarcoplasmic reticulum [35], contributes only to half of the observed diffusion restriction between mitochondrial inner membrane and the surrounding solution in permeabilized rat cardiomyocytes. The other half of the overall diffusion restriction is clearly positioned not on the MOM but on some other location in the cell, on the way between the solution and the MOM. The contribution of this diffusion obstacle is as large as VDAC closure. However, the specific location and the role of these diffusion obstacles in intracellular energetics, signaling, and apoptosis is uncertain.

Table 1
Number of open VDACS and cytosolic diffusion coefficient.

Residual minimum	D $\mu\text{m}^2/\text{s}$	$K_m(\text{ADP})$ mmol/L	Open VDACS per mito
Global	29.2 ± 3.5	0.156 ± 0.013	308 ± 31
On the 0.5-line	22.8 ± 3.4	0.183 ± 0.014	256 ± 26

Many suggested, assuming a relatively fast diffusion in muscle cells [3], that the MOM is a major diffusion obstacle [30–33]. Such obstruction of ATP/ADP diffusion by MOM gathered general support from the demonstration that tubulin interacts with VDAC and reduces VDAC permeability to ATP/ADP. Indeed, in the presence of tubulin there is a population of mitochondria with a high apparent K_m (ADP) for respiration [30]. In addition, in cancer cells, it has been demonstrated that interaction of VDAC and tubulin modulates mitochondrial oxidative phosphorylation [47]. But, to our knowledge, it has not been shown whether tubulin–VDAC interaction is indeed leading to significant diffusion obstacle *in vivo* in the heart. In addition, the strong preference of sarcoplasmic reticulum Ca^{2+} -ATPase to ATP provided by oxidative phosphorylation instead of ATP provided from solution surrounding permeabilized cardiomyocytes [21], and the demonstration of a coupling between ATPases and mitochondrial oxidative phosphorylation [48] clearly suggests that the diffusion between ATPases and MOM is relatively fast, and that there are diffusion obstacles which group ATPases and mitochondria together. In contrast, large diffusion restriction on MOM level would split them apart [37]. In this work, we resolve the controversy by demonstrating the partitioning of intracellular diffusion restrictions into two parts: one is shown to co-localize with MOM and the second is found in the cytoplasm.

The contribution of the cytosolic diffusion obstacles is clearly demonstrated in this work, where we find that they reduce the DC by 6–10 \times compared to those found in skeletal muscle using isotope traces and nuclear magnetic resonance methods [3,49]. Such a difference in the estimation of the DCs in skeletal and cardiac muscle is remarkable and can cause cell-specific properties of local intracellular signaling as well as metabolic regulation. Earlier, on the basis of raster image correlation measurements analysis, we suggested that cytosolic diffusion obstacles are not distributed uniformly within the cytoplasm but are formed by lattice-like structures with the distance between obstacles being in the range of 1 μm [36]. Here, we could not distinguish the homogenous distribution of diffusion obstacle from the lattice-like structures due to the relatively small spatial resolution of our approach. To find the specific spatial distribution of cytosolic diffusion obstacles, some other methods allowing to visualize local diffusion must be employed in future. There is a remarkable similarity in the estimated DC values when comparing our results with earlier estimates. To reduce the number of parameters fitted by the model, we neglected the anisotropy of intracellular diffusion [50]. As shown earlier, depending on the fluorescent dye, the DC in transversal direction is 60–85% of the DC in longitudinal direction [36,50]. Due to the elongated shape of the cells, the DC estimated in this work should mainly correspond to that in the transversal direction. The value of the cytosolic DC found from the analysis of fluorescence heterogeneity in the cardiomyocytes in this work ($\sim 30 \mu\text{m}^2/\text{s}$) is remarkably close the DC of fluorescently labeled ATP ($\sim 24 \mu\text{m}^2/\text{s}$) estimated using raster image correlation spectroscopy [36]. In skeletal muscle, the diffusion coefficient is 6 to 10 \times larger than the diffusion coefficient found in this work for cardiomyocytes. This difference suggests that, in skeletal muscle, the diffusion is mainly restricted on mitochondrial outer membrane level. However, further detailed studies are needed to test this suggestion.

The predicted small number of open or accessible VDACS in mitochondria lead to a significant diffusion restriction for movement of ADP through MOM. Taking into account that the present experiments

were performed at 25 °C, temperature dependence of mitochondrial respiration [51] and larger channels conductivity [52,53], the apparent K_m of oxidative respiration for cytosolic ADP in the vicinity of mitochondria would be ~ 0.25 mmol/L at 37 °C. Assuming that ADP concentration in the cell is about 0.05 mmol/L [54], this indicates an important role of energy transfer systems such as the creatine kinase (CK) shuttle in order to meet the metabolic demands of the working heart. However, a major role of CK shuttle contradicts some recent data. First, on the basis of ^{31}P -NMR magnetization transfer analysis, it has been shown that the CK shuttle can be bypassed by direct ADP diffusion at higher workloads [55]. Second, GuanidinoAcetate MethylTransferase (GAMT) knockout mice lacking a functional CK shuttle, exhibit the same cardiac performance as their wild-type littermates at basal level [56], have unaltered maximal exercise capacity and response to chronic myocardial infarction, and no obvious metabolic adaptations [57]. Intracellular diffusion restrictions and mitochondrial positioning was shown to be the same in cardiomyocytes isolated from GAMT knockouts and their wild-type littermates [19]. Thus, there is a contradiction between a small number of open VDACS found in this study and the non-exclusive role of the CK shuttle in energy transfer suggested earlier. If part of the diffusion restriction at the MOM found in our study on resting cardiomyocytes was due to shielding by the sarcoplasmic reticulum, then this would ensure energy transfer between sarcoplasmic reticulum Ca^{2+} -ATPase and the mitochondria. The sarcoplasmic reticulum would, however, still shield the mitochondria from myosin ATPase, which is the main energy consumer in working heart [58]. Thus, irrespective of the identity of the diffusion barrier at the MOM, the large restriction seems to call for a facilitation of energy transfer between myosin ATPase and mitochondria.

Our finding that only 2% of VDACS are open leads to the question on physiological role of the rest of VDACS in mitochondria. At present, we can only speculate on why 98% of VDACS are closed. Taking into account that VDAC is the main gateway for small molecules into mitochondria, we have to consider that VDAC conductivity may be enhanced in the closed state for some molecules. For example, calcium conductivity was found to be higher at closed state than in the open state [59]. Thus, closure of VDAC may enhance calcium uptake by mitochondria. Additionally, having most of VDACS closed can allow the cardiomyocytes to regulate energy transfer from direct transfer by ATP/ADP diffusion to the CK shuttle, as discussed above. Taking into account the large relative changes in ADP concentrations expected during a beat [54] due to oscillatory nature of acto-myosin ATPase [60,61], reduction of MOM conductivity to ADP would reduce influence of oscillations on mitochondrial oxidative phosphorylation regulation. The large number of closed VDACS could be also used as a reserve that is recruited at some specific conditions, for example during excessive mechanical work. All these questions are still open and are subjects of future research that should find whether more VDACS are open *in vivo*, whether VDAC permeability is significantly different from the one estimated by us at 37 °C, and whether VDAC state is modulated as the cell performs mechanical work.

In summary, we have developed a method and demonstrated as well as quantified two principal intracellular diffusion restrictions in cardiomyocytes to ADP: mitochondrial outer membrane induced by closure of a large number of VDACS and cytosolic diffusion restriction grouping ATPases and mitochondria into a single unit. These diffusion restrictions are expected to play a major role in the regulation of energy transfer and, possibly, in other processes such as signaling and apoptosis in the healthy and diseased heart.

Sources of funding

This work was supported by the European Union through the European Regional Development Fund (CENS Estonian Center of Excellence in Research) and Estonian Research Council (IUT33-7).

Appendix A. Supplementary data

Supplementary data to this article can be found online at <http://dx.doi.org/10.1016/j.yjmcc.2016.04.012>.

References

- [1] J.N. Weiss, P. Korge, The cytoplasm: no longer a well-mixed bag, *Circ. Res.* 89 (2001) 108.
- [2] R. Ventura-Clapier, A. Garnier, V. Veksler, F. Joubert, Bioenergetics of the failing heart, *BBA-Mol. Cell Res.* 1813 (2011) 1360–1372.
- [3] M.J. Kushmerick, R.J. Podolsky, Ionic mobility in muscle cells, *Science* 166 (80-) (1969) 1297–1298.
- [4] R.A. Meyer, H.L. Sweeney, M.J. Kushmerick, A simple analysis of the “phosphocreatine shuttle”, *AJP: Cell Physiol.* 246 (1984) C365–C377.
- [5] S. Kinsey, B. Locke, R. Dillaman, Molecules in motion: influences of diffusion on metabolic structure and function in skeletal muscle, *J. Exp. Biol.* 214 (2011) 263–274.
- [6] S.P. Bessman, P.J. Geiger, Transport of energy in muscle: the phosphocreatine shuttle, *Science* 211 (1981) 448–452.
- [7] B. Glancy, L. Hartnell, D. Malide, Z. Yu, C. Combs, P. Connelly, S. Subramaniam, R. Balaban, Mitochondrial reticulum for cellular energy distribution in muscle, *Nature* 523 (2015) 617–620.
- [8] A. Akki, J. Su, T. Yano, A. Gupta, Y. Wang, M. Leppo, V. Chacko, C. Steenbergen, R. Weiss, Creatine kinase overexpression improves ATP kinetics and contractile function in postischemic myocardium, *Am. J. Physiol. Heart Circ. Physiol.* 303 (2012) H844–H852.
- [9] V. Eisner, G. Lenaers, G. Hajnóczky, Mitochondrial fusion is frequent in skeletal muscle and supports excitation–contraction coupling, *J. Cell Biol.* 205 (2014) 179–195.
- [10] S. Gudbjarnason, P. Mathes, K.G. Ravens, Functional compartmentation of ATP and creatine phosphate in heart muscle, *J. Mol. Cell. Cardiol.* 1 (1970) 325–339.
- [11] R. Fischmeister, L.V. Castro, A. Abi-Gerges, F. Rochais, J. Jurevičius, J. Leroy, G. Vandecasteele, Compartmentation of cyclic nucleotide signaling in the heart: the role of cyclic nucleotide phosphodiesterases, *Circ. Res.* 99 (2006) 816–828.
- [12] G. Csordás, C. Hajnóczky, Sr/er–mitochondrial local communication: calcium and rds, *BBA-Bioenerg.* 1787 (2009) 1352–1362.
- [13] B.Z. Silverman, A. Warley, J.I. Miller, A.F. James, M.J. Shattock, Is there a transient rise in sub-sarcolemmal Na and activation of Na/K pump current following activation of I(Na) in ventricular myocardium? *Cardiovasc. Res.* 57 (2003) 1025–1034.
- [14] M.R. Abraham, V. Selivanov, D. Hodgson, D. Pucar, L. Zingman, B. Wieringa, P. Dzeja, A. Alekseev, A. Terzic, Coupling of cell energetics with membrane metabolic sensing, *J. Biol. Chem.* 277 (2002) 24427–24434.
- [15] V.I. Veksler, A.V. Kuznetsov, V.G. Sharov, V.I. Kapelko, V.A. Saks, Mitochondrial respiratory parameters in cardiac tissue: a novel method of assessment by using saponin-skinned fibers, *BBA* 892 (1987) 191–196.
- [16] L. Kümmel, Ca,Mg-ATPase activity of permeabilized rat heart cells and its functional coupling to oxidative phosphorylation of the cells, *Cardiovasc. Res.* 22 (1988) 359–367.
- [17] A. Kuznetsov, V. Veksler, F. Gellerich, V. Saks, R. Margreiter, W. Kunz, Analysis of mitochondrial function in situ in permeabilized muscle fibers, tissues and cells, *Nat. Protoc.* 3 (2008) 965–976.
- [18] N. Jephthina, N. Beraud, M. Sepp, R. Birkedal, M. Vendelin, Permeabilized rat cardiomyocyte response demonstrates intracellular origin of diffusion obstacles, *Biophys. J.* 101 (2011) 2112–2121.
- [19] J. Branovets, M. Sepp, S. Kotlyarova, N. Jephthina, N. Sokolova, D. Aksentijevic, C. Lygate, S. Neubauer, M. Vendelin, R. Birkedal, Unchanged mitochondrial organization and compartmentation of high-energy phosphates in creatine-deficient *GAMT*^{−/−} mouse hearts, *Am. J. Physiol. Heart Circ. Physiol.* 305 (2013) H506–H520.
- [20] E.K. Seppet, T. Kaambre, P. Sikk, T. Tiivel, H. Vija, M. Tonkonogi, K. Sahlin, L. Kay, F. Appaix, U. Braun, M. Eimre, V.A. Saks, Functional complexes of mitochondria with Ca,MgATPases of myofibrils and sarcoplasmic reticulum in muscle cells, *BBA* 1504 (2001) 379–395.
- [21] A. Kaasik, V. Veksler, E. Boehm, M. Novotova, A. Minajeva, R. Ventura-Clapier, Energetic crosstalk between organelles: architectural integration of energy production and utilization, *Circ. Res.* 89 (2001) 153–159.
- [22] V. Saks, T. Kaambre, P. Sikk, M. Eimre, E. Orlova, K. Paju, A. Piirsoo, F. Appaix, L. Kay, V. Regitz-Zagrosek, E. Fleck, E. Seppet, Intracellular energetic units in red muscle cells, *Biochem. J.* 356 (2001) 643–657.
- [23] M. Sepp, N. Sokolova, S. Jugai, M. Mandel, P. Peterson, M. Vendelin, Tight coupling of Na⁺/K⁺-ATPase with glycolysis demonstrated in permeabilized rat cardiomyocytes, *PLoS One* 9 (2014), e99413.
- [24] V. Saks, A. Kuznetsov, T. Andrienko, Y. Usson, F. Appaix, K. Guerrero, T. Kaambre, P. Sikk, M. Lemba, M. Vendelin, Heterogeneity of adp diffusion and regulation of respiration in cardiac cells, *Biophys. J.* 84 (2003) 3436–3456.
- [25] M. Vendelin, M. Eimre, E. Seppet, N. Peet, T. Andrienko, M. Lemba, J. Engelbrecht, E. Seppet, V. Saks, Intracellular diffusion of adenosine phosphates is locally restricted in cardiac muscle, *Mol. Cell. Biochem.* 256 (257) (2004) 229–241.
- [26] L. Kay, V.A. Saks, A. Rossi, Early alteration of the control of mitochondrial function in myocardial ischemia, *J. Mol. Cell. Cardiol.* 29 (1997) 3399–3411.
- [27] L. Kay, Z. Daneshrad, V.A. Saks, A. Rossi, Alteration in the control of mitochondrial respiration by outer mitochondrial membrane and creatine during heart preservation, *Cardiovasc. Res.* 34 (1997) 547–556.
- [28] S. Boudina, M. Laclau, L. Tariosse, D. Daret, G. Gouverneur, S. Bonoron-Adèle, V. Saks, P. Dos Santos, Alteration of mitochondrial function in a model of chronic ischemia in vivo in rat heart, *Am. J. Physiol. Heart Circ. Physiol.* 282 (2002) H821–H831.
- [29] M.N. Laclau, S. Boudina, J.B. Thambo, L. Tariosse, G. Gouverneur, S. Bonoron-Adèle, V.A. Saks, K.D. Garlid, P. Dos Santos, Cardioprotection by ischemic preconditioning preserves mitochondrial function and functional coupling between adenosine nucleotide translocase and creatine kinase, *J. Mol. Cell. Cardiol.* 33 (2001) 947–956.
- [30] T. Rostovtseva, K. Sheldon, E. Hassanzadeh, C. Monge, V. Saks, S. Bezrukov, D. Sackett, Tubulin binding blocks mitochondrial voltage-dependent anion channel and regulates respiration, *PNAS* 105 (2008) 18746–18751.
- [31] P. Gurnev, T. Rostovtseva, S. Bezrukov, Tubulin-blocked state of VDAC studied by polymer and ATP partitioning, *FEBS Lett.* 585 (2011) 2363–2366.
- [32] M. Gonzalez-Granillo, A. Grichine, R. Guzun, Y. Usson, K. Tepp, V. Chekulayev, I. Shevchuk, M. Karu-Varikmaa, A. Kuznetsov, M. Grimm, V. Saks, T. Kaambre, Studies of the role of tubulin beta II isotype in regulation of mitochondrial respiration in intracellular energetic units in cardiac cells, *J. Mol. Cell. Cardiol.* 52 (2012) 437–447.
- [33] R. Guzun, M. Karu-Varikmaa, M. Gonzalez-Granillo, A. Kuznetsov, L. Michel, C. Cotten-Rousselle, M. Saaremaa, T. Kaambre, M. Metsis, M. Grimm, C. Auffray, V. Saks, Mitochondria–cytoskeleton interaction: distribution of beta-tubulins in cardiomyocytes and HL-1 cells, *BBA* 1807 (2011) 458–469.
- [34] M. Vendelin, M. Eimre, E. Seppet, N. Peet, T. Andrienko, M. Lemba, J. Engelbrecht, E. Seppet, V. Saks, Intracellular diffusion of adenosine phosphates is locally restricted in cardiac muscle, *Mol. Cell. Biochem.* 256–257 (2004) 229–241.
- [35] R. Birkedal, M. Laasmaa, M. Vendelin, The location of energetic compartments affects energetic communication in cardiomyocytes, *Front. Physiol.* 5 (2014) 376.
- [36] A. Illaste, M. Laasmaa, P. Peterson, M. Vendelin, Analysis of molecular movement reveals lattice-like obstructions to diffusion in heart muscle cells, *Biophys. J.* 102 (2012) 739–748.
- [37] H. Ramay, M. Vendelin, Diffusion restrictions surrounding mitochondria: a mathematical model of heart muscle fibers, *Biophys. J.* 97 (2009) 443–452.
- [38] M. Sepp, M. Vendelin, H. Vija, R. Birkedal, ADP compartmentation analysis reveals coupling between pyruvate kinase and ATPases in heart muscle, *Biophys. J.* 98 (2010) 2785–2793.
- [39] J. Schöberl, Netgen an advancing front 2d/3d-mesh generator based on abstract rules, *Comput. Vis. Sci.* 1 (1997) 41–52.
- [40] A. Logg, K. Mardal, G. Wells, Automated Solution of Differential Equations by the Finite Element Method, Springer, Berlin Heidelberg, 2012.
- [41] M. Laasmaa, M. Vendelin, P. Peterson, Application of regularized Richardson-Lucy algorithm for deconvolution of confocal microscopy images, *J. Microsc.* 243 (2011) 124–140.
- [42] M. Aliev, P. Santos, J. Hoerter, S. Soboll, A. Tikhonov, V. Saks, Water content and its intracellular distribution in intact and saline perfused rat hearts revisited, *Cardiovasc. Res.* 53 (2002) 48–58.
- [43] R. Birkedal, H.A. Shiels, M. Vendelin, Three-dimensional mitochondrial arrangement in ventricular myocytes: from chaos to order, *Am. J. Physiol. Cell. Physiol.* 291 (2006) C1148.
- [44] T. Rostovtseva, M. Colombini, ATP flux is controlled by a voltage-gated channel from the mitochondrial outer membrane, *J. Biol. Chem.* 271 (1996) 28006.
- [45] J. Lemasters, E. Holmuhamedov, Voltage-dependent anion channel (VDAC) as mitochondrial governor—thinking outside the box, *BBA-Mol. Basis Dis.* 2006 (1762) 181–190.
- [46] T. Rostovtseva, M. Colombini, VDAC channels mediate and gate the flow of ATP: implications for the regulation of mitochondrial function, *Biophys. J.* 72 (1997) 1954–1962.
- [47] E. Maldonado, K. Sheldon, D. Dehart, J. Patnaik, Y. Manevich, D. Townsend, S. Bezrukov, T. Rostovtseva, J. Lemasters, Voltage-dependent anion channels modulate mitochondrial metabolism in cancer cells regulation by free tubulin and erastin, *J. Biol. Chem.* 288 (2013) 11920–11929.
- [48] E. Seppet, T. Kaambre, P. Sikk, T. Tiivel, H. Vija, M. Tonkonogi, K. Sahlin, L. Kay, F. Appaix, U. Braun, M. Eimre, V. Saks, Functional complexes of mitochondria with Ca,MgATPases of myofibrils and sarcoplasmic reticulum in muscle cells, *BBA-Bioenerg.* 1504 (2001) 379–395.
- [49] R. de Graaf, A. van Kranenburg, K. Nicolay, In vivo 31P-NMR diffusion spectroscopy of ATP and phosphocreatine in rat skeletal muscle, *Biophys. J.* 78 (2000) 1657–1664.
- [50] M. Vendelin, R. Birkedal, Anisotropic diffusion of fluorescently labeled ATP in rat cardiomyocytes determined by raster image correlation spectroscopy, *Am. J. Physiol. Cell. Physiol.* 295 (2008) C1302–C1315.
- [51] V.N. Samartsev, S.A. Chezanova, L.S. Polishchuk, A.P. Paydyganov, O.V. Vidyakina, I.P. Zeldi, Temperature dependence of rat liver mitochondrial respiration with uncoupling of oxidative phosphorylation by fatty acids. Influence of inorganic phosphate, *Biochem. Mosc.* 68 (2003) 618–626.
- [52] I. Biró, S. Pezeshki, H. Weingart, M. Winterhalter, U. Kleinekathöfer, Comparing the temperature-dependent conductance of the two structurally similar *E. coli* porins OmpC and OmpF, *Biophys. J.* 98 (2010) 1830–1839.
- [53] E. Nestorovich, V. Karginov, A. Berezhkovskii, V.A. Parsegian, S. Bezrukov, Kinetics and thermodynamics of binding reactions as exemplified by anthrax toxin channel blockage with a cationic cyclodextrin derivative, *PNAS* 109 (2012) 18453–18458.
- [54] M. Vendelin, O. Kongas, V. Saks, Regulation of mitochondrial respiration in heart cells analyzed by reaction-diffusion model of energy transfer, *Am. J. Physiol. Cell. Physiol.* 278 (2000) C747–C764.
- [55] M. Vendelin, J. Hoerter, P. Mateo, S. Soboll, B. Gillet, J. Mazet, Modulation of energy transfer pathways between mitochondria and myofibrils by changes in performance of perfused heart, *J. Biol. Chem.* 285 (2010) 37240–37250.
- [56] J. Schneider, L. Stork, J. Bell, M. Hove, D. Isbrandt, K. Clarke, H. Watkins, C. Lygate, S. Neubauer, Cardiac structure and function during ageing in energetically compromised guanidinoacetate N-methyltransferase (*GAMT*)-knockout mice – a one year longitudinal mri study, *J. Cardiovasc. Magn. Reson.* 10 (2008) 9.
- [57] C. Lygate, D. Aksentijevic, D. Dawson, M. ten Hove, D. Phillips, J. de Bono, D. Medway, L. Sebag-Montefiore, I. Hunyor, K. Channon, K. Clarke, S. Zervou, H. Watkins, R.

- Balaban, S. Neubauer, Living without creatine: unchanged exercise capacity and response to chronic myocardial infarction in creatine-deficient mice, *Circ. Res.* 112 (2013) 945–955.
- [58] H. Suga, Ventricular energetics, *Physiol. Rev.* 70 (1990) 247–277.
- [59] W. Tan, M. Colombini, Vdac closure increases calcium ion flux, *Biochim. Biophys. Acta Biomembr.* 1768 (2007) 2510–2515.
- [60] M. Vendelin, P.H.M. Bovendeerd, T. Arts, J. Engelbrecht, D.H.v. Campen, Cardiac mechanoenergetics replicated by cross-bridge model, *Ann. Biomed. Eng.* 28 (2000) 629–640.
- [61] M. Kalda, P. Peterson, M. Vendelin, Cross-bridge group ensembles describing cooperativity in thermodynamically consistent way, *PLoS One* 10 (2015), e0137438.

Supporting Information:

Restricted ADP movement in cardiomyocytes: cytosolic diffusion obstacles are complemented with a small number of open mitochondrial voltage-dependent anion channels

Päivo Simson*, Natalja Jephina*, Martin Laasmaa, Pearu Peterson, Rikke Birkedal, and Marko Vendelin
Laboratory of Systems Biology, Institute of Cybernetics, Tallinn University of Technology, Akadeemia Rd 21, 12618 Tallinn, Estonia

* Authors contributed equally to this work

This Supporting Information presents the detailed experimental methods, model and simulation description. In addition, example case is shown where fluorescence was normalized globally, instead of local normalization as presented in the main text. Finally, analysis results for each considered cell are summarized in the table.

1 ISOLATION OF CARDIOMYOCYTES

Cardiomyocytes were isolated as described in [1]. The animals received an i.p. injection of 2500 U heparin and were anesthetized with 0.5 mg/kg ketamine (Bioketan, Vetoquinol Biowet, Gorzów Wielkopolski, Poland) and 125 mg/kg dexmedetomidine (Dexdomitor; Orion, Espoo, Finland). The excised heart was swiftly placed in ice-cold wash solution (see composition below) to minimize ischemic damage. The heart was Langendorff perfused with wash solution at constant pressure of 80 cm H₂O for 5 minutes before the perfusate was changed to digestion solution containing 0.75 – 1 mg/ml of liberase TH (Roche; see composition below). This solution was recirculated with a rate of 5.1 ml/min until the pressure was 0 mm Hg (approx. 40 min). After this, the ventricle was cut into four pieces and transferred into 10 ml digestion solution. It was incubated with gentle shaking in waterbath at 37°C for additional 10 – 20 minutes. When the ventricular tissue pieces began to disassemble, they were transferred to sedimentation solution (see composition below), cut a few times with a scissor and the cells were suspended with a pipette. The cell suspension was passed through a nylon mesh and viable cells separated by sedimentation. Calcium concentration in the cell suspension was increased gradually to 1 mmol/L with repeated wash-sedimentation cycles after which the cells were washed three times with large volumes of Ca²⁺-free solution. The cells were stored in this solution at room temperature until use.

2 SOLUTIONS AND CHEMICALS

Solutions used in isolation of cardiomyocytes. Wash solution contained (in mmol/L): 117 NaCl, 5.7 KCl, 4.4 NaHCO₃, 1.5 KH₂PO₄, 1.7 MgCl₂, 21 HEPES, 20 taurine, 11.7 glucose, and pH was adjusted at 25°C to 7.4 with NaOH. Digestion solution had the same composition as the wash solution with the addition of 3 mg/ml BSA (Roche, 10 775 835 001), 0.25 mg/ml liberase TH (Roche). In some cases, 0.0125 % trypsin was added to the digestion solution. Sedimentation solution had the same composition as the wash solution with the addition of 2 mg/mL BSA (Roche, 10 775 835 001), 10 μmol/L leupeptine (Roche, 11 034 626 001), 2 μmol/L soybean trypsin inhibitor (Fluka, 93619).

Measurements were performed in Mitomed solution. It contained (in mmol/L): 3 KH₂PO₄, 3 MgCl₂, 20 HEPES, 0.5 EGTA, 20 taurine, 0.5 dithiothreitol and 60 lactobionate, 110 sucrose, 5 glutamate and 2 malate, and pH was adjusted at 25°C to 7.1 with KOH. For cell membrane permeabilization 25 μg/mL saponin and 100 μmol/L ADP were added to Mitomed solution.

Concentrations of the uncoupler and respiration blockers were: 10 μmol/L FCCP (Carbonyl cyanide 4-(trifluoromethoxy)phenylhydrazone), 10 μmol/L oligomycin A (Tebu-bio, bia-01059-1) and 5 mmol/L sodium cyanide.

All chemicals were obtained from Sigma-Aldrich if not mentioned otherwise.

3 FLUORESCENCE MICROSCOPY

Experiments were performed on an inverted Nikon Eclipse Ti-U microscope (Nikon, Japan) equipped with two tiers of motorized filter turrets. 60x water-immersion objective (Nikon, Plan Apo VC 60x/1.2 WI, Amstelveen, the Netherlands) was used in the experiments. For images of NADH autofluorescence, light from a Prior Lumen 200 with a 200W metal halide lamp with extended wavelength (Prior Scientific, Cambridge, United Kingdom) was passed via a liquid guide into the upper filter turret. For NADH recordings, the light was passed through a 340/26 nm excitation filter onto a 400 nm long pass dichroic mirror, which deflected the light onto the specimen. Light emitted from the specimen passed back through the upper filter cube to a 510 XR dichroic in the lower filter cube and was reflected through a 460/80 nm emission filter to an Andor Ixon EMCCD camera (Andor Technologies, Belfast, United Kingdom). All filters were obtained from AHF Analysentechnik AG, Germany. Optical sectioning was carried out by a piezoelectric objective positioning system (Piezosystem Jena GmbH, MIPOS 250SG M25, Jena, Germany). To reduce photobleaching through limitation of light exposure, Uniblitz shutter (VCM-D1, Vincent Associates, Rochester, USA) was used. Image acquisition and microscope control during experiments were performed using the software written in our laboratory.

At each experimental condition, such as ADP concentration, exposure to FCCP, or OL+CN, at least three 3D image stacks were acquired. Each 3D stack consisted of 5 images acquired

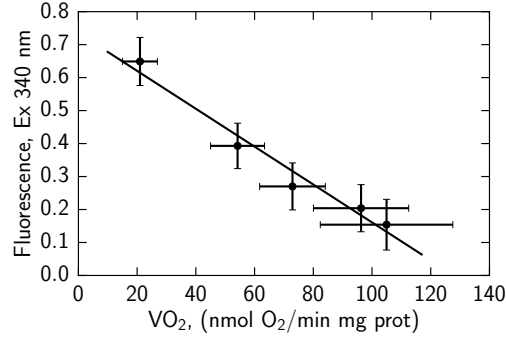


FIGURE S1: Relationship between relative NADH fluorescence and mitochondrial respiration rate in permeabilized cardiomyocytes exposed to the different amount of ADP in solution to stimulate mitochondrial respiration. The experimental points are fitted using linear regression. Data from [2].

at different focal planes. The acquired 3D stacks were averaged leading to 3D image of NADH fluorescence for the corresponding condition. In the analysis, these averaged 3D images were used.

4 REACTION-DIFFUSION MODEL FOR ADP AND ATP

To describe the changes in ADP and ATP concentrations we consider a reaction-diffusion model. We introduce the following notation for the concentrations:

$$u = [ADP], \quad v = [ATP],$$

for the associated maximal reaction rates:

$$V_1 = V_{max}^{ATPsyn}, \quad V_2 = V_{max}^{ATPase},$$

and for the Michaelis constants:

$$K_1 = K_m^{ATPsyn}, \quad K_2 = K_m^{ATPase}.$$

As has been done for representing cardiac electric activation propagation simulations using bidomain models [3], we use continuum approximation of intracellular environment and, in the model, follow changes in ATP and ADP concentrations within cytosol and myofibrils. The model equations, describing ADP/ATP diffusion, ATPase and ATP synthase inside the cytosolic and myofibrillar compartments, are

$$\frac{\partial u}{\partial t} - D\nabla^2 u = V_{ATPase}(v) - V_{ATPsyn}(u), \quad (1)$$

$$\frac{\partial v}{\partial t} - D\nabla^2 v = V_{ATPsyn}(u) - V_{ATPase}(v), \quad (2)$$

where the ATP synthase and ATPase reaction rates are given by Michaelis–Menten formulæ:

$$V_{ATPsyn}(u) = V_1 \frac{u}{u + K_1}, \quad V_{ATPase}(v) = V_2 \frac{v}{v + K_2}.$$

Here we assumed the intracellular diffusion constants for ADP and ATP to be equal, e.g. $D_{ADP} = D_{ATP} = D$. Notice that

the apparent Michaelis constant K_1 reflects stimulation of mitochondrial respiration by cytosolic ADP in the vicinity of the mitochondrion, Mito $K_m(ADP)$ in the main text.

The sum of ADP and ATP concentrations is governed by

$$\frac{\partial}{\partial t}(u + v) + D\nabla^2(u + v) = 0,$$

which is linear and homogeneous diffusion equation. The stationary state solution corresponding to the boundary conditions

$$u|_S = u_{out} = const, \quad v|_S = v_{out} = const,$$

where S denotes the surface of the cell, is

$$u + v = u_{out} + v_{out} = const.$$

Since there is a flow in the chamber, we assume that there is no ATP buildup in the solution ($v_{out} = 0$), and we have

$$v = u_{out} - u.$$

Substituting this relationship into the equation [1], we get a single nonlinear partial differential equation for ADP concentration u inside the cell:

$$D\nabla^2 u = V_1 \frac{u}{u + K_1} - V_2 \frac{u_{out} - u}{u_{out} - u + K_2}.$$

Variational form of this equation is

$$\begin{aligned} -D \int_{\Omega} \nabla u \cdot \nabla v^* d\Omega + \int_S \frac{\partial u}{\partial n} v^* dS \\ = \int_{\Omega} \left[V_1 \frac{u}{u + K_1} - V_2 \frac{u_{out} - u}{u_{out} - u + K_2} \right] v^* d\Omega, \quad (3) \end{aligned}$$

where Ω is the volume of the modeled cell. v^* is the test function required to vanish on the parts of the boundary where u is known. In the present problem this implies that $v^* = 0$ on the whole boundary S , and thus the second term on the left side of the equation [3] vanishes everywhere.

NADH fluorescence is related to respiration rate using a linear approximation of the relationship between respiration rate and the fluorescence [2]. The linear fit through the data points

is shown in Fig.S1 with the coefficient of determination $r^2 = 0.97$. Note that this linear relationship was found in the conditions used in our experiments and is not an universal property of the mitochondrial respiration in the heart.

In our model, NADH fluorescence F_{NADH} at position \mathbf{r} is calculated from local ATP synthesis rate:

$$F_{NADH}(\mathbf{r}) = \gamma \cdot \left(1 - \frac{u(\mathbf{r})}{u(\mathbf{r}) + K_1} \right),$$

where γ is a normalization constant. By convolving the fluorescence signal F_{NADH} with experimentally determined point spread function of the used fluorescence microscope, the images were calculated that were later compared with the measurements (see below).

5 SOLVING THE REACTION-DIFFUSION PROBLEM

Equation [3] was solved numerically by the finite element software package FEniCS [4]. Solutions for each modeled cell for 0.1 mmol/L, 0.3 mmol/L, 0.5 mmol/L and 2.0 mmol/L of exogenous ADP (u_{out}) were calculated for a large set of D and K_1 combinations. The results were compared to experiment and the best fit was found using the methods described below (section Image analysis and data fitting).

6 MODEL PARAMETER VALUES

The maximal mitochondrial ATP synthase activity in the cell, when normalized to cytosolic together with myofibrillar fraction, was $V_1 = 0.54$ mmol/L ATP/s. This was found taking into account ADP/O₂ ratio 6, maximal mitochondrial respiration rate 13.5 $\mu\text{mol O}_2/\text{min}\cdot\text{g dw}$ [5], total dry mass, cellular, and myofibrillar and sarcoplasmic volumes in 1 kg of heart tissue [6].

The maximal ATPase rate, $V_2 = 0.18$ mmol/L/s, was calculated on the basis of the maximal mitochondrial ATP synthase activity taking into account that, in our conditions, the exogenous ATP-stimulated respiration in permeabilized cardiomyocytes was 1/3 from the maximal ADP-stimulated respiration rate [1]. The apparent Michaelis constant for bulk ATPases was taken $K_2 = 0.3$ mmol/L, the upper limit used in [5, 7] on the basis of the fits in [1].

7 EMPIRICAL EQUATION CONNECTING D AND K_1

Regional ATP synthesis rate is approximated by Michaelis-Menten relationship and is dependent on cytosolic ADP concentration in the vicinity of mitochondria:

$$V_{ATPsyn}(u) = V_1 \frac{u}{u + K_1}.$$

Since ATP synthesis rate can be related to respiration rate through linear relationship [8], the found relationships for respiration rate can be directly applied to ATP synthesis rate. For permeabilized cells, the exogenous ADP has to be

~ 0.3 mmol/L to reach half-maximal respiration rate [1]. In the model terms, it can be expressed as

$$\frac{1}{\Omega} \int_{\Omega} V_{ATPsyn}(u^*(\mathbf{r})) d\Omega = \frac{1}{\Omega} \int_{\Omega} \frac{1}{2} V_{max}(\mathbf{r}) d\Omega,$$

where $u^*(\mathbf{r})$ is a solution of the equation [3] that satisfies the boundary condition $u^*|_S = 0.3$ mmol/L. Since in the model we assumed that $V_{max}(\mathbf{r})$ is constant in the cell, we get

$$\frac{1}{\Omega} \int_{\Omega} \frac{u^*(\mathbf{r})}{u^*(\mathbf{r}) + K_1} d\Omega = \frac{1}{2}. \quad (4)$$

This non-linear equation can be solved with respect to D for given K_1 . For that, at each iteration, for given D and K_1 , ADP concentration and average ATP synthesis rate was found by solving Eq. [3] with exogenous [ADP] is 0.3 mmol/L as an boundary condition. By comparing calculated ATP synthesis rate with the expected half-maximal rate, non-linear solver adjusted D until the solution satisfied Eq. [4]. This solution corresponds to D and K_1 values lying on the 0.5-line of Fig.3 A.

8 TOTAL NUMBER OF VDACS PER MITOCHONDRION

To estimate the number of VDACS per mitochondrion, we took into account mitochondrial distribution in rat cardiomyocytes [9] as well as the following morphological data for the heart:

- Total volume of mitochondria, $\Omega_{all\ mitos} = 32.7\%$ of cell volume = 248 ml = $248 \cdot 10^{12} \mu\text{m}^3$ per kg wet weight [6];
- Dry mass of mitochondria, $m_{all\ mitos;dry} = 89.4$ g per kg wet weight [6];
- Total mass of mitochondrial protein $\approx 75\%$ of mitochondrial dry mass [6];
- Total mass of VDACS $\approx 0.3\%$ of all mitochondrial protein [10].

We have earlier shown that mitochondria in rat are distributed in highly ordered pattern along the parallel strands with the longitudinal distance between mitochondrial centers $d \approx 0.95 \mu\text{m}$ and transversal distance $a \approx 1.8 \mu\text{m}$ [9]. Here, we assume that transversally mitochondria are aligned along a hexagon, as in Fig.S2. Assuming that all the mitochondria have the same shape (Fig.S2B, dashed circles denoting the mitochondria), it is clear that the numbered volumes inside the hexagon occupy three times the volume of one mitochondrion. Since the total area of the equilateral triangle is $\sqrt{3}/4 a^2$, the relative volume occupied by mitochondria (32.7% in heart) can be expressed as

$$\frac{\Omega_{all\ mitos}}{\Omega_{cell}} = \frac{3 \times \Omega_{mito} \frac{1}{d}}{6 \times \frac{\sqrt{3}}{4} a^2}.$$

From here, the volume of one mitochondrion equals

$$\Omega_{mito} = 0.327 \frac{\sqrt{3}}{2} a^2 d = 0.872 \mu\text{m}^3.$$

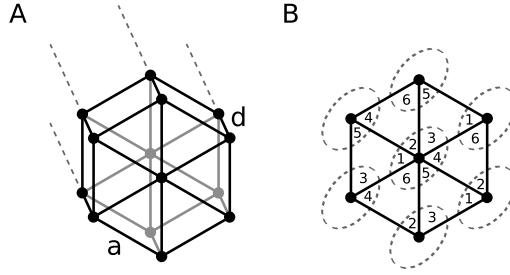


FIGURE S2: Hexagonal arrangement of mitochondria.

Notice that the calculated volume does not depend on the exact shape of the mitochondrion. If the mitochondria can be considered identical, the volume of one mitochondrion is determined by the volume ratio and the spatial arrangement only.

From a single mitochondrion volume, we can get the number of mitochondria per kg of wet weight

$$N_{mitos} = \frac{\Omega_{all\ mitos}}{\Omega_{mito}} = \frac{248 \cdot 10^{12}}{0.872} = 285 \cdot 10^{12},$$

as well as the mass of a single mitochondrion

$$m_{mito;dry} = \frac{m_{all\ mitos;dry}}{N_{mitos}} = \frac{89.4}{285 \cdot 10^{12}} = 0.314 \cdot 10^{-12} g.$$

Thus, the total mass of VDACS per one mitochondrion is therefore

$$\begin{aligned} m_{all\ vdacs\ per\ mito} &= m_{mito;dry} \cdot 75\% \cdot 0.3\% \\ &= 0.314 \cdot 10^{-12} \cdot 0.75 \cdot 0.003 = 0.707 \cdot 10^{-15} g, \end{aligned}$$

and, taking into account VDAC molecular weight [30 kDa = $5 \cdot 10^{-20}$ g, [11]], the number of VDACS per mitochondrion is

$$N_{vdacs\ per\ mito} = \frac{m_{all\ vdacs\ per\ mito}}{m_{vdac}} = \frac{0.707 \cdot 10^{-15}}{5 \cdot 10^{-20}} \approx 14000.$$

Assuming the surface area of the mitochondrion to be $5 \mu m^2$ we get approximately 2800 VDACS per μm^2 and the mean distance between VDAC centers on the mitochondrial outer membrane around 20 nm. Note that the diameter of the VDAC's aqueous channel is 2.6-3 nm [11].

9 NUMBER OF OPEN VDACS

The number of open VDACS is found by taking into account that, at steady state, ADP flux through mitochondrial outer membrane is equal to ATP synthesis rate inside the mitochondrion. At half-maximal respiration rate, for a single mitochondrion, we have

$$p_{mito}(u_{cyto} - u_{mito}) = \frac{V_1}{2} \frac{\Omega_{cyto} + \Omega_{myo}}{N_{mitos}},$$

where p_{mito} is the permeability of mitochondrial outer membrane, u_{cyto} and u_{mito} are ADP concentrations in cytosol and

in the mitochondrial inter membrane space, respectively; Ω_{cyto} and Ω_{myo} are volumes of sarcoplasmic and myofibrillar compartments per kg wet weight, respectively; and N_{mitos} is number of mitochondria per kg wet weight. At half-maximal respiration rate, ADP concentrations would be the corresponding Michaelis-Menten constants leading to

$$p_{mito} = \frac{V_1}{2} \frac{\Omega_{cyto} + \Omega_{myo}}{N_{mitos}} \frac{1}{K_1 - K_m^{ANT}},$$

where K_m^{ANT} is an apparent K_m for adenine nucleotide translocase. From here, assuming that VDAC conductance for ATP and ADP in closed state is negligible, we can get the number of open VDACS N_{vdac}^{open} in single mitochondrion by dividing total mitochondrial outer membrane permeability p_{mito} with a single VDAC permeability $p_{vdac} = 1.1 \times 10^{-2} \mu m^3/s$ [12]:

$$N_{vdac}^{open} = \frac{1}{p_{vdac}} \frac{V_1}{2} \frac{\Omega_{cyto} + \Omega_{myo}}{N_{mitos}} \frac{1}{K_1 - K_m^{ANT}}. \quad (5)$$

For example, for $K_1 = 0.156$ mmol/L found as an average apparent K_m for cytoplasmic ADP of mitochondrial respiration (Table S1), taking into account the myofibrillar and sarcoplasmic volumes in 1 kg of heart tissue [6], assuming that $K_m^{ANT} = 0.015$ mmol/L, we get $N_{vdac}^{open} = 291$ VDACS open for ADP per single mitochondria. This is only 2% of the total number of VDACS on the mitochondrial outer membrane, which was calculated above.

10 IMAGE ANALYSIS AND DATA FITTING

The measured (E) and computed (T) images for each condition s are expressed by three-dimensional arrays:

$$E^s = E_{ijk}^s, \quad T^s = T_{ijk}^s(D, K_1),$$

$$i = 0 \dots 1003, \quad j = 0 \dots 1001, \quad k = 0 \dots 4,$$

where i, j, k are the pixel indexes in x, y, z direction, respectively, and s denotes one of the following conditions: exogenous ADP 0.1 mmol/L, 0.3 mmol/L, 0.5 mmol/L, or 2 mmol/L; inhibitors oligomycin and cyanide OLCN; and uncoupler FCCP.

To correct for the camera image offset and changes in background fluorescence induced by flowing solution, the mean

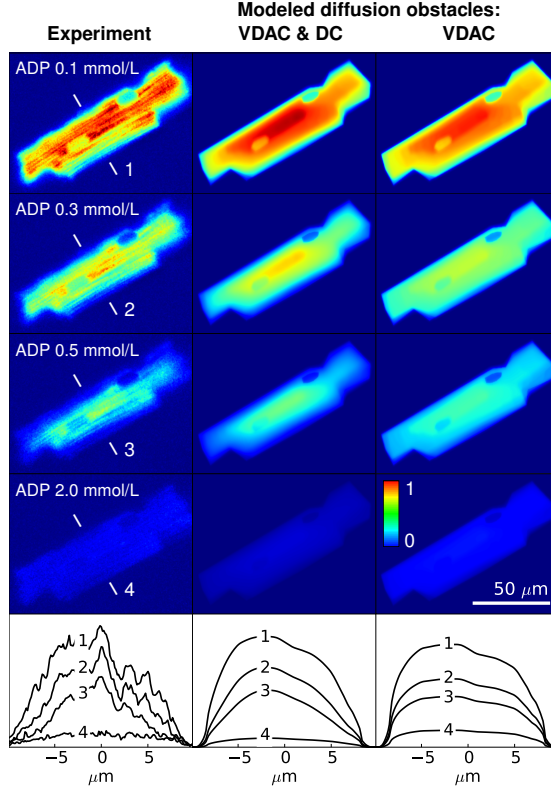


FIGURE S3: NADH autofluorescence of a single permeabilized cardiomyocyte was varied by changing exogenous ADP concentration. The fluorescence images recorded by a camera (left column) on a focal plane are compared with the images calculated by the model (middle and right columns). In the images, the fluorescence intensity is encoded by color, as shown on the bar. The model simulations were performed assuming that diffusion restriction between extracellular solution and mitochondrial inner membrane is either partitioned between cytosolic diffusion obstacles and mitochondrial outer membrane (middle column) or exclusively induced by closure of VDAC in mitochondrial outer membrane (right column). As it is clear from the comparison of the images as well as the intensity profiles shown on the bottom for different ADP concentrations (see experimental images for location of the profile and corresponding ADP concentration), the images calculated by the model for two different diffusion restriction distributions give similar result.

background offset level per pixel is defined for every two-dimensional image:

$$b_k^s = \frac{1}{(i_1 - i_0)(j_1 - j_0)} \sum_{i=i_0}^{i_1} \sum_{j=j_0}^{j_1} E_{ijk}^s,$$

were the indices i_0 , i_1 and j_0 , j_1 define a subregion on the experimental images. This subregion is chosen from outside the cell, appropriately for each experiment.

In addition to the background fluorescence correction, we assumed that, in the presence of FCCP, there is no mitochondrial NADH-induced fluorescence (NADH concentration was expected to be zero in mitochondria). Thus, all experimental images were normalized as in

$$\bar{E}_{ijk}^s = E_{ijk}^s - b_k^s - (E_{ijk}^{\text{fccp}} - b_k^{\text{fccp}}).$$

These level-corrected experimental images were used for comparison with the images calculated by the model.

10.1 Image norm

Let A be an arbitrary array of any dimensions. We define the norm $\|A\|$ as the square root of the sum of the squares of all the array elements. If $A = A_{ijk}$ then

$$\|A\| = \left[\sum_{i,j,k} |A_{ijk}|^2 \right]^{\frac{1}{2}}.$$

10.2 Fitting locally normalized images

Fluorescence distribution heterogeneity is induced by heterogeneity in mitochondrial response, geometry (thickness of the cell) and mitochondrial distribution. To demonstrate the superposition of these effects, experimental and calculated fluorescence image stacks are shown in Fig.S3.

Calculated image stacks corresponding to two different sets of parameters are presented: diffusion is obstructed either mainly

by MOM (Fig.S3, right column) or by combination of MOM and cytoplasmic diffusion obstacles (Fig.S3, middle column). In the both parameter sets used, the diffusion obstacles are such that the apparent K_m of mitochondrial respiration to ADP in solution is 0.3 mmol/L, in accordance with the experimental data [1]. Thus, in the simulation with the combination of two diffusion obstructions (the middle column), the contribution of MOM is reduced when compared to the simulation where only MOM is contributing to overall diffusion restriction.

As in the experiment, the calculated overall fluorescence reduced with the increase of extracellular ADP (Fig.S3). In the both model solutions, there is a marked heterogeneity in fluorescence induced by the heterogeneity of mitochondrial respiration and the differences in thickness of the cell in that particular location (see colormaps and intensity profiles in Fig.S3). However, in the solution with diffusion obstacles mainly attributed to MOM (Fig.S3, right column), the heterogeneity of mitochondrial response is minimal with the differences in calculated fluorescence mainly induced by the differences in cell thickness. Due to the superposition of the heterogeneity of mitochondrial respiration and the differences in thickness of the cell in that particular location leading to the heterogeneity in fluorescence, comparison of the calculated and measured fluorescence heterogeneity poorly differentiated between different combinations of intracellular diffusion obstacles.

To highlight the heterogeneity in mitochondrial response, we found that the sensitivity of the method increases if experimental and calculated data sets are normalized by local maximum fluorescence determined in the presence of oligomycin and cyanide.

Here, for any given (K_1, D) combination, we first determined the gains α^s by minimizing

$$\|\bar{E}^s - \alpha^s T^s\|$$

for each condition separately. Second, we normalized the arrays as follows:

$$\tilde{E}_{ijk}^s = \bar{E}_{ijk}^s N_{ijk}, \quad \tilde{T}_{ijk}^s = \alpha^s T_{ijk}^s M_{ijk},$$

where

$$N_{ijk} = \begin{cases} 1/\bar{E}_{ijk}^{\text{olcn}} & \text{if } \bar{E}_{ijk}^{\text{olcn}}/\alpha^{\text{olcn}} \geq \epsilon \text{ and } T_{ijk}^{\text{olcn}} \geq \epsilon \\ 0 & \text{otherwise} \end{cases}$$

$$M_{ijk} = \begin{cases} 1/(\alpha^{\text{olcn}} T_{ijk}^{\text{olcn}}) & \text{if } \bar{E}_{ijk}^{\text{olcn}}/\alpha^{\text{olcn}} \geq \epsilon \text{ and } T_{ijk}^{\text{olcn}} \geq \epsilon \\ 0 & \text{otherwise} \end{cases}$$

with the cut-off parameter $\epsilon > 0$ was taken equal to 0.01.

The goodness of the fit for any (K_1, D) combination was given by

$$r = \sum_s \|\tilde{E}^s - \tilde{T}^s\|,$$

where s corresponded to exogenous ADP concentrations 0.1 mmol/L, 0.3 mmol/L, 0.5 mmol/L, and 2 mmol/L. As shown in the main text, the calculated normalized image intensities depended on K_1 and D (Fig.2 in the main text, compare to Fig.S3) and r minimum was well determined in parameter space (K_1, D) , Fig.3 in the main text.

10.3 Detailed results

Estimated diffusion coefficient and mitochondrial outer permeability for each studied cell is shown in Table S1.

References

1. M. Sepp, M. Vendelin, H. Vija, and R. Birkedal. Adp compartmentation analysis reveals coupling between pyruvate kinase and atpases in heart muscle. *Biophys. J.*, 98:2785–2793, 2010. ISSN 0006-3495.
2. N. Jephthina, N. Beraud, M. Sepp, R. Birkedal, and M. Vendelin. Permeabilized rat cardiomyocyte response demonstrates intracellular origin of diffusion obstacles. *Biophys. J.*, 101(9):2112–2121, 2011. ISSN 0006-3495.
3. C. S. Henriquez. Simulating the electrical behavior of cardiac tissue using the bidomain model. *Crit. Rev. Biomed. Eng.*, 21(1): 1–77, 1993. ISSN 0278-940X.
4. A. Logg, K. Mardal, and G. Wells. *Automated Solution of Differential Equations by the Finite Element Method*. Springer Berlin Heidelberg, 2012.
5. M. Vendelin, M. Eimre, E. Seppet, N. Peet, T. Andrienko, M. Lemba, J. Engelbrecht, E. Seppet, and V. Saks. Intracellular diffusion of adenosine phosphates is locally restricted in cardiac muscle. *Mol. Cell. Biochem.*, 256-257(1):229–241, 2004. ISSN 0300-8177.
6. M. Aliev, P. Santos, J. Hoerter, S. Soboll, A. Tikhonov, and V. Saks. Water content and its intracellular distribution in intact and saline perfused rat hearts revisited. *Cardiovasc. Res.*, 53(1):48–58, 2002. ISSN 0008-6363.
7. H. Ramay and M. Vendelin. Diffusion restrictions surrounding mitochondria: A mathematical model of heart muscle fibers. *Biophys. J.*, 97(2):443–452, 2009. ISSN 0006-3495.
8. M. Vendelin, O. Kongas, and V. Saks. Regulation of mitochondrial respiration in heart cells analyzed by reaction-diffusion model of energy transfer. *Am. J. Physiol. Cell. Physiol.*, 278(4): C747–C764, 2000. ISSN 0363-6143.
9. R. Birkedal, H. A. Shiels, and M. Vendelin. Three-dimensional mitochondrial arrangement in ventricular myocytes: from chaos to order. *Am. J. Physiol. Cell. Physiol.*, 291(6):C1148, 2006. ISSN 0363-6143.
10. T. Rostovtseva and M. Colombini. Atp flux is controlled by a voltage-gated channel from the mitochondrial outer membrane. *J. Biol. Chem.*, 271(45):28006, 1996. ISSN 0021-9258.
11. J. Lemasters and E. Holmuhamedov. Voltage-dependent anion channel (vdac) as mitochondrial governor—thinking outside the box. *BBA-Mol. Basis Dis.*, 1762(2):181–190, 2006. ISSN 0925-4439.
12. T. K. Rostovtseva and S. M. Bezrukov. Atp transport through a single mitochondrial channel, vvac, studied by current fluctuation analysis. *Biophys. J.*, 74(5):2365–2373, 1998. ISSN 0006-3495.

Table S1: Number of VDACs open for ADP and cytosolic diffusion coefficient.

Experiment No.	Global minimum			Minimum on the 0.5 line		
	D $\mu\text{m}^2/s$	$K_m(ADP)$ mmol/L	Open VDACs per mitochondrion	D $\mu\text{m}^2/s$	$K_m(ADP)$ mmol/L	Open VDACs per mitochondrion
1.	14.8	0.108	440	10.7	0.120	390
2.	42.0	0.163	276	30.2	0.219	201
3.	22.6	0.141	325	16.1	0.178	251
4.	24.5	0.133	347	18.6	0.152	299
5.	32.3	0.152	299	22.2	0.189	235
6.	30.3	0.178	251	23.6	0.208	212
7.	38.1	0.219	201	38.1	0.218	201
Average value \pm standard error of the mean						
	29.2 \pm 3.5	0.156 \pm 0.013	306 \pm 29	22.8 \pm 3.4	0.184 \pm 0.014	256 \pm 26